BIOSYSTEM FOR THE CULTURE AND ELECTRICAL CHARACTERISATION OF EPITHELIAL CELL TISSUES

THÈSE N^{O} 2551 (2002)

PRÉSENTÉE À LA FACULTÉ STI SECTION DE MICROTECHNIQUE

ÉCOLE POLYTECHNIQUE FÉDÉRALE DE LAUSANNE

POUR L'OBTENTION DU GRADE DE DOCTEUR ÈS SCIENCES TECHNIQUES

PAR

Serge HEDIGER

ingénieur microtechnique diplômé EPF
de nationalité suisse et originaire de Reinach (AG)

acceptée sur proposition du jury:

Prof. M. Gijs, directeur de thèse
Dr C. Clément, rapporteur
Prof. J.-D. Horisberger, rapporteur
Prof. J.-J. Meister, rapporteur
Prof. N. de Rooij, rapporteur

Lausanne, EPFL
2002

To my beloved wife and family

ABSTRACT

The aim of this work was to develop a microchamber system for performing electrophysiological measurements on epithelial surface on culture membranes in the mm^2 range. This miniaturised system permits the use of small quantities of epithelial cells, which in relatively short time grow into a tight layer that can be used in electrophysiological (ion transport) experiments. Availability of cells is an issue, for example when the cells originate from human biopsies or from (expensive!) transgenic mice.

Apart from having reduced culture surfaces (for use with scarce biological tissues), there are tremendous advantages in having a cell culture mini-chamber. Our systems are with integrated electrical electrodes, micro-fluidic channels and feed-throughs, making them extremely compact and easy to use, thereby avoiding cell perturbation by manipulations. The structures facilitate control of the cell layer growth, the measurement of the cell layer resistance and the transport and diffusion of biological or pharmacological molecules through the cell layer.

Moreover we have chosen cheap and easy-to-tool materials for the realisation of disposable devices. We have also fabricated modular devices, in which the cell culture membranes can be reversibly placed within or removed from the system, thereby offering flexibility and economic interest.

These microsystems (for biological applications ("biosystems")) are realised using photolithography, various etching procedures (among which powder-blasting), thin film deposition, electrochemical deposition, polydimethylsiloxane (PDMS) moulding and gluing technologies. Both electrical and fluidic characterisation of the biosystems has been performed. Also, a specific study of microelectrode properties of different electrode materials, such as Pt, Ag and Ag/AgCl has been done using various electrochemical experiments and models.

The devices are finally tested in real biological experiments. These experiments were carried on with the collaboration of three different biological academic work groups: the group of Prof. W. Hunziker from the Institute of Biochemistry at the University of Lausanne, the group of Prof. Van der Goot from

the Department of Biochemistry at the University of Geneva and Prof. J.D. Horisberger from the Institute of Pharmacology and Toxicology at the University of Lausanne. The functionality of our devices has been tested and their potential for the study of transport and diffusion of biological or pharmacological molecules through the cell layer via accurate measurement of (bio-) chemically induced resistance variations, has been demonstrated.

VERSION ABRÉGÉE

Le but de ce travail était de développer un système de micro-chambres permettant d'effectuer des mesures électro-physiologiques sur des cultures de cellules épithéliales cultivées sur des membranes de culture de l'ordre du mm^2. Ce type de système permet l'utilisation d'une faible quantité de cellules épithéliales, lesquelles croissent en une durée relativement réduite, en formant une mono-couche serrée qui peut être utilisée dans des expériences électro-physiologiques (transport d'ions). La disponibilité des cellules devient un problème, par exemple quand les cellules proviennent d'une biopsie humaine ou de souris transgéniques (qui coûtent chères).

Indépendamment du fait d'avoir des surfaces de culture réduites (pour l'utilisation de tissus épithéliaux disponibles en quantité réduite), il y a des avantages considérables à avoir une mini-chambre de culture cellulaire. Nos systèmes sont pourvus d'électrodes intégrées, de canaux et de connexions microfluidiques, les rendant extrêmement compacts et d'utilisation aisée afin d'empêcher les perturbations de fonctions cellulaires causées par les manipulations. Les structures facilitent le contrôle de la croissance de la couche cellulaire, la mesure de la résistance de la couche cellulaire, ainsi que le transport et la diffusion de molécules biologiques ou pharmacologiques à travers la couche cellulaire.

De plus, des matériaux bon marchés et faciles à mettre en oeuvre ont été choisis pour la réalisation d'un système jetable. Nous avons également fabriqué un système modulaire permettant le remplacement des membranes de culture cellulaire, offrant ainsi de la flexibilité et un intérêt économique évident.

Ces microsystèmes (pour applications biologiques ("biosystèmes")) ont été réalisés par le biais de la photolithographie, de procédés de gravure variés (parmi lesquels le sablage), la déposition de couches minces, la déposition électrochimique, le moulage de polydimethylsiloxane (PDMS) ainsi que par des techniques de collage. Les caractérisations électriques et fluidiques ont été réalisées. De plus, une étude spécifique a été effectuée sur les propriétés de différents matériaux pour les micro-électrodes comme le Pt, l'Ag, et l'Ag/AgCl, par le moyen d'expériences et d'élaboration de modèles électrochimiques.

Les biosystèmes sont finalement testés dans des expériences biologiques. Ces expériences ont été effectuées avec la collaboration de trois groupes académiques de recherches biologiques: le groupe du Prof. W. Hunziker de l'Institut de Biochimie de l'Université de Lausanne, le groupe du Prof. Van der Goot du Département de Biochimie de l'Université de Genève ainsi que le groupe du Prof. J.D. Horisberger de l'Institut de Pharmacologie et de Toxicologie de l'Université de Lausanne. La fonctionnalité de nos dispositifs a été testée et leur potentiel a été démontré en ce qui concerne l'étude du transport et de la diffusion de molécules biologiques ou pharmacologiques à travers la couche cellulaire par la mesure fidèle de variations de résistances (bio-) chimiquement induites.

TABLE OF CONTENTS

Introduction 1

1 Culture and physiological measurement of cells and tissues 3

1.1 Epithelial tissues 3
1.1.1 Ionic transport through epithelial cells 3
1.1.2 Clinical relevance 6
1.1.3 Epithelial cell culture 6
1.2 How to measure epithelial transport 8
1.2.1 Electrical transport 8
1.2.2 Radioactivity and fluorescence measurements 8
1.3 Electrical characterisation of biological tissues: state of the art 9
1.3.1 “Macro scale” commercial systems for culture and characterisation of epithelial tissues 9
1.3.2 Biological impedance measurements on living single cells or tissues 12
1.3.3 Miniaturised electrical systems for biological applications 13
1.4 Conclusion 15

2 Biosystem design and fabrication 17

2.1 Definition of required features 17
2.1.1 Restatement of the application 17
2.1.2 Biosystem requirements 17
2.2 Design and fabrication 19
2.2.1 Design 20
2.2.2 Fabrication technologies 21
2.2.3 Materials 22
2.2.4 Measurement technique 24
2.3 Device types 25
2.3.1 Silicon based device 25

2.3.2 Glass based device 32
2.3.3 Macro device 36
2.3.4 Linear device 38
2.3.5 Modular device 42
2.4 Conclusion 46

3 Electrochemical characterisation without epithelial tissues 47

3.1 Electrode-electrolyte properties 47
3.1.1 Definition of the interface 47
3.1.2 Double-layer ion distribution models 49
3.1.3 Double-layer circuit model 52
3.1.4 Electrode potential 55
3.2 Impedance measurement technique 56
3.2.1 Two-electrode system 56
3.2.2 Four-electrode system 59
3.2.3 Comparison of the impedance measurement methods 63
3.3 Electrode materials 64
3.3.1 Silver-Silver chloride electrodes 65
3.3.2 Chlorination of silver electrodes 66
3.4 Two-electrode AC impedance measurements 72
3.4.1 Introduction 72
3.4.2 Electrochemical Impedance Spectroscopy 74
3.4.3 Electrical circuit model 77
3.5 Cyclic voltametry 83
3.5.1 Introduction 83
3.5.2 Experiments on different electrodes 84
3.5.3 Potential stability of electrodes 87
3.5.4 Cause of voltage instabilities 91
3.6 Cell culture device resistance 96
3.6.1 Linear device 96
3.6.2 Modular device 98
3.6.3 Polycarbonate membrane 98
3.7 Conclusion 100

4 Biological experiments 101

4.1 Transepithelial resistance study (with Prof. Hunziker) 101
4.2 Transepithelial resistance study (with Prof. Van der Goot) 103

4.3 Transepithelial resistance and ion transport study (with Prof. Horisberger) 105
4.4 Conclusion 107

Conclusions and outlook **109**

Appendix **113**

References **127**

Acknowledgments **139**

Curriculum Vitae **141**

INTRODUCTION

Miniaturised bio-chemical and cell-based measurement systems will have a large impact on the way medical diagnosis will be done in the near future. More particularly, in the field of clinical diagnosis and pharmacology, the use of living cells for fast specific and non-specific chemical sensing is an area of increasing importance [1-3]. A cell or cell layer is a complex system with appropriate response to a variety of external physical and chemical excitations. Experiments on such living biological systems (for example using electrical resistance or fluorescence measurements [4]) can lead to the study of diffusion and transport of biological or pharmacological molecules through the cell or cell layer [5, 6].

The *in vitro* study of the physiological properties of epithelial cells is a very useful tool in biology, both for the fundamental research and for clinical diagnostics. In general, experiments are done in macroscopic tissue resistance measurement chambers [7, 8], with a diameter ranging from a few millimetres up to some centimetres. In these devices, a cell tissue layer is grown on a nano-porous membrane separating two compartments of the chamber and measured with two pairs of electrodes, which are mechanically inserted in the system after cell culture.

There are several circumstances where available cell quantities for establishing those tissue cultures are very reduced: this is the case, for example, when starting those cultures from transgenic mice cells (respiratory epithelium, intestinal, colic, urinary, etc.) or from biopsies obtained from patients (biopsies obtained by digestive endoscopy, bronchial or urinary, for example). The establishment of sufficiently large epithelial cell culture surfaces, enabling electrophysiological studies, is then practically impossible or would take a large amount of time.

The progress in three-dimensional microfabrication technology has opened new possibilities for miniaturising these epithelial cell culture and analysis devices [9]. MEMS (Micro Electro Mechanical Systems), Bio-MEMS or μTAS (Micro Total Analysis Systems) have become a hot topic in today's scientific literature. These are fields, in which sensors, actuators, biological and chemical tools are converging. Thanks to all the new available microfabrication technolo-

gies, a high number of functionalities can be integrated on single miniaturised devices. Many physical and chemical phenomena, known in the “macro” world, are modified in the “micro” world, where, for example, surface interactions start to become more important than bulk phenomena. When scaling down channels, electrodes and different geometrical parameters in a microsystem, one tries to use these new properties advantageously to gain efficiency, resolution and time, to decrease the amounts of reagents and power consumption for the wanted applications.

The aim of our device is to enable both epithelial cell layer culture on small (~1 mm^2) surfaces and characterisation of the electrical transport properties of such cell layers. Apart from having reduced culture surfaces (for use with scarce biological tissues), there are tremendous advantages in having a cell culture mini-chamber. Our systems have integrated electrical electrodes, micro-fluidic channels and feed-throughs, making them extremely compact and easy-to-use, thereby avoiding cell perturbation due to external manipulations. The biosystems therefore facilitate control of the cell layer growth, the measurement of the cell layer resistance, the transport and diffusion of biological or pharmacological molecules through the cell layer and accurate measurement of (bio-) chemically induced resistance variations.

Finally, the biosystems are tested in real biological experiments. The functionality of the devices is demonstrated, showing the potential of such structures for fundamental research and cell based diagnostic applications.

1 CULTURE AND PHYSIOLOGICAL MEASUREMENT OF CELLS AND TISSUES

The cell is the structural and functional unit of living species. It is an open system which needs to exchange material and energy with its environment. It can perceive its environment variation and can react to it. The need to culture cells became obvious when biological experiments needed large quantities of cells, for studies in research and medicine. Biologists dissociated cells from living tissues and separated them by types to obtain quite homogeneous populations that could be analysed directly or after cell culture. Such culture enables the study of cell growth and differentiation, metabolism and cell functionality, response to external stimuli and transport phenomena.

1.1 EPITHELIAL TISSUES

1.1.1 IONIC TRANSPORT THROUGH EPITHELIAL CELLS

Consisting of one or more sheets of very closely associated cells, the epithelial tissue is covering the external surface of the body as well as the organs and the inner cavities [10, 11]. Those coherent cell sheets separate the body from its surroundings and separate its different fluid compartments. Among the important properties of most epithelial tissues is the capacity to transport solutes, in particular electrolytes, from one fluid compartment to another at the expense of metabolic energy. The cells are linked by tight junctions in numerous epithelial tissues. This assembly suits well for the protection function of the epithelium against mechanical lesions, the entry of microorganisms and the loss of liquid from an organism. The structure of an epithelium corresponds to its functionality. There are many specialized types of epithelia. Epithelium can be composed of numbers of cell layers, the stratified epithelium, or just one mono-layer, the simple epithelium. The cells that we are going to use in this thesis are of the second type, the simple epithelium and more specifically, renal and bronchial epithelia.

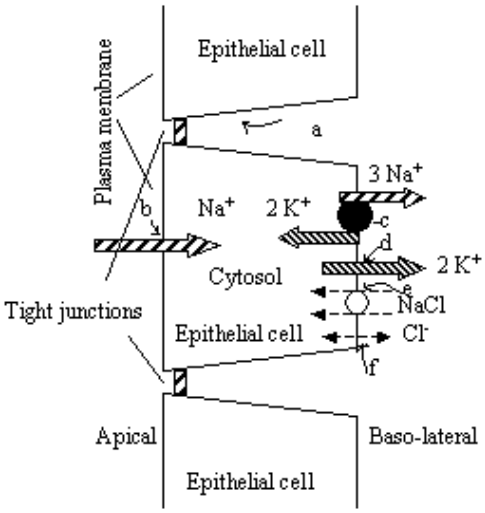

Figure 1.1: A drawing model of the functional unit of a tight epithelium (modified from [10]): (a) tight junction: limits and controls the passage of ions, but the permeability is smaller than other pathways; (b) specific, amiloride-sensitive sodium channel, in the apical membrane; (c) sodium-potassium exchange pump; exchanges 3 Na^+ for 2 K^+ across the basolateral membrane; (d) specific K^+ channels in basolateral membranes; (e) Na + Cl co-transport system (passive); (f) specific chloride channel in basolateral membranes (activated by swelling).

As said before, epithelial cells are linked by tight junctions that limit and control diffusion of substances in between the cells. Figure 1.1 shows that most of the substances that pass those epithelial cells have to go from an extracellular compartment on one side of the epithelial layer through the plasma membrane into the cytosol, and then from the cytosol through a second plasma membrane on the other side of the epithelium into a second extracellular compartment. One of the epithelium's surfaces generally covers a liquid filled cavity, this side is named "apical side or lumen side"; the opposite surface which is usually in contact with the underlying blood vessels is named "baso-lateral or blood side". The permeability characteristics of the two surfaces are different; each of the membranes contains different channels for diffusion and different transport proteins for mediated transport. This difference results in the fact that substances can undergo a dis-

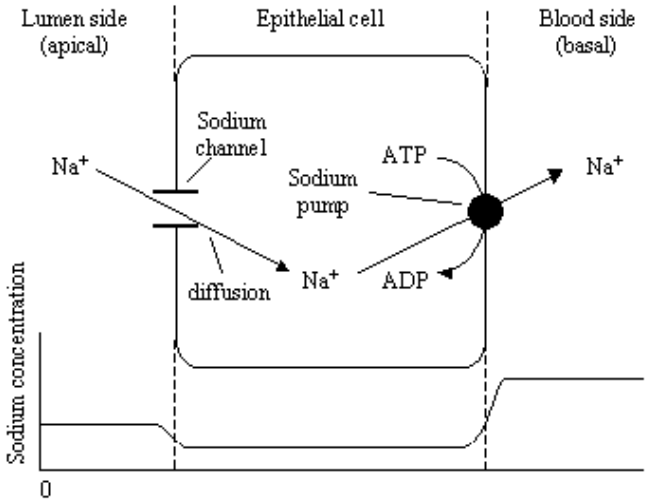

Figure 1.2: Drawing model showing the active transport through epithelial layers (modified from [11]). The transepithelial transport of sodium involves diffusion through channels for a surface followed by active transport through the opposite surface to the outside of the cell.

placement from an area of low concentration on one side of the epithelium to an area of higher concentration on the other side; in other words, substances can undergo an active transport through the epithelial cell layer. Examples of these active transport epithelial processes are the followings: absorption of substances from the gastro-intestinal tube to the blood, secretion of salts and liquids by different glands. Figure 1.2 shows an example of active epithelial transport, the absorption of Na^+. The sodium is actively transported through most of the epithelial surfaces; during the absorption processes, a net sodium movement is occurring from low concentration regions on the lumen side to the high concentration regions on the blood side, and in the opposite way during secretion. The displacement of sodium from the lumen side to the epithelial cell takes place by diffusion through a sodium channel in the lumen membrane. The diffusion takes place into the cell because the intracellular sodium concentration is maintained at a lower level by the active transport of sodium through the plasmic membrane on the surface of the blood side of the cell. All of the Na, K pumps are situated in the blood side membrane of the cell. The sodium concentration in the extracellular liquid of the blood side is much higher than in the cytosol and can even be higher than on the lumen side. It must be said that even when sodium concentrations are the same

on both side of the epithelium, there still is a sodium displacement from the lumen to the blood side (sodium absorption).

1.1.2 CLINICAL RELEVANCE

In the 1950s and 1960s, several inherited diseases of the fluid and electrolyte metabolism were described, in which the principal problem appeared to be a specific functional defect in the renal tubule [12]. In the past ten years, genetic and molecular approaches have elucidated the underlying molecular defects in several of these diseases. However, further questions were raised about the physiology of epithelial functioning. In several cases, the discovery of the molecular defect in a rare Mendelian disorder has provided important insights into complex traits, such as hypertension and hypercalciuria. A variety of inherited disorders alter specific renal epithelial transport functions such as the Liddle syndrome [12] and the pseudohypoaldosteronism type I [13], which are both induced by an epithelial sodium channel dysfunction.

The excretion of sodium and chloride by the skin or the digestive tract is usually very low, but it can significantly rise during untimely sweating, diarrhoea or vomiting. A bleeding can of course lead to big losses of water and salt. The renal sodium, chloride and water excretion control therefore consist of the most important mechanism for homeostatic regulation of those ions and water. With our biosystem, we will characterise the ionic transport properties of such cell layers, more specifically the sodium transport through the epithelial cell sodium channels [14].

1.1.3 EPITHELIAL CELL CULTURE

In an epithelial cell tissue growth experiment, tissue samples are removed from sacrificial animals, cells are dissociated, treated to avoid infection, and placed under culture conditions (plastic dish or different cell culture chambers with nutritive solution and controlled conditions such as temperature, atmosphere, etc.). Cell cultures can then be realised from two types of cell suspensions: the primary culture which is realised directly from the cells of removed tissues, and culture from cell lines (cells often treated such as to multiply almost indefinitely, which can be frozen for conservation and defrosted for taking a sample of cells for culture). However, certain cells, particularly the epithelial cells, are not adapted to a suspension type of culture and need a solid substrate on which they can grow and multiply. These substrates are usually the bottom of a cell culture chamber or a porous membrane. The cells in suspension in the physiological solution progressively fall on the membrane and adhere to it. They grow and multiply until they

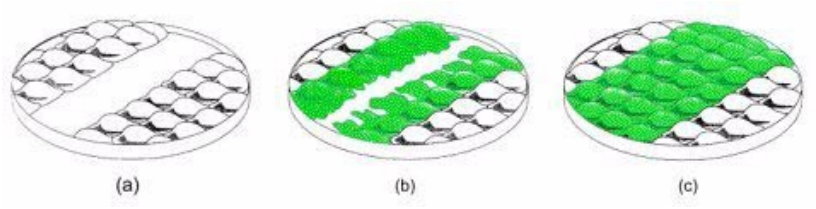

Figure 1.3: Diagram showing the contact inhibition principle [15]: When a tissue is positioned on the membrane edge (a), the cells near the tear start growing and dividing (b), until the layer is completed (c), then the cell proliferation ends.

get in touch with neighbouring cells: it's the contact inhibition principle shown in figure 1.3.

Cell culture is performed in an incubator, where the temperature is maintained at 37 °C, a 95/5% O_2/CO_2 atmosphere and saturated with water. The physiological solution used in the culture chambers is often the following:

Compound	Molarity
NaCl	0.12 M
KCL	5 mM
$NaHCO_3$	25 mM
Na-Pyruvate	1 mM
Na-Phosphate	0.9 mM
D-Glucose	10 mM
$MgCl_2$	1 mM
$CaCl_2$	1.8 mM

Table 1.1:Physiological solution composition

1.2 HOW TO MEASURE EPITHELIAL TRANSPORT

1.2.1 ELECTRICAL TRANSPORT

A valuable tool in epithelial transport studies for “tight” epithelia is the short-circuit technique [16]. In this procedure the spontaneous potential difference produced across an epithelium by ionic currents is reduced to zero with the aid of an external electrical circuit, while the current flowing through this circuit and the tissue preparation is recorded simultaneously (short-circuit current). If this is done with identical liquid solutions on both sides of the tissue, it is clear that there is neither a potential gradient nor a concentration gradient for any of the molecular species present in the solution. Any current measured must therefore originate from active transport of ions. When unidirectional ionic fluxes of sodium are measured (using radioactive labels) under short-circuit conditions, it becomes evident that the net flux of sodium alone accounts for the short-circuit current through the tissue. The net flux of chloride under these conditions (115 mM Cl^- on both sides) is virtually zero [10].

In order to use this short-circuit technique, the evolution in time of two electrical parameters has to be measured:

- the transepithelial resistance Rte: by following the time evolution of transepithelial resistance Rte, one can know at what time (after how many days of culture) the epithelial cell monolayer is completed, as the resistance comes to a plateau (maturation process).

- the transepithelial voltage Vte: as previously explained, because of identical solutions on the two sides of the tissue, there is no potential gradient in the solution. Hence, the spontaneous potential difference is a consequence of the net sodium flux.

1.2.2 RADIOACTIVITY AND FLUORESCENCE MEASUREMENTS

For measuring other epithelial cell properties than the ion transport, such as transport and diffusion of biological or pharmacological molecules through the cell layer, radioactivity and fluorescence measurements can be performed. After marking molecules on one side of the epithelial cell layer with radioactivity or fluorescence, on can follow the transport of these molecules through the cell layer by collecting the entire solution on the other side of the membrane after experience, and analysing this solution.

1.3 ELECTRICAL CHARACTERISATION OF BIOLOGICAL TISSUES: STATE OF THE ART

The results detailed in this chapter represent an overview of what has been done in the field of electrical characterisation of various types of biological entities, such as living bodies, tissues and single cells. The "macro-scale" commercially available systems for electrically characterising cell tissues will first be listed. A non-exhaustive list of impedance measuring systems will be mentioned as well as microsystems for characterising tissues or cells using impedance or conductometric techniques.

1.3.1 "MACRO SCALE" COMMERCIAL SYSTEMS FOR CULTURE AND CHARACTERISATION OF EPITHELIAL TISSUES

- Figure 1.4 shows the commercial tissue culture multi-well plates that can be found from different companies [7, 8]. The culture substrate can be of different synthetic material such as polycarbonate.

- The EVOM™ was the first instrument designed to perform routine Trans Epithelial Electric Resistance (TEER) measurements in tissue culture research [17]. TEER measurements are now universally established as a non destructive and reliable method to monitor the *in vitro* growth of

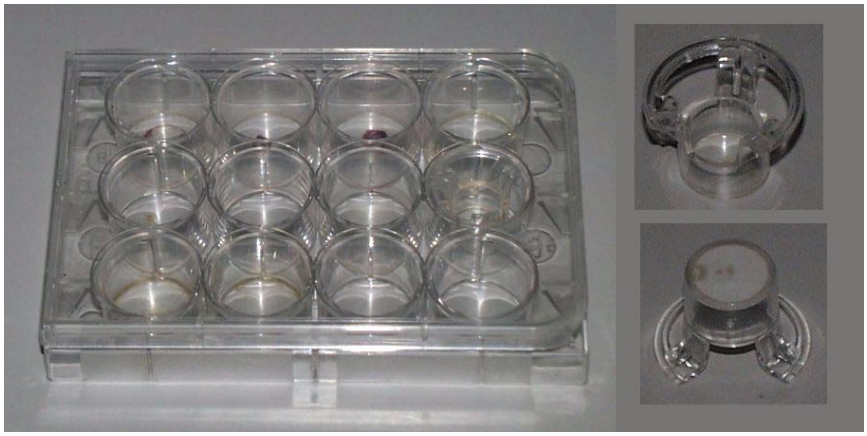

Figure 1.4: Photographs of multi-well plates and adapted culture cups with cell culture substrates.

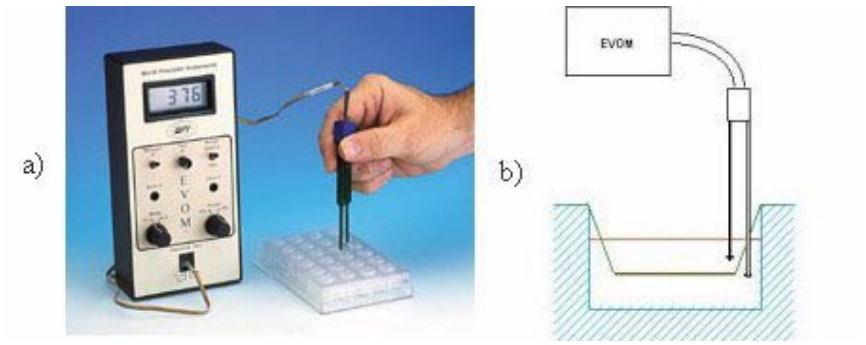

Figure 1.5: a) Photograph of the EVOM™ instrument and electrode system from WPI Inc. [17] b) Principle-of-use schematic of the STX2 electrodes system.

epithelial and endothelial tissue cultures. The confluence of the cellular monolayer during growth is easily determined by a sharp increase in TEER, detected using a four-point (at 12.5 Hz) electronic circuit of EVOM™ and STX2 electrodes shown in figure 1.5. The STX2 electrodes consist of a fixed pair of double electrodes, 4 mm wide and 1 mm thick. Each stick of the electrode pair contains a silver/silver-chloride pellet for measuring voltage and a silver electrode for passing current. The small size of each electrode is designed to facilitate placement of the electrodes into cell culture wells. STX2 can be used with all tissue culture inserts currently on the market. The problems with this system are the minimum culture surface size which is of 6 mm in diameter, the non-reproducibility in TEER measurements due to the manual insertion of the electrodes and contamination as an external part (the electrodes) has to be inserted in the solution everyday.

- Figure 1.6 shows the Endohm™ chambers that can provide more reproducible resistance measurements of endothelial tissues (minimum diameter size of 6 mm). Culture cups are transferred from their culture wells to the Endohm™ chamber for measurement rather than using hand-held electrodes. The chamber and the cap each contains a pair of concentric electrodes: a voltage-sensing silver/silver chloride pellet in the centre and an annular current electrode made of medical grade stainless steel. The height of the top electrode can be adjusted to fit cell culture cups of different manufactures. The reproducibility of the measurements is improved compared to the STX2 electrode system, but the

Figure 1.6: Photograph of the Endohm™ chambers from WPI Inc. [17].

manipulation of cell culture cups is tedious and still contamination problems can occur.

- The REMS AutoSampler shown in figure 1.7, automates measurements of electrical resistance of transepithelial, transendothelial or Caco-2 cell membranes being grown to confluence on microporous filters of high throughput screening (HTS) 24 well microplates. It is a PC-controlled, tissue resistance measurement system that offers reproducibility, accuracy, flexibility and ease of operation for this kind of measurement. Automated measurements of tissue resistance in cell culture microplates

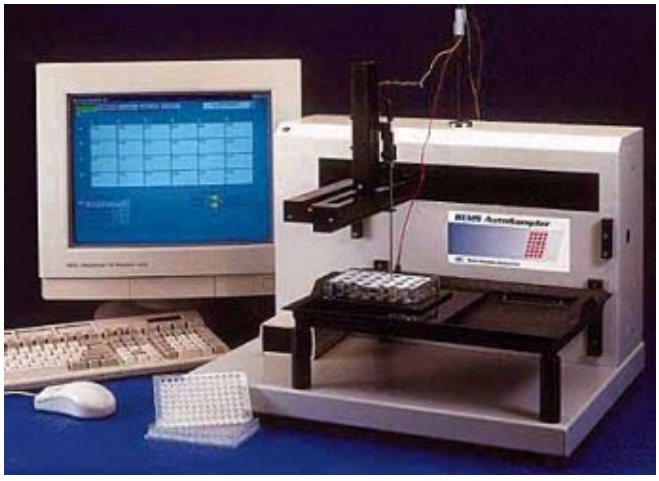

Figure 1.7: Photograph of the REMS AutoSampler *from WPI Inc.*

provide the important advantages of speed, precision, decreased probability for contamination and the instant availability of measured resistance data on a computer. These measurements are useful in applications such as drug bioavailability studies and studies on the mechanisms of drug transport. The minimum culture surface size (6 mm in diameter), is still a problem, as well as the cost of the AutoSampler.

1.3.2 BIOLOGICAL IMPEDANCE MEASUREMENTS ON LIVING SINGLE CELLS OR TISSUES

- Skin, body and blood impedance or conductometric measurements using simple and compound electrodes: One example is the impedance plethysmography. The technique consists of a non-invasive measurement that measures the change in blood volume for a specific body segment. As the blood volume changes, the electrical impedance also changes. However the skin-electrode impedance instability is a problem and is studied in [18-20]. Other physiological events, causing changes in dimension, dielectric properties or conductivity can be measured using non-invasive impedance techniques applied to the human body [21]. Another example is the electrical conductivity of blood measurement [22]. The conductivity of blood is an important quantity, as it influences the measurement results of various methods used in the study of heart and circulation research (such as the above mentioned impedance plethysmography).

- The membrane patch-clamp measurement technique (for single cells) [3, 23, 24] was developed in the late 70's by Erwin Neher and Bert Sakmann (Nobel Price 1991). The principle of this method is to isolate a patch of membrane electrically from the external solution and to record current flowing into the patch, to monitor ionic membrane channels. This is achieved by pressing a fire polished glass pipette with an internal Ag/ AgCl wire electrode, which has been filled with a suitable electrolyte solution, against the surface of a cell and applying light suction. The glass pipette consists of a capillary tube with a small open tip. In general, they are made by pulling a glass capillary with high softening point to a diameter smaller than 0.5 μm at the tip. A high electrical sealing resistance of more than 10 GΩ can then be formed. This giga-seal is needed for electrical isolation. Figure 1.8 summarizes the main modes of giga-seal recordings. This method needs an important set-up, including a good microscope with an x-y stage and substantial high input resistance amplifiers for the recordings. There is a serious interest in achieving this

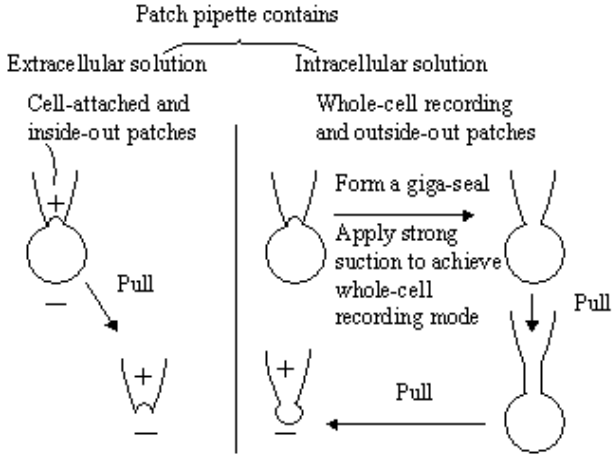

Figure 1.8: Diagram illustrating the method of making cell attached and inside-out patches, and whole cell and outside-out patches [24].

patch clamp method on-chip and considerable progress in this direction is made [25].

1.3.3 MINIATURISED ELECTRICAL SYSTEMS FOR BIOLOGICAL APPLICATIONS

The main advantages of miniaturising systems for chemical or biological analysis are the following:

- decrease of the analysis time due to smaller volumes in channels and reaction chambers, hence a higher interaction rate between analytes, solutes, electrodes and surfaces.
- decrease of analytes, reactants and solutes quantities.
- large possible number analysis in parallel.
- possibility of integrating numerous features on one device such as a coupling of separation, sensing and analysis.
- batch fabrication processes.
- cost reduction.
- ease of handling of microscale object (cells, all kinds of molecules).

- Cell sorting or counting:
  - The Coulter counter method of counting and determining size of particles is based on measurable changes in electrical resistance produced by non-conductive particles suspended in an electrolyte. Some examples of realised microchips using this principle can be found in references [26-31].
  - The precise positioning of cells on sensor microstructures is a major problem when using cells in biosensors and test systems. A method for hydrodynamic positioning of cells on substrates with electrically contacted micro electrodes is presented in references [32, 33].

- Separation methods: microfabricated devices have been demonstrated for capillary electrophoresis, synchronized cyclic electrophoresis, free flow electrophoresis, and open channel electrochromatography [34-37].

- Cell culture and neuronal network bio-electrical signal recording systems:
  - Impedance analysis of epithelial and endothelial cell monolayer cultures on gold surfaces has been demonstrated [38]. This study describes a new method to determine transepithelial and transendothelial electrical resistance (TEER) of culture cell monolayers. Cells are cultured on a microscope glass slide covered with gold electrodes. This method enables TEER measurements using a considerable set-up for impedance spectroscopy, but no transport through the cell monolayer can be measured. It is therefore a useful, but incomplete, tool.
  - Multi-electrode arrays (MEA) are used for extracellular measurements of neural activity. The external electrodes sense the outside electrical field around the cells and thereby measure the potential changes of cell membranes. Simultaneous monitoring of several cells in culture is possible, thus enabling the study of cell conductivity in the cell network. MEA devices consist of a biocompatible culture chamber with planar electrodes deposited on the substrate. The tissues can be laid in the chamber and kept alive during measurement. Most realised structures are based on a regular matrix design [39-45].

- Conductivity sensors: different microsystems where conductivity measurements are the basis for the characterisation of the biological

tissues, have been developed [46-49]. A commonly used design is the interdigitated electrode structure. However, a major problem encountered when miniaturising conductivity cells is the overwhelming influence of the double-layer capacitance between the metal electrode and the cell solution (see also chapter 3.1). The use of four-electrode structures is an elegant method to overcome this problem.

1.4 CONCLUSION

In this chapter, the importance of physiological measurements on epithelial cells was underlined, granting the need of further development of the existing epithelial cell culture and characterisation systems, especially for the study of scare epithelial cells. The evolution of microfabrication technologies and materials for integrating several functions on a microsystem (MEMS and μTAS) shows the potentiality of miniaturised biosystems for culture and electrical and/or optical characterisation.

2 BIOSYSTEM DESIGN AND FABRICATION

When developing a new system for a specific application, one needs to be aware of the essential requirements in order to realise the simplest possible operational system. In our case, biocompatibility is perhaps the most important consideration, as the epithelial cells need to be in a favourable environment to be maintained alive, but even more, to be able to grow and divide.

2.1 DEFINITION OF REQUIRED FEATURES

2.1.1 RESTATEMENT OF THE APPLICATION

1) Epithelial cell culture device: epithelial cell suspensions are to be introduced in the microsystem and have to demonstrate growth and division as to form a cell monolayer on a substrate.

2) Electrical characterisation: the transepithelial electrical resistance (TEER or Rte) has to be monitored to reveal the moment when the monolayer formation is terminated. The transepithelial current (TEC or Ite) has to be measured during and after formation of the cell layer, so that characterisation of the transport of biological or pharmacological molecules and diffusion through the cell layer, or sodium transport through the epithelial cell sodium channel, can be monitored.

2.1.2 BIOSYSTEM REQUIREMENTS

No electrical source or instrument, as well as no temperature, humidity or partial CO_2 pressure control system, is integrated in the device. The device is aimed to be used in an incubator controlling those parameters, and is to be connected to adequate instruments for electrical characterisation.

- Biocompatibility: to suit the first point of paragraph 2.1.1, all the surfaces in contact with the cells and the physiological solution have to be

biocompatible. This includes the substrate, electrodes, chamber housing, adhesives, sealants, tubing and covers. Biocompatibility can be expressed at different levels, depend on the application. In our device, cells need to be cultured for a period between 5 and 10 days and then kept alive for a few more days to allow characterisation of the desired property. It means that the materials in contact with the cells or physiological solution do not have any toxic, harmful, or other damaging effect to the biological function. The cells need to be kept alive with all their biological function effective, as in their usual environment.

- "User-friendliness": not to be forgotten is the fact that this device has to be used by biologists or laboratory assistants who need a device which is easy to manipulate. Therefore, the microchambers have to be provided with all the required elements for maintaining culture, such as a direct access for sample introduction, a system enabling the renewal of culturing solution, the administration of growth factors, hormones and drug substances. The biosystem also needs a packaging, facilitating insertion of the cell culture system into the measurement electronics while protecting the living system from the external environment. Therefore, it needs to have external electrical ports for collecting data that can be easily connected to. Altogether, everything has to be of easy use to avoid cell function perturbation by manipulations.

- Environment resistance: the microsystem will stay a minimum of 5 days in the incubator. Therefore, it has to be able to resist to a particular environment, such as temperature (37°C), partial CO_2 and O_2 pressures, and humidity (95%). It also has to resist to transepithelial hydraulic pressures during the culturing solutions replacement, as well as the sterilisation process (temperature of 110°C and humidity).

- Electrical characterisation method: for both applications, i.e. the characterisation of biological or pharmacological molecules transport and diffusion through the cell layer, or sodium transport through the epithelial cell sodium channel, we want to measure the trans-epithelial tissue resistance Rte and trans-epithelial current (Ite) or voltage (Vte). Hence, we need electrodes on both sides of the cell monolayer. For the characterisation of sodium transport through the epithelial cell sodium channel, we could use a non-permeable substrate with deposited electrodes for the cell monolayer and the other electrodes on top of the cells. But for the study of molecular transport, we need to be able to collect the solution from either side of the cell layer. Consequently, the

substrate has to be permeable. As for the commercial systems presented in figure 1.4, a standard biocompatible nano-porous (0.2 to 2 µm of diameter pores) polycarbonate cell culture substrate can be used. This implies that there will be an upper chamber above and a lower chamber beneath the cell monolayer on a porous membrane, each compartment containing its electrodes. Concerning the impedance measurement method, a two-electrode or a four-electrode system can be chosen, which will be discussed later on.

- Low cost: of course, as in any project, the device needs to be the cheapest possible. If not considering the development costs (we are in an academic project) but just the fabrication costs, one has to minimise the fabrication steps and use the cheapest possible materials. The choice of thin film deposited electrodes is obvious, as reproducible measurements are required, thus we will work with pre-positioned and integrated electrodes. The work in a clean room is known as being expensive, but it has its advantages. When working in a clean room, a so called batch process can be elaborated, that is to say, a fabrication process is developed and can then be reproducibly applied to many wafers in parallel or in series. If several devices or parts of the device are on each wafer, the fabrication costs in clean room will greatly decrease. The etching of channels and vias can be realised by microfabrication technologies in a clean room [9, 50, 51], but can as well be done by alternative etching techniques, such as to decrease the clean room working time. A capital choice for costs reduction is the way the microsystems will be used: a re-usable device is of course a nice solution in the sense that several cell culture experiments can be realised with the same device. The problem will then be in the degree of user-friendliness. The device needs to be easy cleanable and re-sterilisable between two experiments with no changes of biocompatibility and characterisation elements. Another possibility is to realise a disposable device (for single use). This needs to be fabricated with very few processing steps and low cost materials.

2.2 DESIGN AND FABRICATION

The design choices of materials and fabrication methods are in fact not decoupled. They are dependant on one another in the sense that a certain design will influence the choice of a material and a corresponding fabrication method and, inversely, using certain fabrication technologies will pose limiting factors on materials and design. Anyway, as we want to realise a miniaturised device, we

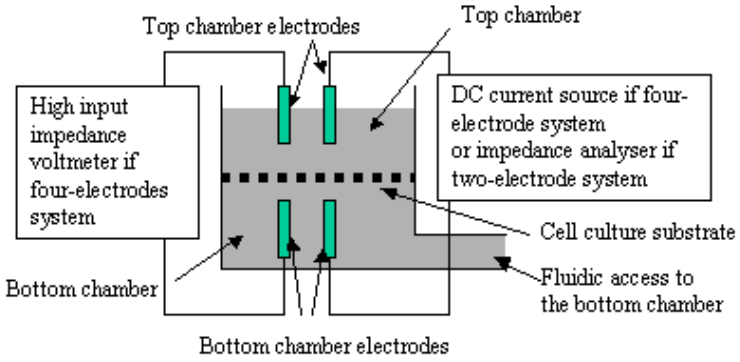

Figure 2.1: Functional schematic of the desired biosystem.

know that some parts of the device will be machined with microfabrication technologies [9, 50, 51].

2.2.1 DESIGN

For choosing an adequate design for our microsystem for culture and electrical characterisation of epithelial tissues, a functional schematic based on the defined requirements of the preceding section can be defined as shown in figure 2.1. The basic design is a porous membrane cell culture substrate, separating two physiological solution chambers. The top chamber has a direct access to the membrane and the bottom chamber has fluidic connections for solution renewal or sample collecting. One or two pairs of electrodes are positioned on either side of the membrane, depending on the chosen impedance measurement method. Each electrode must have external electrical connectors for connection to measurement instruments.

We want to have a device with multiple cell culture sites to enable multiple tissue culture and characterisation in uniform conditions. We have chosen for four culture sites on one device, a number which can be increased further when needed.

We have chosen different chamber configurations:

- Each culture site with its own top and bottom chamber.
- Common bottom chamber.
- Common top chamber.

We have also chosen different geometrical designs:

- Linear shape design with cell culture sites distributed on one line.
- Square shape design with cell culture sites distributed on a square.

We have also tried different device approaches:

- Disposable device (for single use).
- Modular device (with re-usable parts and removable parts).

2.2.2 FABRICATION TECHNOLOGIES

Most of today's microfabrication technologies [9, 50, 51] are available at the EPFL centre of microtechnology (CMI), which consists of several class 100 clean rooms. Used techniques include photolithographic processes, various etching techniques such as wet chemical etching, dry chemical or physical etching, metallic or oxide deposition, high temperature oxidation and nitridation, anodic bonding and all kinds of characterisation techniques (see appendix 1).

In a first design, silicon was chosen as substrate material for most of the microsystem's parts [52]. Therefore, many of the above mentioned microfabrication technologies have been used: photolithographic processes, deep plasma etching (Reactive Ion Etching (RIE)) for vertical side walls, KOH silicon etching for oblique side walls, metallic deposition, oxidation and anodic bonding. This means that most of the fabrication of the device is done in the clean room.

When changing the material of the device from silicon to glass, only the photolithographic process followed by a metal deposition step remains as clean room processing. We introduced powder-blasting as etching technology for the channels and vias in glass [53, 54].

For the device assembling after substrate dicing, a gluing technology was developed.

Finally, aluminium wire bonding was chosen to connect the thin films electrodes to copper tracks on printed circuit boards (PCB) using the Kulicke & Soffa© model 4123 wire bonder. A silicone protection and isolation layer (Dow Corning® 734 Flowable sealant) is added on the wires and connections pads.

2.2.3 MATERIALS

The most common materials used in MEMS are silicon, glass (floatglass, pyrex and quartz) and polymers (plastics, polyimide, silicone etc.). Most of them are biocompatible. As said before, the choice of materials is tighly bound to the fabrication technologies.

- Substrate (see also appendix 2):
  - A first design was done using silicon as principal substrate. Silicon is the base material for integrated circuits. Therefore, all the micromachining technologies for silicon are well developed and all kinds of designs can be realised. Yet there are two main drawbacks for our application. First, silicon is not an insulating material, hence it has to be oxidised in order to be used in impedometric applications. Secondly, silicon is not transparent, which prevents observation within micro-channels and cavities.
  - Pyrex was used for the first type of device as bottom layer, in order to enable backside observation of the device. Moreover, the anodic bonding technology for Pyrex and silicon is part of the standard microfabrication technologies.
  - The second and third generation of devices are essentially made of floatglass, which is a cheap standard glass type.

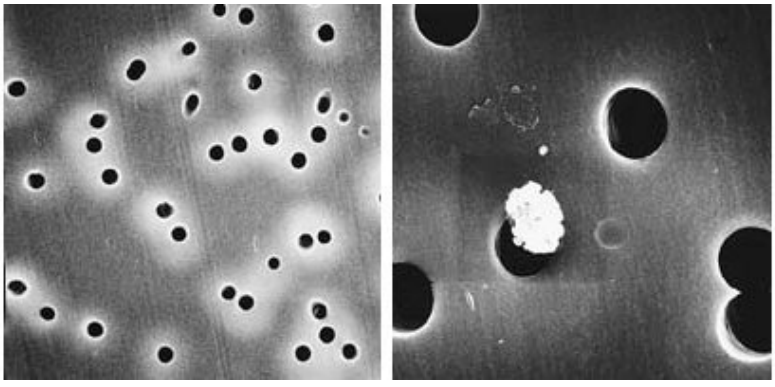

Figure 2.2: SEM photographs showing a porous polycarbonate membrane [55].

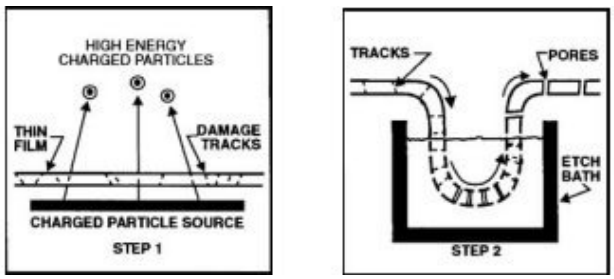

Figure 2.3: Schematics showing the polycarbonate membrane two-step fabrication process [55].

- Cell culture membrane:
  - We chose a standard cell culture substrate, which is a porous polycarbonate membrane shown in figure 2.2. Poretics® Polycarbonate (PC) Track-Etch screen membranes (PCTE)) [55] are biologically neutral, being neither cytotoxic nor bactericidal. Cells and bacteria will grow on PCTE membranes when proper nutrients are supplied. These membranes can be obtained with different pores sizes or densities. We again chose a quite standard type for epithelial cell culture, that is to say 0.4 µm pores and a pore density of 1×10^8 pores/cm^2. The fabrication of those membranes is done in a two-step process: In the first step, a thin PC film is exposed to ionizing radiation, forming damage tracks. In the second step, the tracks are preferentially etched out into pores by a strong alkaline solution (see figure 2.3).

- Physiological solution reservoirs:
  - We chose a two-part silicone elastomer, polydimethylsiloxane (PDMS) Sylgard® 184 that can be purchased from Dow Corning [8]. It can be used for encapsulating applications but is also well known as a biocompatible material, hence is often used in biological applications [56]. We decided to use it as a material for channels or reservoirs for physiological solution after moulding in plastic moulds.

- Electrode material:
  - We have tried different materials for realising the electrodes: Au, Pt, Ag and AgCl electrodes were used and characterised in terms of impedance and voltametric properties, adhesion and lifetime (see chapter 3).

- Glue:
  - We will need glue for the integration of the cell culture substrate within the device. As a first glue, we used Araldit® which is an epoxy glue. It is not known to be biocompatible, but this will be discussed in chapter 4.1. In further fabrication, a biocompatible silicone adhesive was used, the MED1-4213 from Polytec GmbH (Germany).

2.2.4 MEASUREMENT TECHNIQUE

As stated in section 2.1.1, the biosystem needs to be able to measure the transepithelial resistance Rte and the transepithelial current Ite:

- Transepithelial resistance Rte measurement:

  We have investigated different configurations, the two-point (two electrodes) impedance measurement technique and the four-point impedance measurement technique. A discussion about the drawbacks and advantages of each technique is given in section 3.2.

- Transepithelial current Ite measurement:

  The simplest way to measure the transepithelial current is to measure the potential difference across the cell monolayer and deduce the transepithelial current knowing the transepithelial resistance. The short-circuit technique detailed in section 1.2.1 can be used as well. The success of such measurements is based on the choice of adequate microelectrode material, showing no potential offset at Ite = 0. This choice will be discussed in section 3.3.

2.3 DEVICE TYPES

During this thesis, different generations of device have been designed and fabricated. Five of them will be presented here. They are given different names for better understanding: the silicon based device, the glass based device, the macro device, the linear device and the modular device. The evolution from one device to the next one as well as the improvements in performance will be discussed in chapter 3.

2.3.1 SILICON BASED DEVICE

Figure 2.4 shows a schematic cross-section of the basic silicon based tissue measurement structure [52]: it consists of an assembly of two micro-machined silicon wafers, with a nano-porous polycarbonate membrane glued in between. The surface of a single culture device (determined by the free area of the membrane) ranges between 1 and 4 mm^2. Before assembly, a two-electrode system, that is to say one top and one bottom Pt electrode (with a thin Ta film as adhesion layer) are micro-patterned on the upper silicon wafer (forming the top reservoir) and on the lower Pyrex wafer respectively. All the photolithographic masks have been designed with the CleWin 2.5 mask designer software from Delta Mask in the Netherlands (see appendix 7). They were then printed via a 3600 dpi printer on a transparent sheet, which is a very economic process as long as mask details are

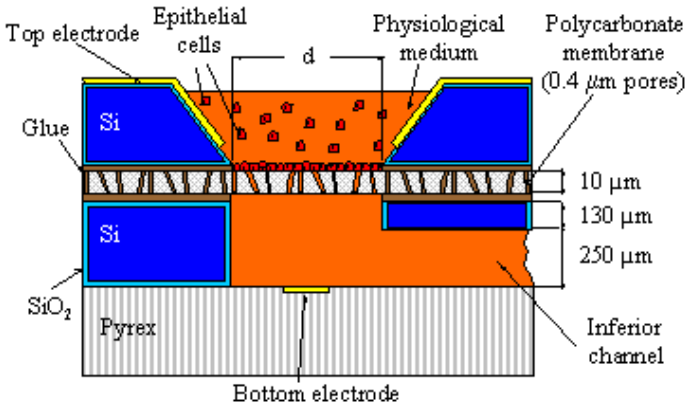

Figure 2.4: Schematic cross-section of the basic silicon based tissue measurement structure showing epithelial cell layer covered nano-porous membrane separating the top from the bottom reservoir.

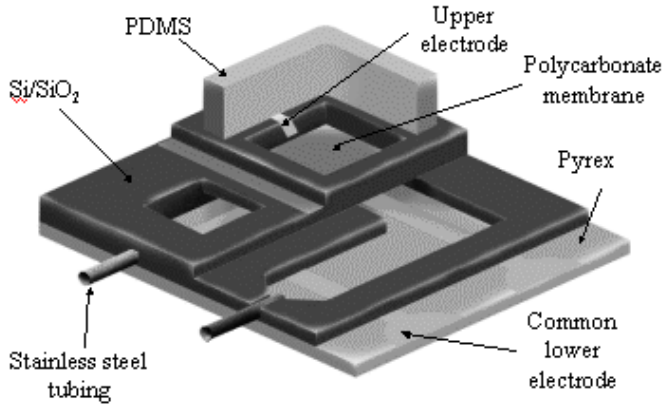

Figure 2.5: Artist impression, showing an oblique view of a partially sectioned device revealing the various patterned layers.

bigger than about 20 µm. This sheet can simply be scotched on a glass mask or reproduced on a chromblank (glass mask with a Cr layer and a photoresist layer on one side) for better manipulation and reproducibility. The basic silicon tissue measurement structure of figure 2.4 is repeated to form four separate and identical cell culture wells on one device. Figure 2.5 is an artist impression, showing an oblique view of a partially sectioned device revealing the various patterned layers. This figure clearly shows the external fluidic connections to the lower reservoir underneath the membrane, as well as a top removable reservoir, made out of Polydimethylsiloxane (PDMS) elastomer which is needed for providing a sufficiently large quantity of biological solution (withstanding evaporation) during the three days of the cell growth. The figure also shows the bottom electrodes in the lower micro-fluidic channel and the upper electrodes on the top wafer.

Figure 2.6 shows the batch process for the realisation of the silicon based tissue culture measuring device. Five lithographic masks are used for the whole processing sequence (see appendix 3). The fabrication technologies are deep plasma etching for the cell culture via and for the micro-fluidic channel in the lower silicon wafer, wet etching for the top silicon well, metallic thin film deposition, anodic bonding of a Pyrex glass wafer with the lower silicon wafer and, finally, an appropriate gluing procedure for sandwiching the polycarbonate membrane in between the two silicon wafers.

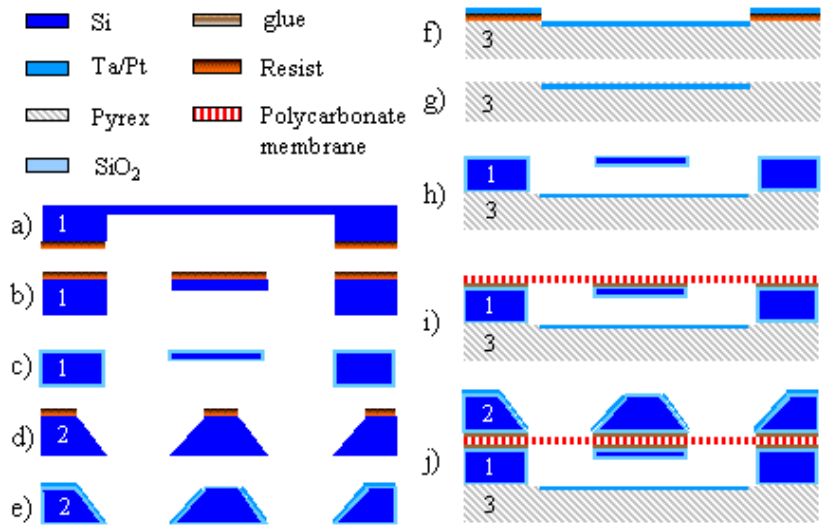

Figure 2.6: Batch process for the realisation of the silicon based tissue culture measuring device, using two silicon wafers (1,2) and one Pyrex wafer (3).

We start with a 380 µm thick 4" (100) silicon wafer with a resistivity of 0.3 Ω cm, on which we structure a photoresist mask for the dry etching of the vias and micro-fluidic channels in the lower silicon wafer (denoted by 1 in figure 2.6). We used a SF_6 deep plasma etch, combined with a C_4F_8 sidewall passivation process in a RIE reactor, resulting in vertical etch profiles and etch rates of about 5 µm/min. (fig. 2.6a and b). The same kind of silicon wafer (denoted by 2 in figure 2.6) is used as top substrate for the etching of the wells in a classical KOH solution in order to obtain oblique sidewalls (fig. 2.6d). After a thermal oxidation step giving rise to an oxide thickness of about 0.5 µm on every outer silicon surface, including the via, well and the micro-fluidic channel (fig. 2.6c), the top Ta/Pt electrodes (typically 20/200 nm) are sputtered through a shadow mask. The electrical contacts on the Pyrex wafer (denoted by 3 in figure 2.6) are realised using a lift-off process (fig. 2.6f, g). However, prior to the Ta/Pt deposition, we use the lift-off stencil to etch a 0.5 µm deep recess in which the Ta/Pt contacts will be buried (fig. 2.6f). This procedure gives rise to a flat top wafer surface, which lends itself excellently to an anodic bonding assembly with the top silicon wafer (fig. 2.6h). Figure 2.6i represents the gluing of the nano-porous membrane on the structure of figure

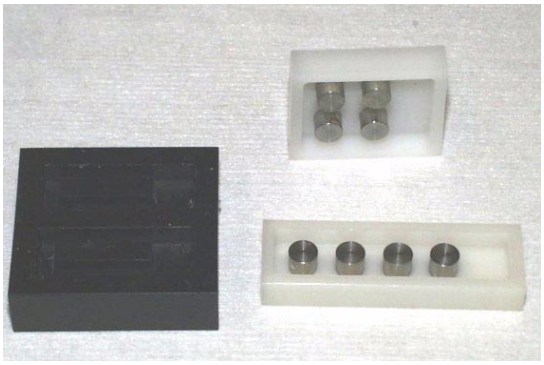

Figure 2.7: Photograph of different POM moulds for top PDMS reservoirs.

2.6h. The structure is completed by gluing the structured silicon wafer of figure 2.6d on top of the membrane, forming the upper reservoirs. One can add an additional polydimethylsiloxane (PDMS) top reservoir to avoid physiological solution evaporation (represented on figure 2.5). This reservoir is realised by moulding (see appendix 4) in a machined plastic mould (Polyoxymethylene (POM)). Figure 2.7 shows examples of POM moulds.

One of the most critical steps for the fabrication of the tissue culture measurement device is the polycarbonate (PC) membrane gluing. The whole difficulty lies in the fact that the polycarbonate membrane has to remain free of glue on each of the cell culturing sites. The method used is schematically shown in figure 2.8. It consists of applying an ultra-thin layer of liquid glue (Araldit®) on a paraffin foil using a rolling procedure and bringing it into contact with the part of the

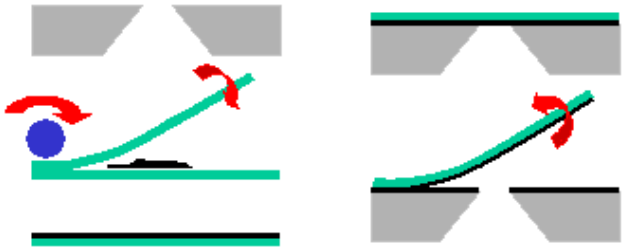

Figure 2.8: Schematic of the gluing procedure chosen to obtain a membrane free of glue.

device on which the membrane has to be glued. By carefully lifting the paraffin foil, a smooth and thin (~1 µm) gluing layer is left on the surface. The gluing procedure appeared to be very critical in the fabrication process; when the gluing layer is not sufficiently thin, small residues of glue tend to spread on the polycarbonate membrane, thereby filling the nano-pores and preventing later cell culture at such site. Evidently, when the nano-porous membrane surface is partially covered with glue, this will result in an arbitrary and variable enhancement of the measured perpendicular resistance. This would be an additional origin in a spread of resistance values of grown cell layers during later device applications. For experiments with grown cell layers, we have used only devices with a nano-porous membrane fixed using our special gluing procedure and, hence, completely free of residual glue on the membrane.

Figure 2.9 shows photographs of a finalised silicon based device. One can observe the fluidic and electrical external connectors, as well as the PDMS moulded top reservoir. The culture sites have a surface of 4 mm^2 and just one top electrode per site (the system uses a two electrode set-up). The PCB has a large through-hole (figure 2.9b), allowing the possibility of backside observation.

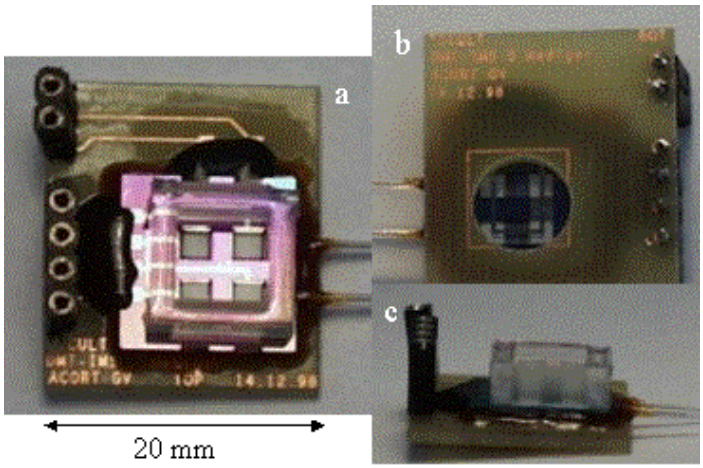

Figure 2.9: Optical photographs showing a finalised silicon based device: a) top view showing a PCB mounted device with fluidic and electrical connectors and the top PDMS reservoir. b) backside of a device. c) side view of a device.

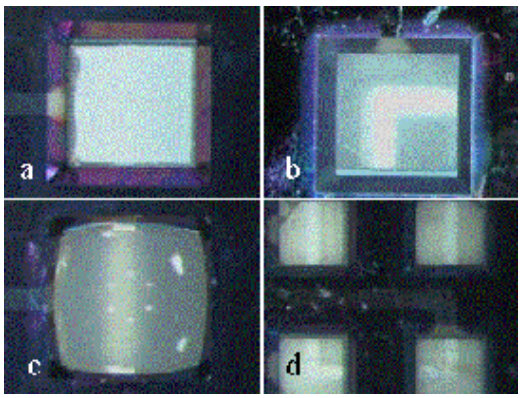

Figure 2.10: Optical photographs showing frontsides of silicon based devices: a) a glue-free dry culture site with top KOH etched well and integrated top electrode. b) a membrane being wetted, one can see the bottom electrode through it. c) physiological solution starting to pass though the membrane and filling the top reservoir. d) four culture sites with wet membranes, one can observe the bottom electrode.

Figure 2.10 shows different optical photographs of one or four culture sites. One can see that if the PC membrane is in the dry state, it becomes quite transparent when wetted. Figures 2.11 a and b are backside pictures of the silicon based devices. The common bottom electrode in the bottom channel can be seen as well as a dry etched input channel for fluidic connection.

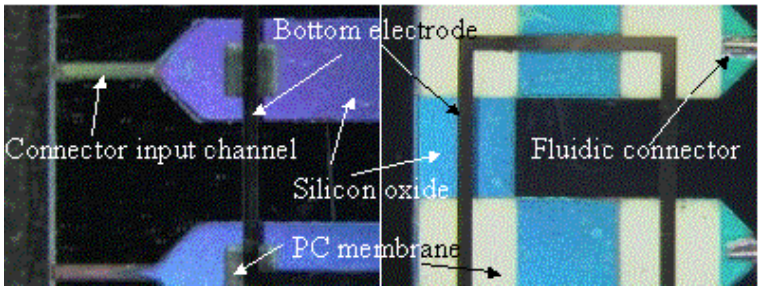

Figure 2.11: Optical photographs showing the backside of the silicon based device through the Pyrex layer. The left hand photograph shows a 1 mm^2 culture site and the photograph on the right hand side shows 4 mm^2 culture sites.

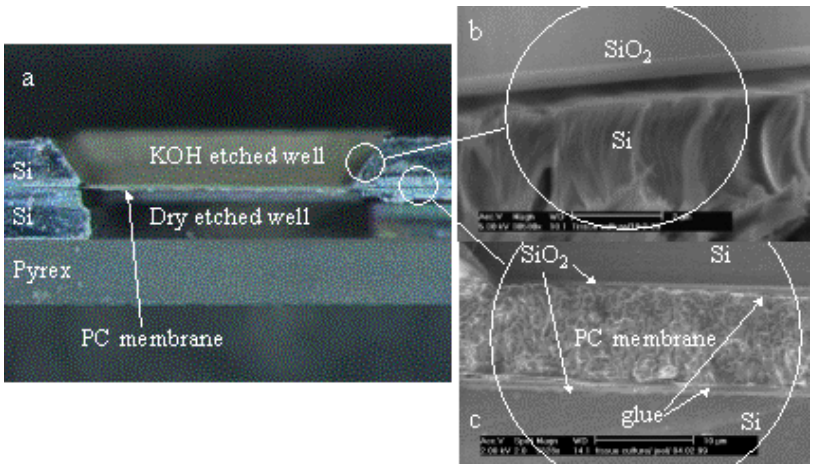

Figure 2.12: a) Optical photograph showing the three layers of the silicon based device and the sandwiched polycarbonate membrane. b) SEM photograph showing the 0.6 µm silicon oxide layer on silicon. c) SEM photograph showing the PC membrane sandwiched between the two silicon layers. One can see the 1 µm thick glue layer as well as the silicon oxide layer.

Figure 2.12a is a cross-section of a diced silicon based device where the three substrates and the PC membrane can be seen. Figures 2.12b and 2.12c are enlargements of figure 2.12a of, the oxide layer on silicon and the glued PC membrane in between two silicon wafers, respectively.

Figure 2.13 exposes the gluing problem. One can see the difference between a PC membrane with diffused glue filling up the pores and a membrane free of glue. On the SEM photograph of figure 2.13b, pores can hardly be seen as they are completely filled up with diffused glue. This can be avoided by using the gluing method described before and by using a glue with an adequate viscosity to avoid diffusion on the membrane.

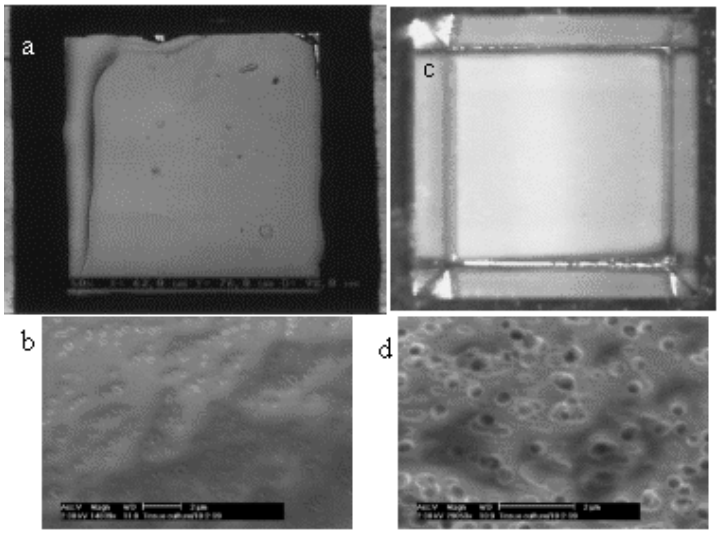

Figure 2.13: a) Optical photograph showing a PC membrane with diffused glue. b) SEM photograph of a PC membrane with glue filling up the pores. c) Optical photograph showing a glue-free PC membrane. d) SEM photograph of a PC membrane with glue-free pores.

2.3.2 GLASS BASED DEVICE

Realising a device with just floatglass wafers and no silicon highly reduces the clean room fabrication steps. On the other hand, for the etching of vias and channels, we have to introduce a new etching technology, the powder-blasting technology [53, 54]. The powder-blasting etching process is based on the erosion of brittle materials (such as glass, silicon or ceramics) due to multiple impacts of accelerated 30 micrometer size alumina particles (Al_2O_3), projected in an air flux through a nozzle. Figure 2.14 shows a schematic view of the cracks generated by an indenting particle. The etching procedures were performed using a Texas Airsonics abrasive jet machine, type HP-2. In this apparatus, the powder is dosed by a vibration feeder in an air flow and transported to a nozzle. Selective erosion can be performed by positioning a wax sealed metallic mask (thickness of 0.5 mm) (see appendix 6) on the substrate in order to realise patterned microstructures of various shapes and sizes varying from 50 µm up to 3 mm. The whole surface of the substrate is uniformly exposed to the powder beam by using two translation stages: one for the substrate which can move along the x-axis and a second one for the nozzle which moves along the y-axis (see appendix 5). Powder-blasting

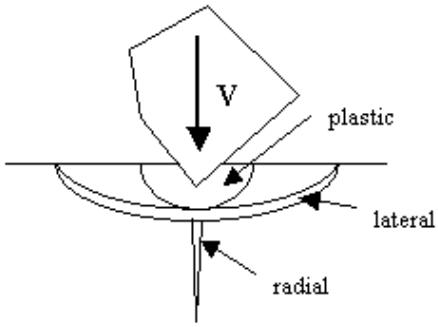

Figure 2.14: Schematic view of the cracks generated by an indenting particle (modified from [53]).

parameters used for etching glass wafers during this thesis are presented in appendix 5.

Figure 2.15 shows a schematic cross-section of the basic glass based tissue measurement structure [52]: it consists of an assembly of two micro-machined floatglass wafers, with a nano-porous polycarbonate membrane glued in between.

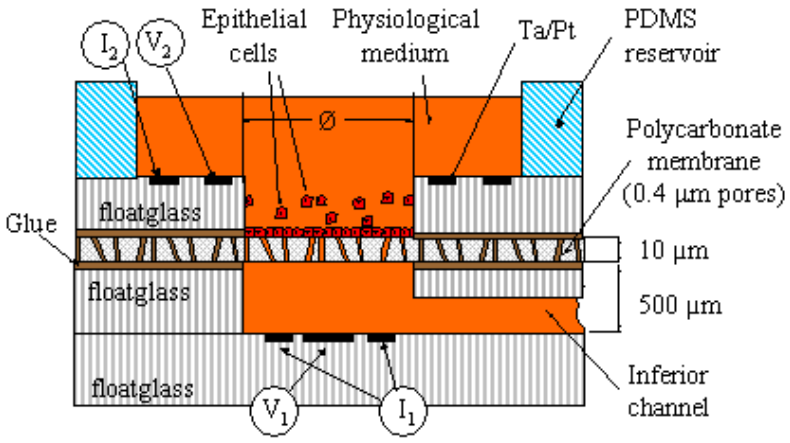

Figure 2.15: Schematic cross-section of the basic glass based tissue measurement structure, showing an epithelial cell layer covered nano-porous membrane separating the top from the bottom reservoir.

Compared to the silicon based device, a four-electrode system is introduced [4]. Figure 2.16 shows the batch process for the realisation of the glass based device. The sequence is similar to the one used for the silicon based device. The plasma and KOH etching procedures are replaced by a powder-blasting erosion process using metallic contact masks. The various structured layers are bonded simply by gluing.

We start with a 530 µm thick 3" floatglass wafer (denoted by 1), on which we pattern a channel and in- and outlet vias using powder-blasting through a metal contact mask (fig. 2.16a, b). The top and bottom Ta/Pt electrodes are then realised by sputtering on two other floatglass wafers (denoted by 2 and 3) using a lift-off process (fig. 2.16c, d and e). The glass wafer of figure 2.16e (which will be the wafer containing the top electrical contacts of our device) is powder-blasted through a metallic mask, and will later form the top cell culture chambers (fig. 2.16f). The same gluing technology as for the silicon based device is then used to glue the bottom wafer to the glass wafer containing the channels of figure 2.16d (fig. 2.16g). The nano-porous membrane and the top glass wafer are as well glued with the same gluing technology to obtain the finalised device (fig. 2.16h, i).

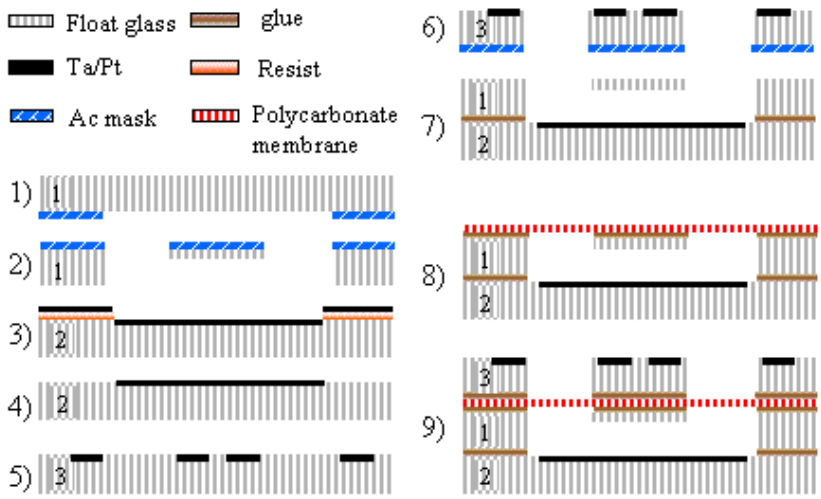

Figure 2.16: Batch process for the realisation of the glass based tissue culture measuring device using floatglass substrates.

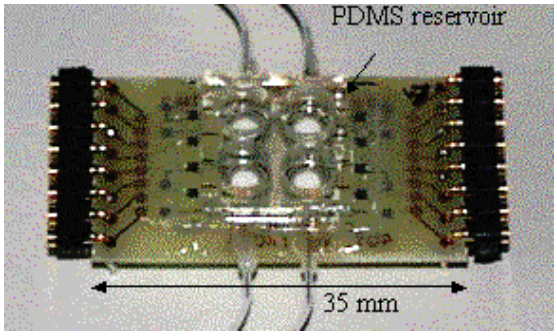

Figure 2.17: Optical photograph showing a completed glass based device

Figure 2.17 shows a completed glass based device. One can observe the four culture sites with fluidic and electrical external connection. The back and the side view of the device are shown in figure 2.18 a and b respectively. As for the silicon based device, a window has been cut out of the PCB such as to show the backside of the PC membrane and the bottom electrodes. In this device, each culture site is completely separated from the others, thus having a bottom and a top pair of electrodes. A version of this glass based device with common top electrodes has also been designed and realised. This design can be seen on the left-hand side of figure 2.19a presenting the result of the batch process with the deposited electrodes on floatglass wafers and the powder blasted vias. Using a dicing machine (see appendix 1), the wafers are diced for separating the devices after having properly protected the electrode side with a blue-tape (adhesive tape for dicing). Figure 2.19b shows a top and a bottom pair of electrode (without PC membrane in between) and the powder blasted through hole.

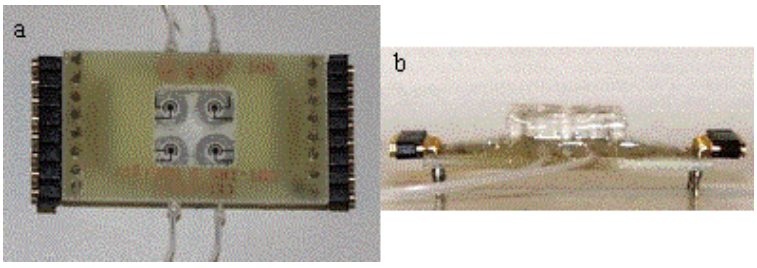

Figure 2.18: Optical photographs showing a completed glass based device: a) back view showing the bottom electrodes through a hole cut in the PCB. b) side view.

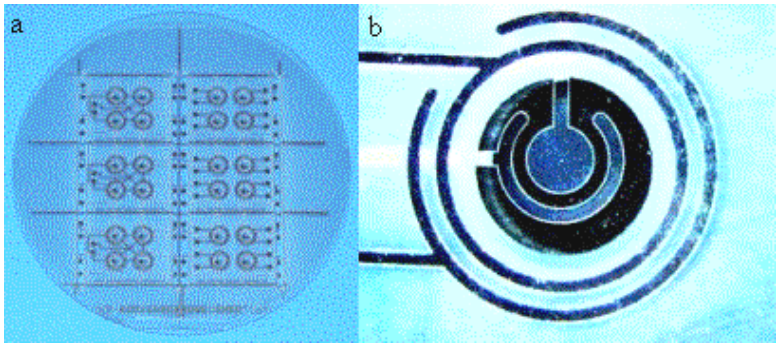

Figure 2.19: Optical photographs showing: a) Bottom and top wafer temporarily assembled before dicing showing the powder blasted holes and the deposited electrodes. b) Enlargement showing a top and a bottom pair of electrode (without PC membrane).

2.3.3 MACRO DEVICE

As developed further in chapter 3, we experienced some adhesion problems of thin film Ag/AgCl electrodes in the linear and modular devices. We have designed a "macro" device, so-called because no microfabrication steps were used for its realisation, for continuing biological experiments while the microsystems were inoperative. The advantage of this macro device is that the electrodes are not thin films but Ag wires (99.99% Ag purity, Ø 0.37 mm). As the electrodes are of Ag "bulk" material, there are no adhesion problems of Ag on a substrate such as glass, and the AgCl layer can also be much thicker, hence having a better lifetime. It is a reusable device, as the modular device.

The macro device shown in figure 2.20 consists of three separate parts:

- The lower part which is a polycarbonate machined chamber with a Ag electrode for current input and a Ag/AgCl electrode for voltage measurement.
- A disposable PDMS moulded middle part with four upper chambers and a polycarbonate membrane under each chamber defining cell culture sites.
- A machined polycarbonate part composed of four guides for the top pairs of electrodes, each pair consisting of a Ag electrode for current input and a Ag/AgCl electrode for voltage measurement.

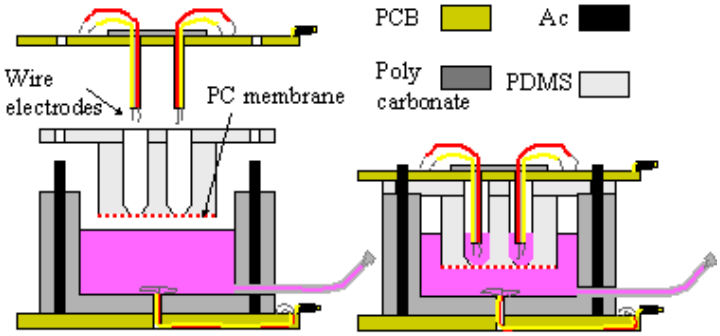

Figure 2.20: Schematic cross-section showing the three levels of the macro device and the assembled structure.

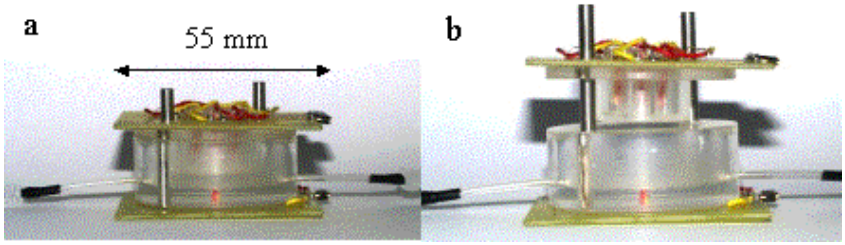

Figure 2.21: Optical photographs showing a completed glass based device: a) back view showing the bottom electrodes through a hole cut in the PCB. b) side view.Photograph of the POM mould and its cover for the middle part of the macro device

Figure 2.21a shows a completed macro device. The device can be separated as shown on figure 2.21b, to remove the PDMS element on which the PC membrane is glued. The top part of the device, represented on figure 2.22a, is a PCB with a glued PC element which consists of four PC tubes as guides for a pair of electrodes for each culture site. The bottom part (figure 2.22b) is a PC reservoir glued on a PCB with two fluidic accesses and a pair of common bottom electrodes.

Figure 2.23a shows the POM mould for the PMDS piece that can be seen on figure 2.23b. One can observe the four aluminium pins which are removed after curing, giving rise to four separate top reservoirs for physiological solution and cells.

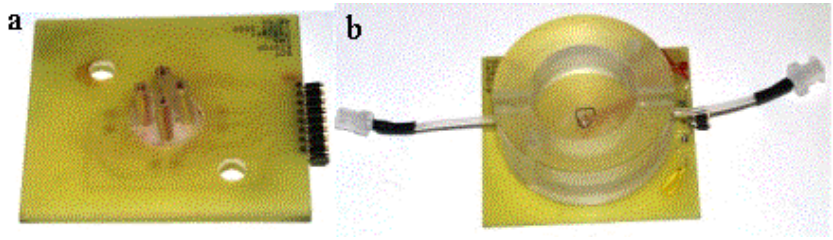

Figure 2.22: a) Optical photograph of the top part of the macro device with four pairs of electrodes. b) Optical photograph of the bottom part of the macro device with the polycarbonate reservoir and one common pair of electrodes.

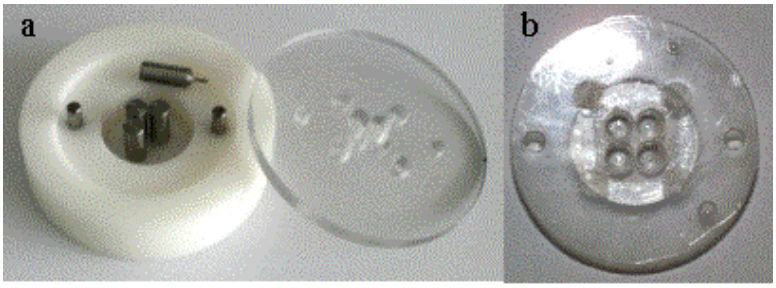

Figure 2.23: a) Optical photograph of the POM mould and its cover for the middle part of the macro device. b) Optical photograph of the PDMS moulded part.

2.3.4 LINEAR DEVICE

The so-called “linear” device was designed and realised as a follow-up version from the “glass based” device. A linear design (shown in figure 2.24) was chosen to reduce the number of corners in the bottom channel, hence decreasing the bubble formation during filling with a liquid solution. In comparison with the glass based device, the middle glass wafer containing the bottom channel and vias is replaced by a moulded PDMS element, and consequently, the volume of the bottom reservoir (channel) is not any more limited by the thickness of the standard floatglass wafer (500 µm). Moreover, a supplementary moulded PDMS layer is added on top of the porous polycarbonate membrane, as to determine the cell culture surface (see figure 2.25), which permits a much better reproducibility than

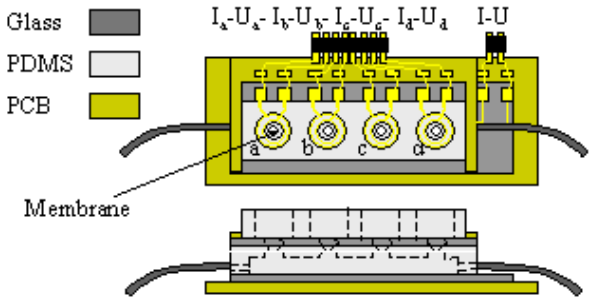

Figure 2.24: Schematic drawing showing the entire linear device.

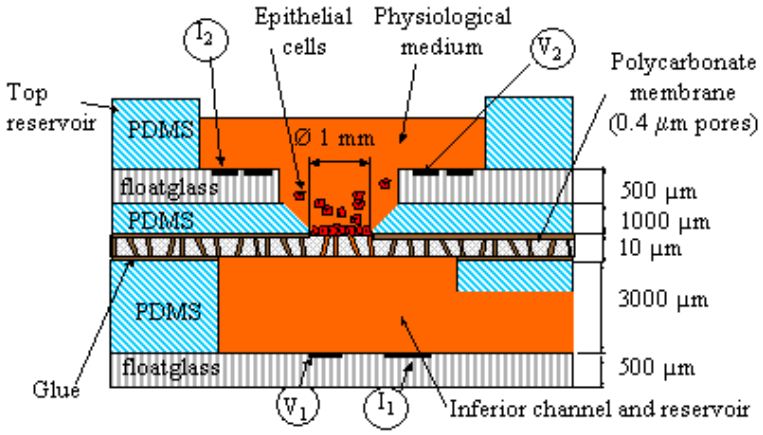

Figure 2.25: Schematic cross-section of the basic linear tissue measurement structure showing epithelial cell layer covered nano-porous membrane separating the top from the bottom reservoir

using a powder-blasted hole in glass, as for the glass based device (see figure 2.15). The four-electrode impedance and voltage probe set-up of the glass based device is maintained but the electrodes material is no longer Ta/Pt. We use Ag electrodes for the injection of current (I_1 and I_2) and Ag/AgCl electrodes for the voltage measurements (V_1 and V_2). The adhesion Ta film is replaced by a Ti film (typically 20-50 nm) or Ti/Pd (typically 20/20 nm). The choice of this adhesion

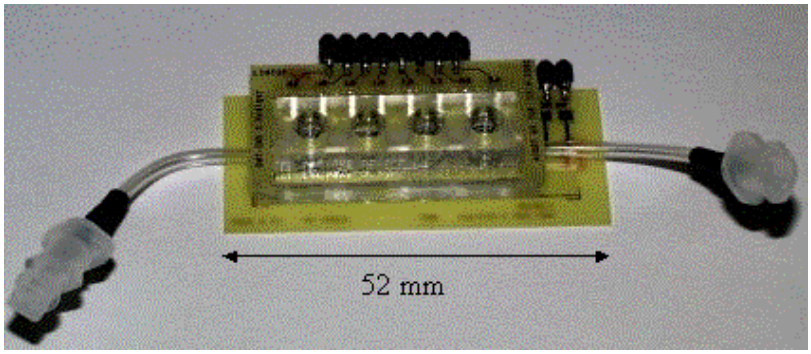

Figure 2.26:Optical photograph showing a completed linear device.

layer will be discussed in chapter 3 as well as the chlorination step of the Ag electrodes for the obtaining of Ag/AgCl electrodes.

Figure 2.26 shows a completed linear device. Well visible are the four in-line culture sites and the bottom reservoir inlet tubes with standard syringe connectors. There are five main parts for the assembly of the linear device. Figures 2.27 a and b show the PCB mounted top and bottom floatglass substrates respectively. One can see, on the top substrate, four pairs of deposited electrodes and, on the bottom substrate, a common pair of electrodes. Three PDMS moulded elements complete the device. On figure 2.27c one can see the PDMS moulded channel. It consists of a common bottom reservoir for physiological solution with access holes to the PC membrane to be glued on top of it. Two side fluidic channels for fluidic connection purposes can be distinguished. Figure 2.27d shows the middle PDMS moulded layer, determining the size of the culture sites (1 mm of diameter as standard size). This element can be modified to have different culture site diameters (up to 2.5 mm) without modifying the other elements of the linear device. Four separate top reservoirs, with 5 mm diameter and a height of 4 mm, form the third PDMS moulded part shown in figure 2.27e.

The PDMS mould for the channel element of figure 2.27c is represented on figure 2.28. It is composed of two polyoxymethylene (POM) machined parts, a bottom part with the channel shape and a top lid. On can notice the two side pins which can be removed after moulding, forming two fluidic connector input channels, as well as the four pins which determine the bottom culture membrane access holes.

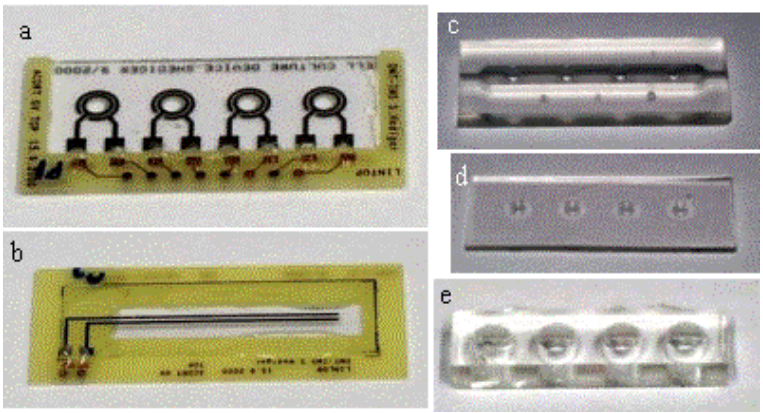

Figure 2.27: Optical photographs showing the five main parts of the linear device: a) Top substrate with a pair of electrodes for each culture site. b) Bottom substrate with on common pair of electrode. c) PDMS moulded channel. d) Middle PDMS moulded layer (determining the size of the culture sites. e) Top PDMS moulded reservoir.

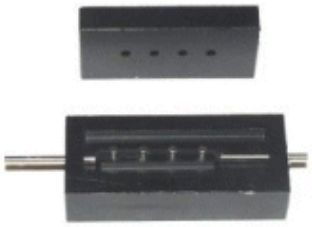

Figure 2.28: Optical photograph of the PDMS channel mould. One can see the two side pins which can be removed after moulding, leaving the fluidic input channels, as well as the four pins which determine the bottom culture membrane access vias.

Figure 2.29a shows the middle PDMS layer with a glued PC membrane determining a culture site (1 mm in diameter). One notices that it has a cone-shaped hole, allowing an approach of the pipette to deposit the cells as near as possible to the membrane. Figure 2.29b shows the top floatglass substrate with the top electrodes and the centred powder blasted through hole (2.5 mm in diameter).

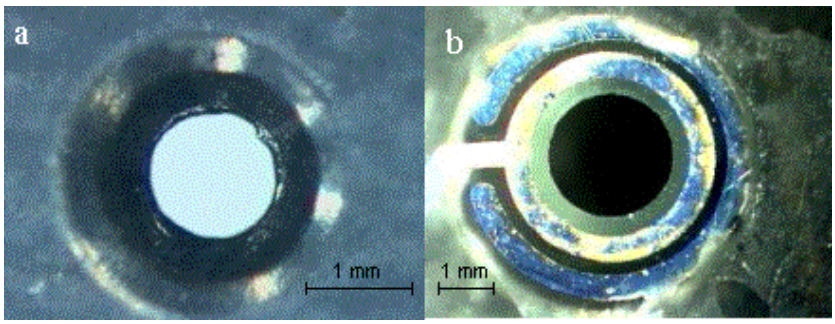

Figure 2.29: Optical photographs showing: a) A 1 mm diameter culture site glued under the middle PDMS layer which has a cone-shaped hole, allowing an approach of the pipette to deposit the cells as near as possible to the membrane. b) Concentrical top electrodes with the powder blasted via in the centre.

2.3.5 MODULAR DEVICE

Contrarily to the already presented devices which are disposable (for single use), the modular device shown in figure 2.30 is designed for multiple use [57].

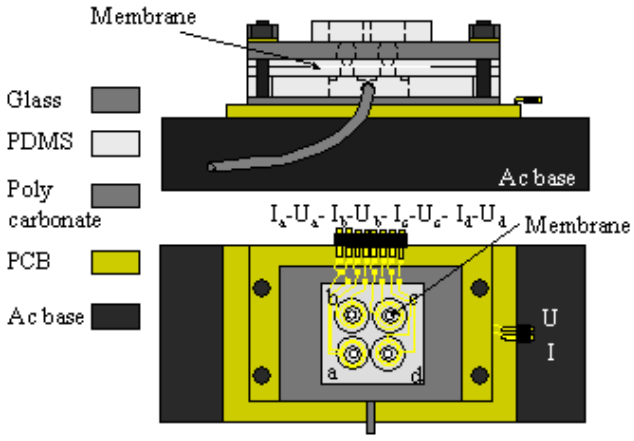

Figure 2.30: Schematic drawing showing the entire modular device.

Figure 2.31 shows a schematic cross-section of the basic modular tissue measurement structure: it consists of an assembly of three different stacks. The first level is a glued assembly of a floatglass wafer and a machined 2 mm thick polycarbonate plate (a thicker floatglass wafer than standard (0.5 mm) was chosen to avoid bending and rupture when pressing the complete structure together). Ag micro-patterned electrodes are previously deposited on the floatglass wafer, namely the lower current electrode (I_1) and the concentrical lower voltage electrode (V_1). The polycarbonate plate is manufactured in order to obtain a sufficiently large bottom fluidic reservoir to have enough physiological solution for the cells. The second level of the device is composed of two PDMS moulded layers with a nano-porous polycarbonate membrane glued in between. The diameter ∅ of a single culture site (determined by the free area of the membrane) is 1 mm. The third level is similar to the first one with two concentrical electrodes (I_2 and V_2) and vias. The basic structure of figure 2.31 is repeated to form four separate and identical cell culture wells on one modular tissue measurement device. The complete stack is formed simply by mechanically pressing the three levels together, thereby using the elastic properties of the PDMS to have a microfluidic seal. The stack can be separated after culture and electrical characterisation to enable optical investigation of the cell layer using only the second level. The final step before use

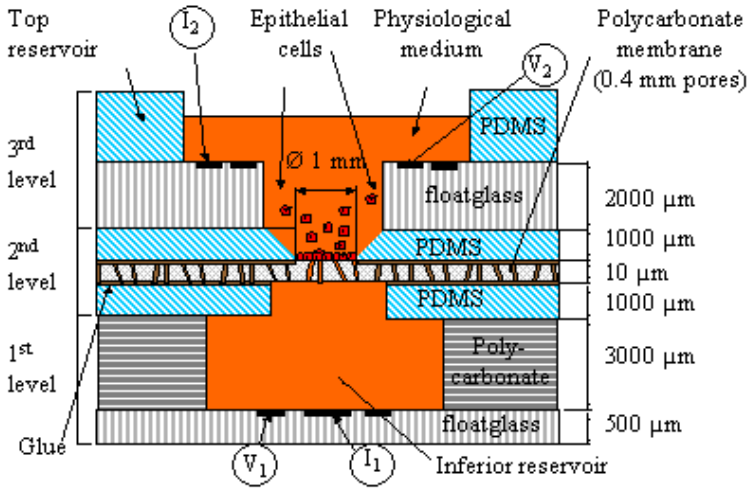

Figure 2.31: Schematic cross-section showing the three levels of the basic modular tissue measurement structure.

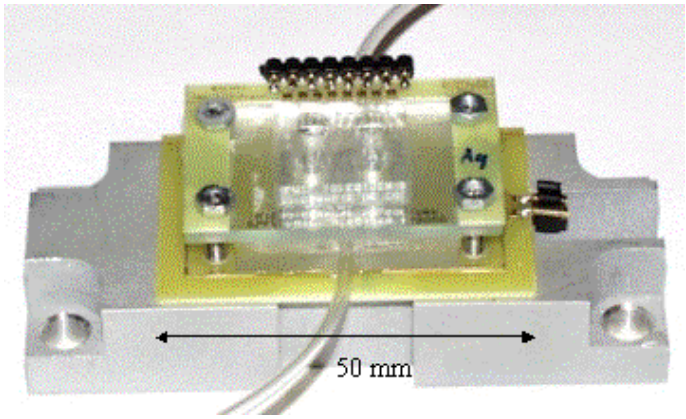

Figure 2.32: Optical photograph showing a completed glass modular device on its aluminium base.

is the chlorination of the voltage electrodes (V_1 and V_2) which will be discussed in chapter 3.

Figure 2.32 shows a ready-to-use modular device. It is mounted on its aluminium base and the three levels are pressed together using four nuts. The filling is done from the 1st level through the membrane to the 3rd level.

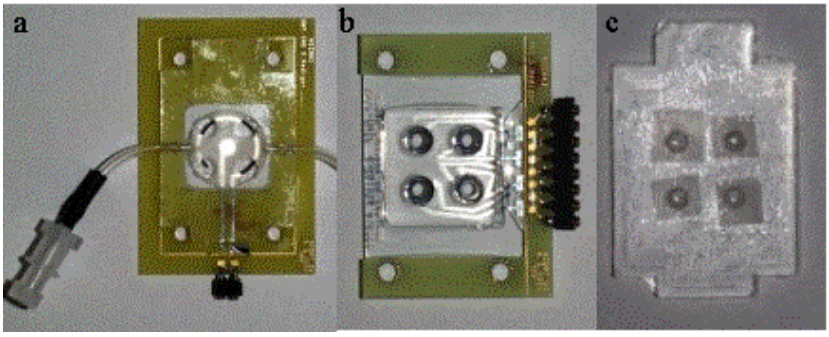

Figure 2.33: Optical photographs showing: a) 1st level of the modular device, the bottom layer with one common pair of electrodes. b) 3rd level of the modular device with top PDMS reservoir and four culture sites. c) 2nd level of the modular device, a PC membrane sandwiched between 2 moulded PDMS layers.

Figure 2.33 a is an optical photograph of the finalised first level mounted on a Printed Circuit Board (PCB), showing the outward electrical connectors, as well as the two fluidic connections to the lower channel. On can also see the bottom PC reservoir with four access holes to the backside of the culture membrane. Figure 2.33b is an optical photograph of the third level, where a powder blasted via and the concentrical top current and voltage electrodes can be seen. Figure 2.33c shows the second level, an assembly of two PDMS moulded layer with the PC membrane glued in between

Figure 2.34 is an optical photograph mounting schematically representing the different levels of the modular tissue culture device. The structures of levels 1 and 3 are to be cleaned for each cell culture experiment and are re-usable; level 2, the PDMS sandwiched membrane, is to be changed for each new experiment. The three levels of the structure are mounted on an Al base using four nuts.

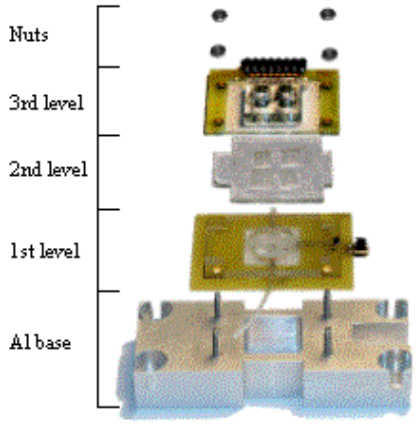

Figure 2.34: Photographic images showing the mounting of the modular device before use. One can see the 2nd level, consisting of a PC membrane sandwiched between two moulded PDMS layers, which form the only disposable part of the device.

2.4 CONCLUSION

Several devices were designed and realised, proposing different solutions to the requirements of a biosystem for culture and characterisation of epithelial cell tissues, such as biocompatibility, "user-friendliness", environment resistance, electrical characterisation method and cost. The choice of the materials is tightly bound with the micro-fabrication technology used. The powder-blasting technology was introduced as a non-standard micro-fabrication technology for etching glass wafers, thereby limiting the clean-room fabrication steps. PDMS moulding was used as a simple method to produce disposable elements with favourable properties such as the biocompatibility and the sealing potential (2^{nd} level of the modular device). Different electrode, channel and reservoir configurations were designed and realised, offering a complete overview of biosystems for the culture and characterisation of epithelial cell tissues.

3 ELECTROCHEMICAL CHARACTERISATION WITHOUT EPITHELIAL TISSUES

Today, electrodes are widely used to measure bioelectric events and to stimulate living tissues. Starting in the early 1800s, after the principles of electricity had been discovered, the interaction of electric currents with biological media was a subject of interest for scientists [58-62]. However, until now and despite considerable experimental and theoretical research, electrode properties are still very difficult to predict. In the last decade, the research concentrated more on microelectrodes, as new fabrication technologies emerged. Recently, they have found various applications in bio-analytical science. As a direct consequence of their reduced size, microelectrodes have demonstrated an enhanced analytical performance, for example, through a more efficient diffusion of analytes to the electrochemical surface. In this thesis, different electrochemical measurements and analysis were performed on our electrode systems and using different electrode materials, to develop an analytical model concerning our specific application.

3.1 ELECTRODE-ELECTROLYTE PROPERTIES

3.1.1 DEFINITION OF THE INTERFACE

In order to explain what is happening at the electrode interface with the physiological solution, which, due to its ionic character, acts as an electrolyte, we have to define the different elements involved in this interaction. An electrolyte is a substance with ionic dc conductivity. In water, the ionic bonds between unequal atoms are broken and the ions split, thereby causing ionic conductivity. Thus, the charge carriers are ions and there is no separate flow of electrons which are bound to their respective atoms. As we want to measure electrical characteristics of cells, we can consider them as electrolytic conductors. Actually, the intra- and extracellular liquids contain ions free to migrate, the currents are therefore ionic. On the contrary, in metals, the electrons are free to move and the current is electronic. Electron transport in a metal does not involve any transport of metallic ions. Con-

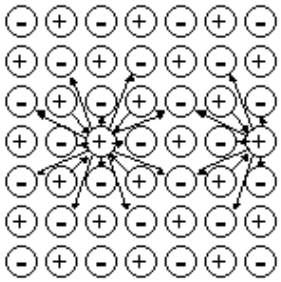

Figure 3.1: Schematic showing the coulombic forces on ions in the bulk and on the surface of an ionic crystal. The arrows to the central ions indicate repulsive forces and the arrows pointing from the central ions indicate attractive forces (illustration modified from [63]).

sequently, for passing a current from a metal to an electrolyte, there must be a charge exchange between electrons and ions. The electrode is the site where this charge carrier shift transition takes place. An electrode reaction takes place at the surface of the electrode which is in contact with the electrolyte. This region, called the interface, is where electrode and solution meet and where their properties differ from those in the bulk. Considering an ionic crystal placed in vacuum, we can represent the coulombic forces acting on an ion in the bulk and on an ion at the interface (figure 3.1). The arrows to the central ions indicate repulsive forces and the arrows pointing from the central ion indicate attractive forces. One can see that the forces acting on an ion on the bulk are symmetrical (in all directions), but for an ion at the interface, the forces work in half the direction. This means that the surface layer of a solid must be structurally different from the inside layers, as a consequence of this change in forces. A similar phenomenon occurs for species in a liquid. This difference in interaction at interfaces leads to the existence of surface tension (formation of drops and behaviour of liquids in capillaries).

Now, if a metal is immersed into a polar liquid, two processes take place:

1) The dipoles of the liquid orient themselves toward the metal in a way to counterbalance the force of the free electrons and the cations of the metal.

2) Some metal ions will dissolve, leaving a negative charge on the metal. This charge will polarise the surface layer of the solvent and the cations in solution will polarise the surface layer of the metal.

The result is that the surface layer of the metal acquires a charge which is equal in magnitude and opposite in sign to the charge of the electrolyte at the interface. Hence, there must be a neutral region in the interface region as separation of charges occurs. As the distance between the two charged layers is very small, an analogy can be made with a parallel-plate condenser. The concept of capacity and potential difference across the condenser follow. The interface is therefore called the *double-layer*. Depending on the applied potential, the metal charge can be either positive or negative with regard to the electrolyte. The composition of the double layer thus depends on the potential and the chemical nature of present ions. Moreover, if the electrode-solution interface acts like a parallel-plate condenser, when direct current flows through the cell and there is no change of potential in time, there is no capacitive current. This means that direct current must be passed by another mechanism. Here we reach the basic principle of electrodics:

The continuous flow of direct current through an electrolytic or galvanic cell is always associated with two electrode reactions [63].

3.1.2 DOUBLE-LAYER ION DISTRIBUTION MODELS

Electrode polarisation is an interfacial phenomenon occurring at the electrode-electrolyte interface. “To polarise an interface means to alter the potential difference across it, to be polarisable means to be susceptible to changes in potential difference” [64]. Electrode polarisation has been a field of investigation since the beginning of the 19^{th} century until nowadays. The first step in modelling the electrode-electrolyte interface [62] was taken by Helmholtz [65] in 1879, who proposed that a double layer of charge existed at the interface (figure 3.2), hence a capacitance must be included in the model. Moreover, as mentioned in the preceding paragraph, because a direct current can pass through the interface, in an electrolytic cell, a resistance must also be a component of any model. One electrode reaction takes place at the cathode surface and the other at the anode surface. Once the current has crossed the electrode-solution interface, it is carried by ions through the solution until it reaches the other electrode-solution interface where it is transferred to the metallic conductor again. This current is called charge transfer current or faradaic current. The resistive component in the models is then called the charge transfer resistance (R_{ct}). However, some electrodes-electrolytes couples do not contain reactive species and allow large scale potential variation with no electrochemical reactions occurring, hence no measurable faradaic current. An electrode with this property is called “ideally polarisable”.

- Helmholtz model: the first and simplest model (figure 3.2) which supposes that positive and negative charges are situated in two plates

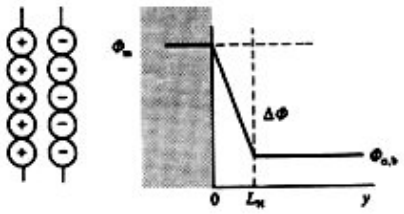

Figure 3.2: Schematic showing the Helmholtz model of the double layer. Φ *represents the potential*

separated by a distance L_H of 0.2 to 0.3 nm, corresponding to the distance separating hydrated ions from the surface of the electrode. According to this model, the double layer is equivalent to a parallel-plate condenser. The double layer capacitance C_d is therefore:

$$C_d = \frac{\varepsilon_r \varepsilon_0 A}{d} \qquad \text{Eq. (3.1)}$$

where ε_r is the relative dielectric constant of the electrolyte, ε_0 is the permittivity of free space ($\varepsilon_0 = 8.86 \times 10^{-12}$ C V^{-1} m^{-1}), A is the electrode surface and *d* is the plate separation. However, this model is not perfect as, according to equation 3.1, the double layer capacitance is a constant. In practice, C_d depends on concentration and potential.

- Gouy-Chapman model: ion concentration influences the double layer capacitance. This behaviour, contrary to the Helmholtz model (where there is a rigid sheet of solvated ions), results from thermal agitation of

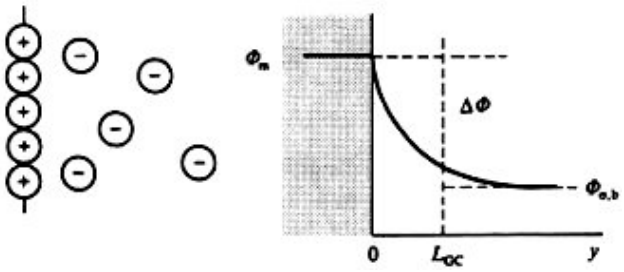

Figure 3.3: Schematic showing the Gouy-Chapman model of the double layer.

the ions. The ions are not in fixed plane but follow a Boltzmann distribution in a region situated near the surface which is called diffuse double layer or Gouy-Chapman layer (shown in figure 3.3). This allows the capacitance to change by thermal movement of ions, in response to an applied potential. Without exposing the more complicated equation for the capacitance, it is known that the Gouy-Chapman model is an improvement to the Helmholtz model, but that it generally overestimates the interfacial capacitance.

- Stern model: this model (shown in figure 3.4) is a combination of the Helmholtz and the Gouy-Chapman models. The potential difference between the electrode and the solution consists of two terms: $\Delta\Phi_H$ due to a compact layer (Helmholtz) and $\Delta\Phi_{GC}$ due to a diffused layer (Gouy-Chapman). The total capacitance is then C_H and C_{GC} in series:

$$\frac{1}{C_d} = \frac{1}{C_H} + \frac{1}{C_{GC}} \qquad \text{Eq. (3.2)}$$

The resulting total capacitance thus depends on the smallest of the two capacitances. For low ionic concentrations (1 to 10 mM), the diffuse layer has a dominant effect, and for higher concentrations, the Helmholtz layer increases in importance. The Stern model gives a good description of the electrical behaviour of the metal-electrolyte interface of certain systems, but can not explain every experimental result. Moreover, it does not include the influence of crystalline orientation and chemical nature of ions.

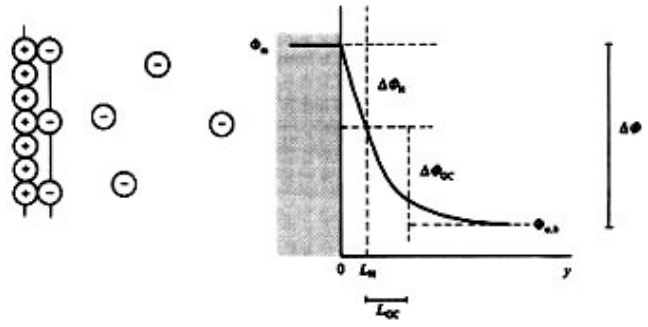

Figure 3.4: Schematic showing the Stern model of the double layer.

3.1.3 DOUBLE-LAYER CIRCUIT MODEL

When elaborating an analytical electric circuit model for the electrochemical processes at the metal-solution interface, the aim is that the model reflects primarily the experimental phenomena and the measured values. The elements of the model do not necessarily exist as isolated physical entities but they can simulate the electrical behaviour of the interface. The best way to establish a model is to consider the interface as a black box, make extensive measurements on it, and find the electrical circuit that matches the electrical impedance-frequency response. The aim is to be able to anticipate the behaviour of a certain metal-solution interface by simulating it with the circuit model with some fixed parameters deduced from anterior measurements on similar interfaces, and to possibly isolate interfacial parameters, corresponding to a certain electrical behaviour.

After a brief presentation of the simple existing models of the metal-solution interface, different electrochemical characterisation methods will be used on our devices for the elaboration of a circuit model which simulates best the electrical behaviour of our specific metal-solution interface. The model will help us to extract that part of the total measured electrical signal we are interested in, i.e. the impedance of the cell monolayer and the transepithelial current.

- Simple electrochemical process:

  An equivalent electronic circuit (circuit model) for a simple electrochemical process is shown in figure 3.5. It is based on the theory elaborated by Helmholtz as exposed in section 3.1.2. The passive elements composing this model are:

  - the ohmic resistance R_Ω which represents the potential drop in the electrolyte between the reference electrode and the working

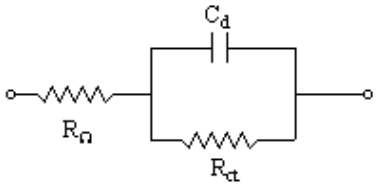

Figure 3.5: Schematic showing the equivalent electronic circuit for a simple electrochemical process.

electrode. It is a function of the conductivity of the electrolyte and the geometry of the electrochemical cell.

° the double layer capacitance C_d, induced by the charge separation at the interface. The value of the double layer capacitance depends on many variables including electrode potential, temperature, ionic concentration, types of ions, oxide layers, electrode roughness, impurity adsorption, etc.

° the charge-transfer resistance R_{ct}, which represents the resistance for the direct current to pass through the interface, which depends on electrode reactions with the electrolyte at the interface.

• Advanced electrochemical process:

An equivalent electronic circuit for an electrochemical process, where a diffusion limited faradaic process occurs, is shown in figure 3.6. There is an additional passive element in this model:

The Warburg impedance Z_W is an impedance describing the current limiting due to diffusion mass transport. When the electron transfer flux and the chemical reaction rate are so high, that the faradaic current is limited by diffusion alone (transport process dependant only on concentration gradients), one more element, Z_W, can be added to the circuit model. The diffusion may be of reactants to the electrode, or of

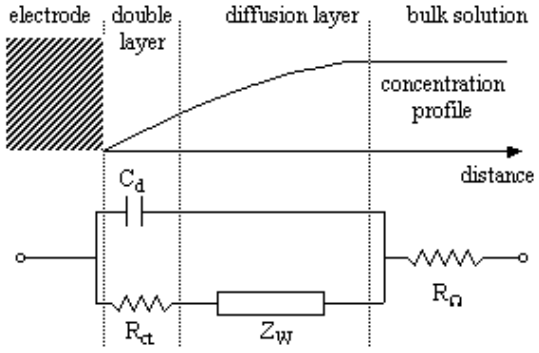

Figure 3.6: Schematic showing the correlation of the different equivalent components of a faradaic process with electrochemical phenomena.

reaction products away from the electrode. Warburg (in 1899) [62] was the first to study and develop a theory about this process. Z_W is not an ideal component, as it changes with frequency. For a diffusion-controlled faradaic reaction, the phase of the current is shifted 45° with respect to the applied potential in the Warburg impedance. Equation 3.4 shows the literal value of Z_W [66, 67]. It is calculated by supposing high charge transfer rates, thus the potential at the electrode corresponds to the Nernst equation (eq. 3.7) at every time.

Considering the following redox reaction (eq. 3.3):

$$ox + ne \rightarrow red \qquad \text{Eq. (3.3)}$$

$$Z_W = \frac{\sigma}{\omega^{0.5}} - j\frac{\sigma}{\omega^{0.5}} \text{ and } |Z| = \sqrt{2}\frac{\sigma}{\omega^{0.5}} \qquad \text{Eq. (3.4)}$$

$$\sigma = \frac{RT}{cn^2F^2A(2D)^{0.5}} \qquad \text{Eq. (3.5)}$$

where:

σ is the Warburg coefficient

R is the universal gas constant R=8.3144 [J•mol^{-1}•K^{-1}]

F is the Faraday constant F=9.6885•10^4 [C•mol$^-$]

T is the temperature in [K]

n is the number of electrons in the unit reaction

$\omega = 2\pi f$ in [Hz]

c is the concentration of the reduced ions in [mol•l^{-1}]

D is the diffusion coefficient of the reduced ions in [cm^2•sec^{-1}]

A is the surface of the electrode [cm^2]

This diffusion process impedance model is only valid for systems where the electrode is operated near equilibrium using an AC excitation and does not predict the DC behaviour, where the double layer capacitance C_d is the dominant factor.

3.1.4 ELECTRODE POTENTIAL

We have just discussed the notion of interface and more specifically the metal-solution interface. In our microsystem, there are at least three components involved for measuring the impedance of the epithelial cell mono-layer, two electrodes and an electrolyte. When no dc current is flowing through the cell, a half-cell reaction takes place at each electrode-solution interface, and a electrical potential difference occurs over the interface (which is not due to polarisation as no dc current is flowing). The equilibrium potential or reversible potential of an electrode represents the electrical potential difference between the metal and the solution at equilibrium. The potential of an electrode can not be measured in absolute values, one can only measure the potential difference between two electrodes. We call a half-cell potential, the electrode potential developed when a metal is in contact with an electrolyte. As we want to separate the two half-cell reactions of an electrochemical cell, a constant and stable reference electrode must be used for measuring a half-cell potential. By international convention, the potential at a normal hydrogen electrode (NHE) (platinum wire placed in a solution with constant hydrogen activity) is defined to be zero at all temperatures [68-70]. It corresponds to the following reaction:

$$2H^+ + 2e \Leftrightarrow H_2 \qquad \text{Eq. (3.6)}$$

All half-cell potentials are referred to this standard. However, this NHE is not very practical for every day use. More used are the secondary reference electrodes, especially the calomel (Hg_2Cl_2 paste in saturated KCl solution) and the silver-silver chloride (Ag/AgCl in saturated KCl solution). A special study on Ag/AgCl electrodes will be developed in the following section 3.2. All reference electrodes are based on the Nernst equation.

The Nernst equation (eq. 3.7) relates the redox processes and the potential to the concentration/activity of the ions in the solution of an electrolytic cell. It provides a value for the redox equilibrium potential V with no dc current flow. Referring to the redox reaction (eq. 3.3):

$$V = V_0 + \frac{RT}{nF} \ln \frac{a_{ox}}{a_{red}} \qquad \text{Eq. (3.7)}$$

where:

V_0 is the standard electrode potential of a redox system (with respect to the hydrogen reference electrode at 1 mole concentration) in [V]

n is the number of electrons in the unit reaction

R is the universal gas constant R=8.3144 [$J \bullet mol^{-1} \bullet K^{-1}$]

F is the Faraday constant F=$9.6885 \bullet 10^4$ [$C \bullet mol^{-}$]

T is the temperature in [K]

a_{ox} and a_{red} are activities, $a = \gamma c$, where c is the concentration and γ is the activity coefficient. $\gamma = 1$ for low concentrations (no ions interactions), but < 1 at higher concentrations.

3.2 IMPEDANCE MEASUREMENT TECHNIQUE

As previously mentioned in section 2.2.4, we have used two impedance measurement systems, namely the two-electrode system and the four-electrode system. The principle of these measurement systems is presented in the following sections.

3.2.1 TWO-ELECTRODE SYSTEM

In our first device, the silicon based device, we have used a two-electrode (or two-point) system shown in figure 3.7. One can observe the two electrode-solution interface (represented by the equivalent electronic circuit for a simple electrochemical process as shown in figure 3.5) and the ohmic resistance R_Ω which counts for the electrolyte resistance, the polycarbonate membrane and the cell monolayer. The measurements are performed using a Hewlett-Packard® impedance analyser, the HP 4194A. A very small sinusoidal potential (10 mV peak-to-peak amplitude) is applied to the cell culture device via the two integrated electrodes and the resulting AC current is measured. The result of this measurement, that is to say the impedance of the device over a wide frequency range (from 100 Hz to 1 MHz), is represented in a Bode plot which is the standard technique to represent an electronic transfer function (for example filters). The absolute imped-

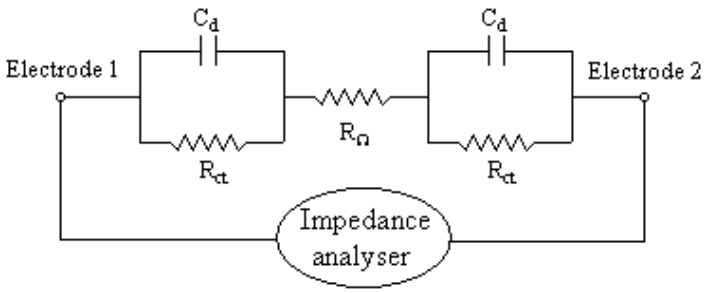

Figure 3.7: Schematic showing the two-electrode system electrical model.

ance $|Z|$ and the phase-angle θ, are plotted as a function of frequency in a log-log plot (see also section 3.4).

Figures 3.8 and 3.9 show the Bode plot for the impedance measurements of one cell culture site of a silicon based device (1 mm^2 of free membrane surface) and a glass based device (4 mm^2), respectively. Both devices contain physiological solution and Pt electrodes. As expected, the impedance is increasing at lower frequencies due to the polarisation effect at the two electrode-solution interfaces. The double-layer capacitance C_d is short-circuited at higher frequencies, in this case starting at approximately 10 kHz, and the total impedance corresponds to the ohmic resistance R_Ω. This measurement technique can be improved by using adequate electrodes, that is to say, by using low surface impedance metals. One very effective electrode material for this application is the black platinum (or platinised platinum) [71]. An electrochemical deposition via a specific platinum containing solution transforms the surface of the platinum electrode in a black platinum layer which has a higher effective surface area, thereby reducing the electrode impedance. Another possibility to reduce the electrode surface impedance is to use iridium oxide electrochemically deposited on Pt. It also increases the effective electrode surface area and a hydrous oxide grows when it is electrochemically activated, which provides a very high charge capacity as well as the ability to deliver large amounts of charge to the aqueous solution. This two-point impedance measurement method can therefore be used to measure the resistance of our devices.

However, there are several drawbacks:

- The resistance measurements at high frequencies cannot be applied to silicon based devices. Indeed, one can observe that the impedance at 1

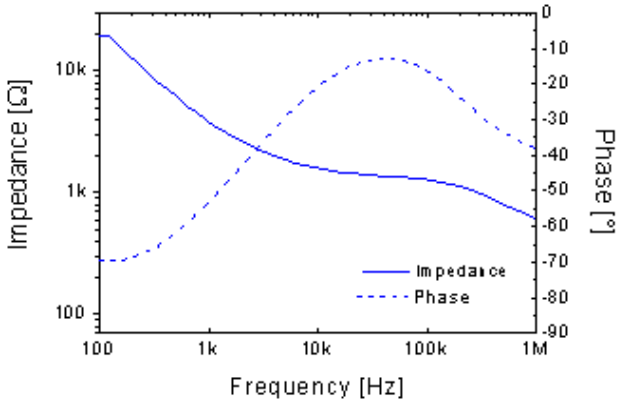

Figure 3.8: Bode plot representing a two-electrode impedance measurement for one cell culture site of a silicon based device using physiological solution as electrolyte.

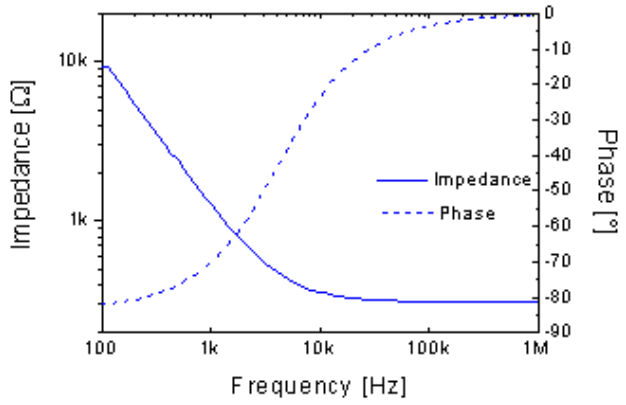

Figure 3.9: Bode plot representing the two-electrode impedance measurement for one cell culture site of a glass based device using physiological solution as electrolyte.

MHz for the glass based device represented in figure 3.9 is totally resistive (the phase is zero). On the other hand for the silicon based device, the impedance decreases for frequencies higher than 100 kHz. Actually, the silicon structures of the device have been oxidised for

electrical isolation. As the silicon dioxide is a dielectric, it can be represented by a capacitance. This silicon dioxide layer is short-circuited at higher frequencies, inducing an electrical short-circuit to the microfluidic cell.

- Impedance analysers such as the HP 4194A are quite expensive and represent an effective overkill for the simple measurements required for the epithelial cell layer resistance measurement. Moreover, our devices are meant to be used by biologists who have no access to such expensive and voluminous instruments.

Therefore, we have decided to abandon the two-electrode measurements and have chosen for the four-electrode system for the next generation of devices.

3.2.2 FOUR-ELECTRODE SYSTEM

In the glass based device, the linear, modular and macro devices, we have used a four-electrode (or four-point) system shown in figure 3.10. The circuit elements are the same as for the two-electrode system (figure 3.7). The principle of this measurement technique is based on the injection of a known current via two current-carrying electrodes and the measurement of the resulting voltage via two voltage electrodes positioned in the pathway of the current [20, 21, 71-76]. This method has its origin in the measurement of solid-state materials formed into flat samples of uniform thickness and arbitrary shape (for example a thin film). For the measuring of the voltage response to the current, a high input impedance (>1 GΩ) voltmeter is used. No current is then flowing in the voltage electrode leads,

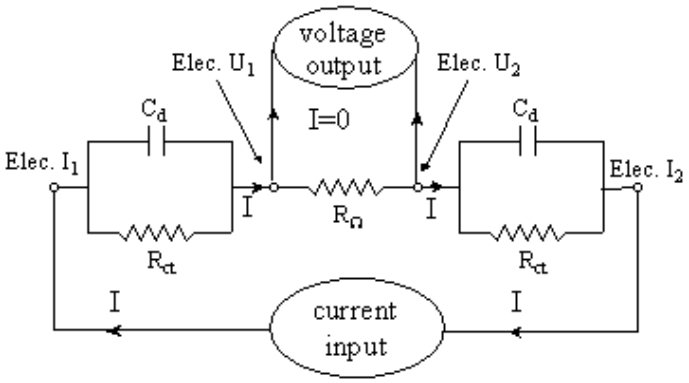

Figure 3.10:Schematic showing the four-electrode system.

thus no polarisation is occurring. The resistance is calculated following the Ohm law:

$$U = R \bullet I \qquad \text{for DC circuits} \qquad \text{Eq. (3.8)}$$

$$u = Z \bullet i \qquad \text{for AC circuits} \qquad \text{Eq. (3.9)}$$

Three different four-electrode measurements set-up have been tested:

1) Epithelial Tissue Voltohmmeter, the EVOM™:

We have tested the epithelial tissue voltohmmeter presented in chapter 1 (figure 1.5). It is used with the STX2 electrodes which consist of a fixed pair of double electrodes. Each stick of the electrode pair contains a silver/silver-chloride pellet for measuring voltage and a silver electrode for passing current. The AC input current is ± 20 µA at 12.5 Hz and the EVOM™ has an input impedance of >10 GΩ for the voltage measurements.

2) Four-point AC measurement set-up:

Figure 3.11 shows the four-point AC measurement set-up which consists of a function generator (the arbitrary waveform generator HP 33120A) for applying an AC voltage to the current-carrying electrodes of the device in series with a known resistance (1 kΩ). The voltage drop across this resistance is measured using a voltmeter (HP 34401A) to determine the current flowing into the device.

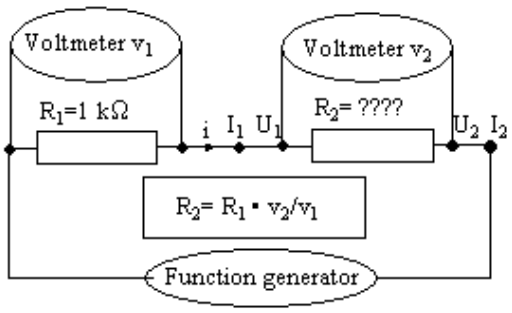

Figure 3.11: Schematic showing the four-electrode AC measurement system using a function generator and two voltmeters.

3) Four-point DC measurement set-up:

For this method, we use a controlled DC current supplied by a galvanostat (EG&G 263A) for current injection via the current carrying electrodes. The voltage is measured as for set-up n°2 with a high input impedance voltmeter. This method is based on the measuring principle of standard voltage-current clamp amplifiers, used for biological electrical characterisation. The controlled current actually has a pulse-type waveform, with inversion of polarity every second. This is necessary as we want to avoid electrode modification of the silver current carrying electrodes, as well as charge separation in the electrolyte by ion migration.

The design parameters for a four-electrode impedance measurement system are the following:

- Size: the surface area of the current carrying electrodes need to be as large as possible for lowering the surface impedance. The surface area of the voltage electrodes is of no influence as no current is flowing to the external leads. However, if the voltage electrodes are too large, they can influence the current path.

- Position: the two voltage electrode need to be in the current pathway, i.e. between the two current electrodes. For an absolute value of the resistance between the voltage electrodes (delimiting the sample to be measured), the voltage electrodes need to be in a region of parallel current lines. Figure 3.12 shows a four-point resistance measurement in a column with square cross-section, using Pt planar electrodes deposited on one side of the column and filled with a NaCl 1 M solution. A schematic top-view of the test structure is represented on the right-hand side of the graph. When fixing the sample of the column to be measured, that is to say by keeping the distance l between the voltage electrodes constant, one should measure a constant value for the resistance, independently of the position of the current electrodes, as long as the voltage electrodes are in the current pathway (linear region of both curves, with $l' > 5$ mm). This is no longer the case when the current electrode is positioned closer to the voltage electrode ($l' < 5$ mm). The reason for this non-linearity is the non-parallel current lines at the level of the voltage electrode. This can be visualised in figure 3.13, showing two simulations of current flowing through the cell. One can see that the minimum separation distance l' between the current and voltage electrode corresponds to the height h of

the electrolyte reservoir, in order to measure the voltage in a parallel current lines region.

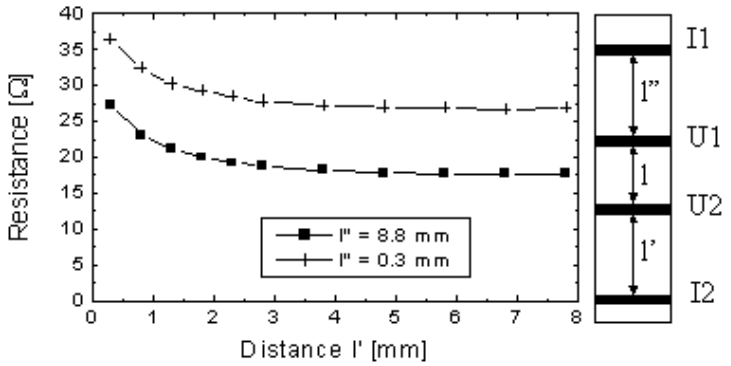

Figure 3.12: Graph showing four-point resistance measurements in a column of height h = 5 mm and width w = 5 mm and a length l = 3.8 mm, using Pt planar electrodes and filled with a NaCl 1 M solution. A schematic top-view of the test structure is represented on the right-hand side.

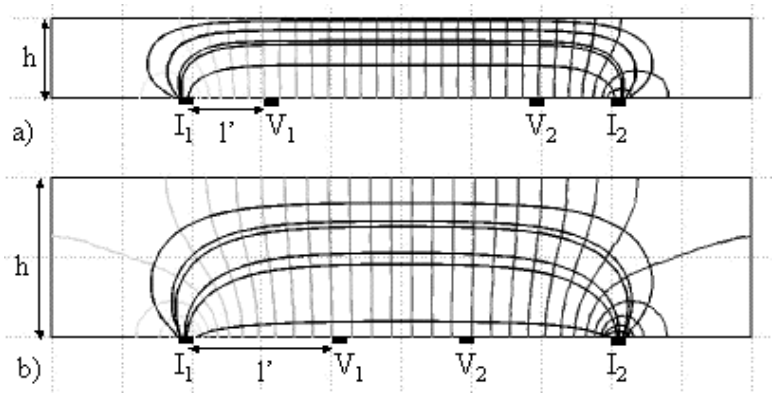

Figure 3.13: 2D Femlab simulations showing the equipotential and current lines with the same test structure as in figure 3.12. The height of electrolyte reservoir h is doubled for simulation b, compared to simulation a.

Remark: Note that for our device, we don't need to measure an absolute value of the resistance, we need to measure the increase of resistance when epithelial cells grow such as to form a monolayer. Therefore the minimum distance between the current and the voltage electrode does not need to be chosen. However, the phenomenon has been explained to be able to understand certain scaling behaviour of the microfluidic resistance chamber.

3.2.3 COMPARISON OF THE IMPEDANCE MEASUREMENT METHODS

Figure 3.14 shows a graph comparing the AC two- and four-point impedance measurement technique. One can observe that the AC four-point impedance is independent on frequency, as expected (no polarisation of the voltage electrodes, hence no capacitive effect), and its resistance value corresponds to the high frequency AC two-point impedance value.

The AC two- and four-point, and the EVOM™ impedance measurement method presented above are compared in figure 3.15 for a sample of NaCl 1 M solution of length l in a square cross-section column. One can first of all observe the perfect match between the EVOM™ and our AC four-point impedance measurement method, as well as the linearity with distance l. Concerning the two-point method (measured at 1 MHz), one can first notice the 20 Ω offset at l = 0 mm, corresponding to the resistance of the contact lines and wires to the impedance ana-

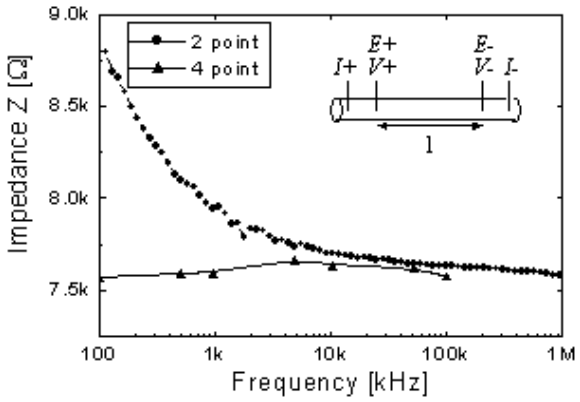

Figure 3.14: Graph comparing AC frequency-dependent two- and four-point impedance measurements in a plastic tube of 1.4 mm of diameter and 20 mm length (l = 20mm) filled with a physiological solution (ρ = 60 Ω cm), using steel needles as electrode.

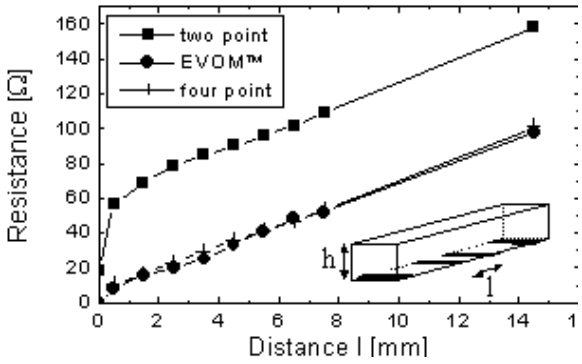

Figure 3.15: Graph comparing the resistance measurement methods for a column of section 5x5 mm^2 filled a NaCl 1 M solution, using planar Pt electrodes, l being the distance between the measuring electrode (voltage electrodes for the four-point method).

lyser. The offset then increases until about 60 Ω. This effect is a consequence of the non-uniform current lines between the two electrodes (the voltage electrodes are used for the two-point method), as explained above, as the electrodes are planar and therefore non-symmetrical with respect to the column section. This effect cannot be seen for the EVOM™ and our AC four-point impedance measurement method, as the current electrodes are far enough from the voltage electrodes in order to produce parallel current lines at the voltage electrode level (see figure 3.12).

3.3 ELECTRODE MATERIALS

During the development of our microsystems for culture and characterisation of epithelial cell tissues, different electrode materials were used. The choice of those materials follows from the requirements of the electrode system (change from a two-electrode system to a four-electrode system), as well as the necessary

	Au	Pt	Ag	Ag for Ag/AgCl
Thickness [nm]	200	200	300 and 500	500 and 700

Table 3.1: Overview of electrode materials used in our microsystems

	Au	Pt	Ag	Ag for Ag/AgCl
Deposition method	Joule-effect evaporation	Sputtering	Joule-effect evaporation	Joule-effect evaporation
Adhesion layer	Cr	Ta	Ti	Ti/Pd
Adhesion layer thickness [nm]	50	20	20	20/20
Deposition method (adhesion layer)	e-beam evaporation	Sputtering	e-beam evaporation	Sputtering
Substrate	silicon	floatglass	floatglass	floatglass
Device	silicon based device	glass based device	linear and modular devices	linear and modular devices

Table 3.1: Overview of electrode materials used in our microsystems

adhesion properties. The choice of Au and Pt was obvious as they are noble metals (high resistance against oxidation); therefore they are the most commonly used electrodes in MEMS. Ag/AgCl electrodes are chosen for their pseudo-reference properties (see following section), as stability in potential is a condition for measuring the Ite (see section 2.2.4). Table 3.1 shows an overview of the clean-room deposited thin-film electrodes used in our different microsystems.

3.3.1 SILVER-SILVER CHLORIDE ELECTRODES

The silver-silver chloride electrode (Ag/AgCl) is generally represented as Ag | AgCl | Cl^- [70, 77]. There are three phases, the metallic silver substrate, a AgCl phase coating the substrate, and an electrolyte solution which contains a soluble chloride such as NaCl or KCl. Under conditions of reversibility (currents relatively small to maintain an unchanged chemical environment), the potential of a silver-silver chloride electrode is determined by two equilibrium reactions:

$$Ag\ (solid) \Leftrightarrow Ag^+\ (solution) + e^-\ (metal\ phase)$$

$$Ag^+\ (solution) + Cl^-\ (solution) \Leftrightarrow AgCl\ (solid)$$

The standard equilibrium electrode potential for AgCl is:

$$E^0=220 \text{ mV vs NHE.}$$

If the Ag/AgCl electrode is used as the anode of an electrochemical cell, AgCl will be deposited on the electrode and increase the AgCl layer thickness, and if it's the cathode, the AgCl layer is reduced, Ag^+ and Cl^- ions are freed in the electrolyte, the AgCl layer will decrease in thickness and eventually be stripped off. As introduced in section 3.1.4, the Ag/AgCl electrode follows the Nernst law (eq. 3.7). Thus if a stable constant electrode is needed, the Ag/AgCl electrode is immersed in a saturated KCl solution, and is then called a reference Ag/AgCl electrode. It consists of a silver wire coated with an AgCl layer immersed in saturated KCl and located in a glass tube. The electrochemical contact to the external solution is made via a porous plug or a fritted disk. The potential of the saturated Ag/AgCl reference electrode is +197 mV with respect to the NHE. These electrodes are used for signal recording or potentiostatic applications, and therefore are operated with high-input impedance circuits.

In biological fluids, such as the physiological solution used for cell culture, the chloride ion concentration is nearly constant at 0.09 M. A simple Ag/AgCl wire or plane electrode can then be used as a so-called pseudo-reference electrode, as the potential generated at this electrode will practically remain constant.

3.3.2 CHLORINATION OF SILVER ELECTRODES

The chlorination of silver consists in forming a silver chloride phase on top of the silver wire or thin-film. Both electrochemical (potentiostatic (controlled voltage) and galvanostatic (controlled current) chlorination) and chemical depositions method have been carried out. The electrodes silver surface have to be cleaned or polished before deposition. The best way to obtain a uniform silver chloride layer on a silver thin film is to proceed to the chlorination just after the deposition or following the lift-off procedure, in order to avoid formation of a silver oxide passive film on top of the silver. If the silver thin film is stored for a few days, a cleaning step using diluted (10-20%) sulphuric acid is necessary before chlorination to obtain a pure silver surface.

- Chemical deposition:

The chemical deposition is based on the following reaction:

$$FeCl_3 + Ag \Leftrightarrow FeCl_2 + AgCl$$

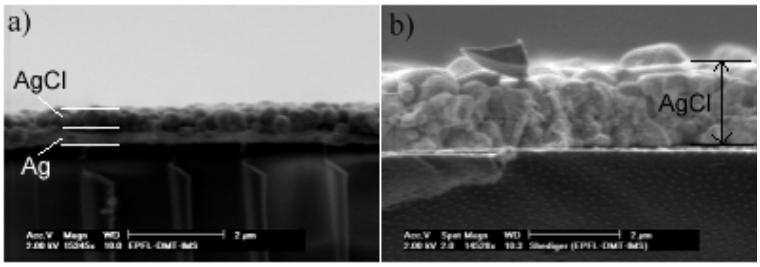

Figure 3.16:SEM photographs showing the cross-section of chemically deposited Ag/AgCl layers. a) 1 min. in $FeCl_3$.b) 5 min. in $FeCl_3$.

A part of the silver layer is transformed to silver chloride by immersion in a 1 M $FeCl_3$ solution at 30°C [69, 78-80]. Based on the literature, two immersion times have been tested, 1 and 5 min. Figure 3.16 shows SEM photographs showing the cross-section of chemically deposited Ag/AgCl layers. One can observe on figure 3.16a that only a part of the Ag layer has been converted to AgCl, while the total Ag layer has been converted to AgCl for a 5 min immersion, as shown in figure 3.16b. Moreover, the AgCl layer of figure 3.16b is no longer attached to the substrate (glass substrate and a Ti adhesion layer), as all the silver deposited on the adhesion layer has been converted to AgCl. This chemically deposited AgCl layer seems to be adequate for our application (good adherence for the 1 min. immersed layer). However, this method has one main drawback for the fabrication of our systems: the current and the voltage electrodes, being on the same substrate, require an additional photolithographic process in order to protect from chlorination both the current electrodes and the silver pad used for wire bonding to the PCB.

- Galvanostatic deposition:

  The galvanostatic as well as the potentiostatic deposition in NaCl solution is based on the following reactions [81]:

  At the anode:

$$Ag \rightarrow Ag^+ + e^-$$
$$Ag^+ + Cl^- \Leftrightarrow AgCl$$

At the cathode:

$$Na^+ + e^- \rightarrow Na$$
$$2\ Na + 2\ HOH \Leftrightarrow 2\ NaOH + H_2 \uparrow$$
$$NaOH \Leftrightarrow Na^+ + OH^-$$

Different deposition parameters are tested in the literature [77, 82-85]. We chose to use a NaCl 1 M solution as Cl containing media and a Pt counter-electrode. The controlled current was supplied by a galvanostat (EG&G 263A) and a measurement of the applied voltage was achieved via a multimeter (HP 34401A). Figure 3.17 shows the voltage applied by the galvanostat during a controlled chlorination current. First a cathodic current of 10 µA is applied for 10 seconds as a cleaning and activating procedure, followed by 10 seconds with no current and finally an anodic current is applied during 20 seconds. The silver thin film electrode surfaces are 1 mm^2 in size, whereas for the platinum counter electrode, the surface was 25 mm^2. For the characterisation of the chlorination of silver thin film electrodes, we used test structures with silver electrodes of defined surfaces.

We have applied different current densities and deposition times. Figure 3.18 shows SEM photographs of galvanostatically grown silver chloride electrodes.

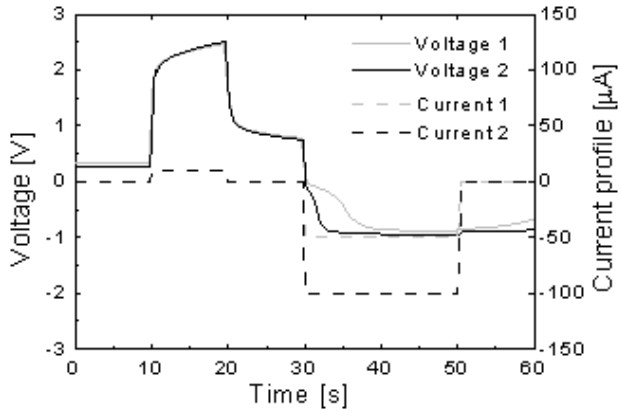

Figure 3.17: Graph showing the voltage applied for a galvanostatic deposition of AgCl on Ag in NaCl (0.1 M) on a 1 mm^2 surface. First, a cleaning and activation 10 µA cathodic current is applied for 10 s, followed by 10 sec without current and finally the deposition anodic current for 20 s (50 µA for experiment 1 and 100 µA for experience 2).

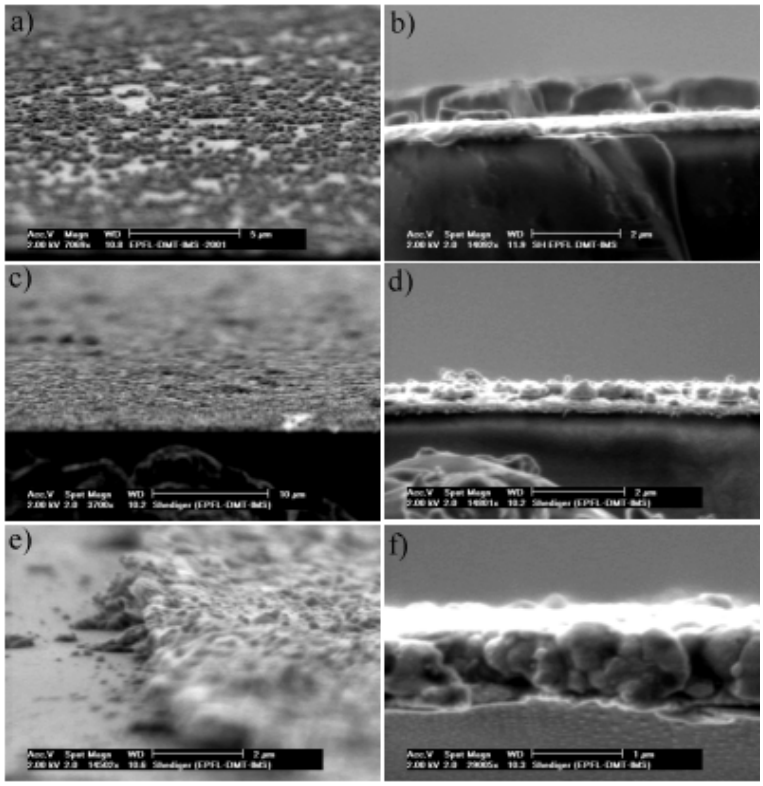

Figure 3.18: SEM photographs showing the surface and the cross-section of thin film silver galvanostatically chlorinated electrodes: a) and b) current density of 2 mA/cm^2. c) and d) 4 mA/cm^2. e) and f) 8 mA/cm^2.

The thin film, before chlorination, has the following composition: Ti/Ag [69] with respective thickness of 20/300 nm. The deposition time for the AgCl has been kept to 20 s. and the current density is varied. One can observe that with increasing current densities, the surface is more and more covered with AgCl until finally the total thickness of the silver layer is consumed.

The chlorination parameters finally chosen as “standard” for a homogeneous AgCl layer on Ag are the following: the current density used is 5 mA/cm^2 for a period of 20 seconds for chlorination of about 30% of the 500 nm thick Ag film

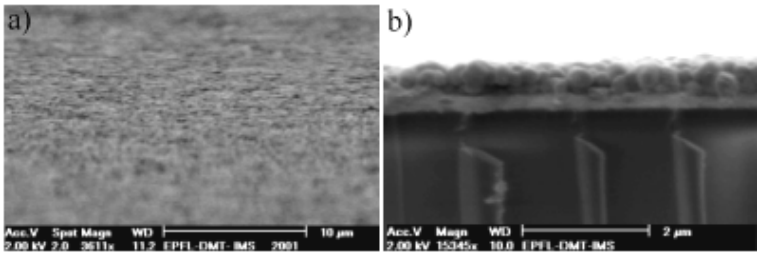

Figure 3.19: SEM photographs showing the surface and a cross-section of a silver chloride electrode galvanostatically grown with the chosen "standard" parameters.

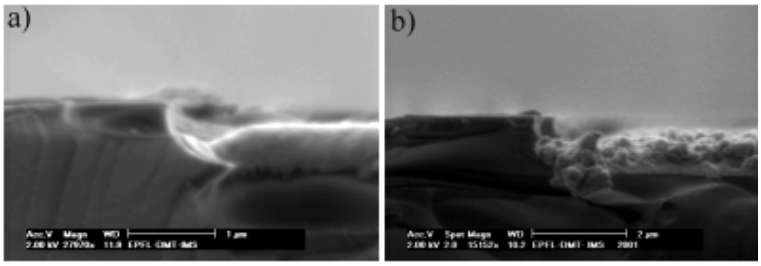

Figure 3.20: SEM photographs showing: a) HF isotropically etched groove with recessed 500 nm thick silver thin film. b) Same sample as for a) after a galvanostatic chlorination with the chosen "standard" parameters.

in NaCl 1 M with a Pt counter electrode. The percentage of silver converted to silver chloride has an influence on electrode stability as well as on electrode adhesion on its substrate, as previously demonstrated [77, 81, 83, 86]. Figure 3.19 shows a silver chloride electrode chlorinated with the above "standard" parameters. Finally, figure 3.20 is a side view of a silver thin film electrode, before and after chlorination. One can identify the HF etched groove in the glass substrate with the recessed deposited thin-film electrode.

- Potentiostatic deposition:

  The potentiostatic method is the most applied method for chlorination of silver electrode for biomedical applications [87]. Macroscopic electrodes (millimetre size silver wire or silver ink) are regularly re-chlorinated

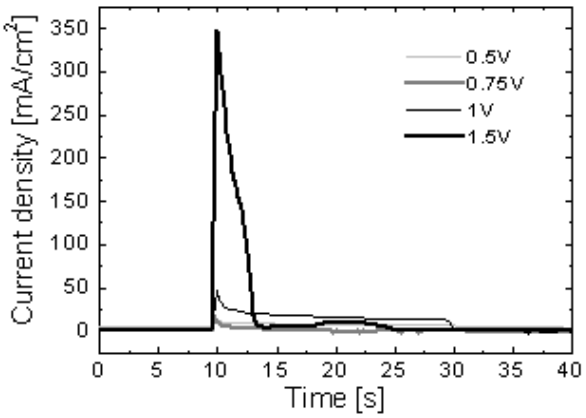

Figure 3.21: Graph showing the current applied for a potentiostatic deposition of silver chloride. Four different voltages have been tested on 1 mm^2 thin film silver electrodes (Ti/Ag 20/500 nm) for a period of 20 s.

using a simple 1.5 V battery in a 1 M NaCl or KCl solution for several minutes. The reactions involved are the same as for the galvanostatic deposition. We have applied this method on our thin films using a potentiostat (EG&G 263A), for better control of the applied potential. The current applied to the system was recorded using a multimeter (HP 34401A). Figure 3.21 shows the current density applied for four different voltages on 1 mm^2 thin film silver electrodes (Ti/Ag 20/500 nm) for a period of 20 seconds. One can observe the particular shape of the current as a result of the charging of the double-layer capacitance as well as ion diffusion into the solution. If this deposition method with variable current works well for bulk electrodes (silver wire shown in figures 3.22 and 3.23), as no control of AgCl thickness is needed, it is unsuitable for thin-film layers where the process has to be controlled such as to avoid the conversion of the total Ag thickness to AgCl.

Figure 3.22: Optical photographs showing 3 steps of the potentiostatic chlorination of a silver wire with 1.5 V applied for 60 s. in NaCl 1 M.

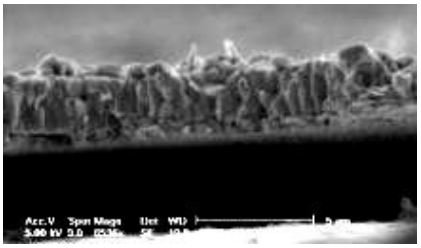

Figure 3.23: SEM photograph showing the 4 µm thick AgCl layer (partially detached from the silver wire during the cutting of a section of the wire) potentiostatically grown with 1.5 V during 60 s. in NaCl 1 M.

3.4 TWO-ELECTRODE AC IMPEDANCE MEASUREMENTS

3.4.1 INTRODUCTION

The Electrochemical Impedance Spectroscopy (EIS) experiment is based on the application of a AC potential and the measurement of the corresponding current [68, 69, 88, 89]. A very small sinusoidal potential (5 to 10 mV peak-to-peak amplitude) is applied to the electrochemical cell and the resulting AC current is measured. The result of this measurement is the impedance of the electrochemical cell over a wide frequency range (from 1 mHz to 1 MHz). The final goal of this experiment is to elaborate an equivalent electronic model and to correlate that

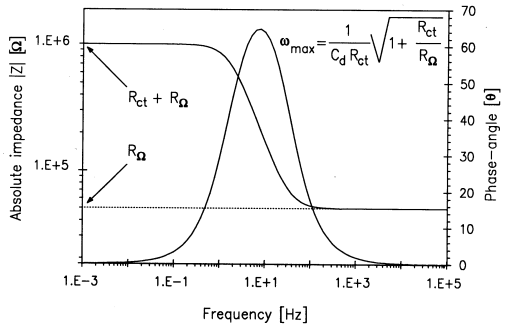

Figure 3.24: Simulated AC impedance measurement Bode plot of the simple circuit shown in figure 3.5 (R_Ω = 50 KΩ, R_{ct} = 950 KΩ, C_d = 100 nF) [69].

model with electrochemical phenomena. The impedance informations as a function of frequency can be represented in different ways:

- Bode plot: it is the standard plot function used to represent a electronic transfer function (for example filters). The absolute impedance $|Z|$ and the phase-angle θ, are plotted as a function of frequency in a log-log plot. Figure 3.24 shows a simulated Bode plot of the simple circuit shown in figure 3.5. One can derive all the component of the circuit on this ideal circuit Bode plot. However, depending on the value of the capacitance and the frequency range of the measurement instrument, some components can not be as clearly derived from the plot.

- Nyquist plot: in electrochemistry, one prefers to use the Nyquist plot, which is a polar diagram. The negative imaginary impedance is plotted versus the real impedance. Figure 3.25 shows a simulated Nyquist plot of the simple circuit shown in figure 3.5. In this ideal circuit case, one can

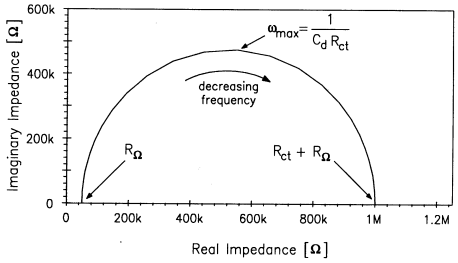

Figure 3.25: Simulated AC impedance measurement Nyquist plot for the same circuit as for figure 3.24 *[69].*

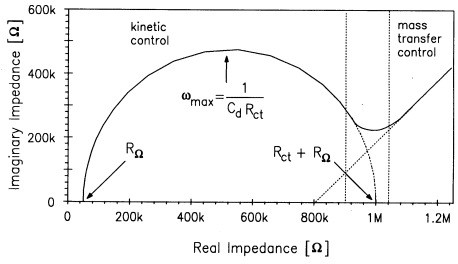

Figure 3.26: Simulated AC impedance measurement Nyquist plot for a diffusion controlled reaction [69].

also derive all the components from this curve. If the electrochemical reaction is diffusion controlled (see section 3.1.3), the Nyquist plot will look more like the one presented in figure 3.26. At low frequencies, the nyquist diagram is reduced to a 45° line.

3.4.2 ELECTROCHEMICAL IMPEDANCE SPECTROSCOPY

EIS measurements were first performed via an impedance analyser, the Hewlett-Packard® HP 4194A with a 100 Hz to 2 MHz frequency range. EIS measurements can be achieved using a Pt counter electrode with a more than 10 times larger surface than the working (to be characterised) electrode. We have chosen to use a symmetrical type of test structure with same working and counter electrodes. Therefore, we have two identical electrode/solution interfaces in series. Figure 3.27 shows the Bode plot of the EIS measurements for Pt, Ag and Ag/AgCl thin film 2 mm^2 electrodes in a NaCl 0.1 M solution. First of all, one can see that much less information can be deduced from this plot than from a simulated Bode plot shown as example in figure 3.24. In fact, the impedance analyser HP4194A does not perform measurements at frequencies lower than 100 Hz, which is too high for obtaining certain informations, like the value for the charge-transfer resistance. Nevertheless, we can observe that the impedance for each of the three electrode materials is, as expected, totally resistive at frequencies higher than 100 kHz. On the other hand, the ohmic resistance (resistance of the electrolyte between the two electrodes) can be derived directly from the plot (about 1 kΩ for our test structures). For the measurements at low frequencies, we can also deduce that the charge-transfer resistance is higher for Pt than for Ag, which is as well higher than for Ag/AgCl, even though no value can be assigned.

Consequently, we have decided to use a more specific set-up for EIS measurements, the Electrochemical Workstations IM6 from Zahner® measurement systems. This set-up allows EIS measurements down to 1 mHz although we decided to stop at 10 mHz (standard value on the used set-up to avoid environmental noise). Figure 3.28 shows the Bode plot for the same electrodes as used for the EIS measurements represented in figure 3.27. One notices that for obtaining the charge-transfer resistance directly from the plot, the measurement should be carried out at yet lower frequencies. However, by having Bode plots four decades of frequency lower than with the EIS measurements achieved via the HP4194A impedance analyser, one can observe a double peak in the phase of the Ag/AgCl electrode, probably due to a double interface with the electrolyte. An adequate fitting can then be achieved (next section) such as to enable the comparison between the different electrical elements of a chosen circuit model for the electrochemical cell and confirm the double interface theory.

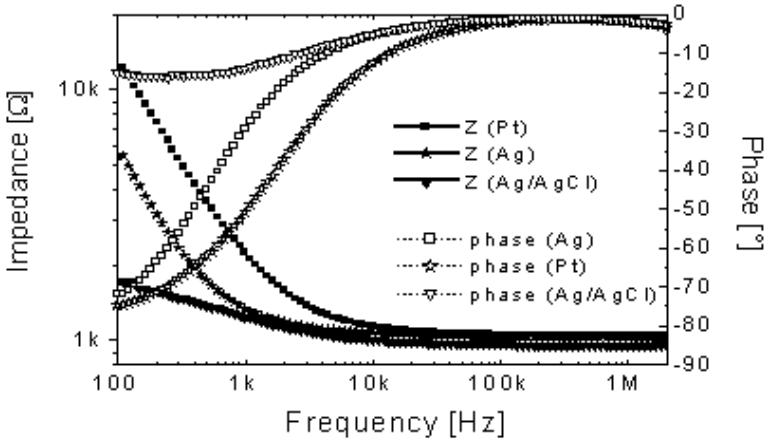

Figure 3.27: Bode plot of the EIS measurement for three different thin film 2 mm^2 electrodes using the HP4194A impedance analyser (100 Hz to 2 MHz).

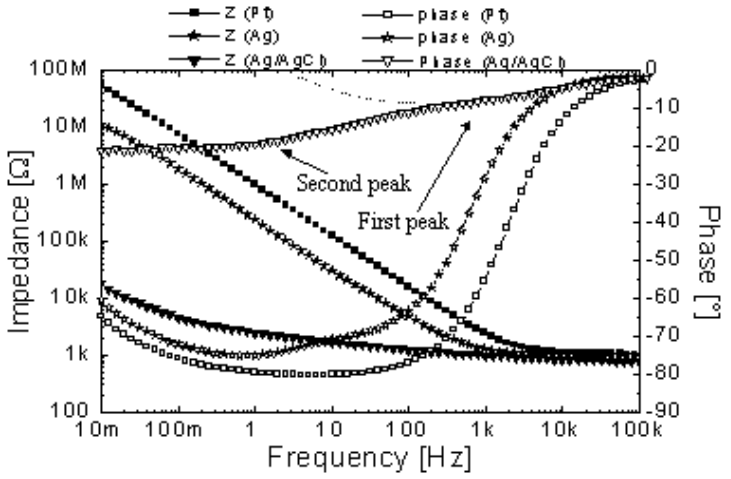

Figure 3.28: Bode plot of the EIS measurement for three different thin film 2 mm^2 electrodes using the Zahner® measurement systems (10 mHz to 100 kHz).

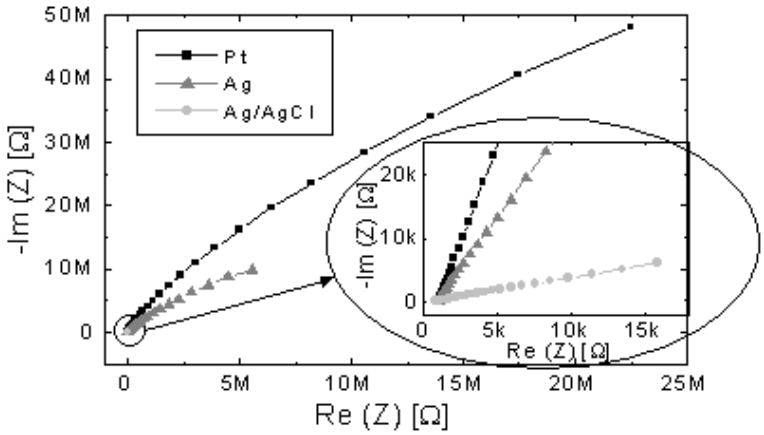

Figure 3.29: Nyquist plot of the EIS measurement represented in figure 3.28. The insert shows an enlargement of the origin region.

Figure 3.29 shows the Nyquist plot of the EIS measurement represented in figure 3.28. Again, the parameters that we wanted to derive from the plot are not directly available as shown on an ideal Nyquist plot exposed in figure 3.25. The loci of figure 3.29 look more like the tail of the locus represented in figure 3.26. However, in many situations, the high-frequency impedance characteristic is not as expected. This phenomenon has been underlined by McAdams in [67], showing that the impedance locus of a solid metal electrode is represented by a straight line at an angle Φ to the real axis and given by the following empirical equation [90]:

$$Z_I = K (j\omega)^{-\beta} \qquad \text{Eq. (3.10)}$$

where K is a measure of the magnitude of Z in ($\Omega s^{-\beta}$), β is a constant which has a value between 0 and 1. The phase angle Φ is related to the fractional power β in the following way: $\Phi = \beta\pi/2$ radians.

Many researchers have tried to explain this phenomenon [91-94], however without real success. The most accepted causes for the frequency dependence of Z_I are specific adsorption and surface roughness effects (Sluyters-Rechbach & Sluyters in [95]). From figure 3.29, one can observe a low value of Φ for the Ag/AgCl electrode, which can be explained by a very large surface area due to the porous AgCl layer [90, 96].

3.4.3 ELECTRICAL CIRCUIT MODEL

After having realized the EIS measurements, we have fitted the obtained curves shown in figure 3.28 using the Thales software which is included in the Zahner® measurement system. This software allows fitting via user defined electrical circuit models composed by the components presented in section 3.1.3, until finding the best appropriate model and components values. Yet a new electrical circuit component has to be introduced based on the considerations expressed in the preceding section: the constant phase element (CPE). Actually, capacitors in EIS experiments often do not behave ideally (the surface under investigation is never completely homogeneous). This lack of homogeneity is modelled with a constant phase element.

$$Z_{CPE} = (j\omega C)^{-\alpha} \qquad \text{Eq. (3.11)}$$

where C is the ideal capacitance, and α is an empirical constant, with values between 0 and 1. If $\alpha = 1$, the CPE acts like an ideal capacitor.

Remark: although two electrode-solution interfaces are present in our electrochemical system, only one interface will be represented in our models as the two interfaces are identical (cf. section 3.4.2).

- Electrical circuit model for Pt and Ag thin films:

The electrical circuit model for a simple electrochemical process as shown in figure 3.5 has been used for the Pt and Ag electrodes, though the capacitor has been replaced by a constant phase element (see figure 3.30).

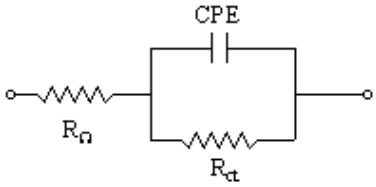

Figure 3.30: Schematic showing the electronic circuit model for Pt and Ag thin films.

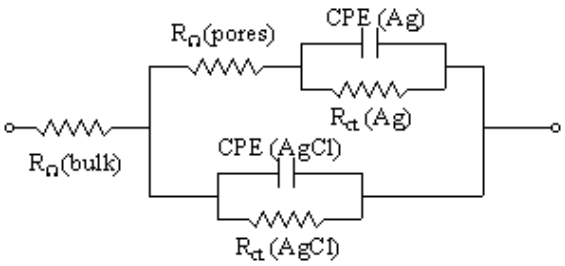

Figure 3.31: Schematic showing the electronic circuit model for a Ag/AgCl thin film.

- Electrical circuit model for Ag/AgCl:

Figure 3.31 shows the chosen electrical circuit model for our Ag/AgCl test electrode. It is composed of an ohmic (bulk) resistance R_Ω representing the resistance of the solution between the two electrodes, followed by two parallel branches. A first branch counts for the Ag-electrolyte interface with an ohmic resistance R_Ω (pores) representing the resistance of the electrolyte in the pores of the AgCl layer (through which the ions have to migrate before reaching the Ag

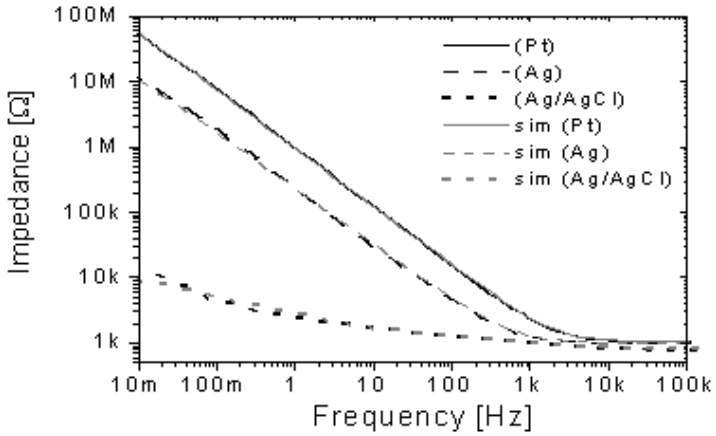

Figure 3.32: Bode plot showing the impedance measurements and the impedance simulations using the respective electrical models for Pt, Ag and Ag/AgCl thin film electrodes.

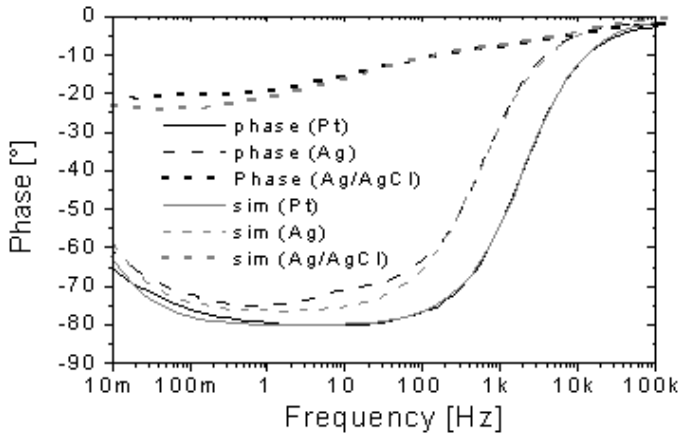

Figure 3.33: Bode plot showing the phase measurements and the phase simulations using the respective electrical models for Pt, Ag and Ag/AgCl thin film electrodes.

surface). A second branch represent the AgCl-electrolyte interface. Both interfaces are composed of a charge transfer resistance in parallel with a constant phase element.

Figure 3.32 and 3.33 show the impedance and the phase of EIS measurements, respectively, and simulation using the respective electrical models for our investigated Pt, Ag and Ag/AgCl thin film electrodes. One can observe that the simulated curves fit quite well the measured values. This does not mean that the models chosen are the only ones for representing our electrochemical systems, especially for the Ag/AgCl system. That model is only one of the possible representations, which we have chosen for closest fitting reasons.

Table 3.2 and 3.3 present the values for each components of, the electrical circuit model for Pt and Ag (figure 3.30), respectively, and the electrical circuit model for Ag/AgCl (figure 3.31), after fitting the experimental EIS measurements. The values presented are qualitative in the way that they depend on the thin film deposition parameters, the cleaning or polishing procedure and on the electrolyte. However, one can see that the charge-transfer resistance is many orders lower than for the Pt and even for the Ag. A way to decrease the value of a metal's charge-transfer resistance is to increase the surface of the electrode. We have performed Atomic Force Microscopy (AFM) experiments to measure the roughness of our electrodes. Figure 3.34 a and b show the AFM measurement for Pt and Ag

Component n°	RΩ	Rct	CPE/α
Pt	1.04 kΩ	169.1 MΩ	77.87 nF / 0.89
Ag	998.5 Ω	33.16 MΩ	249.4 nF / 0.85

Table 3.2: Component values corresponding to the electrical circuit model represented in figure 3.30 for the Ag and Pt electrode EIS simulations.

Compo-nent n°	1 Rct Ag	2 CPE/α Ag	3 Rpore	4 Rct AgCl	5 CPE/α AgCl	6 RΩ
Ag/AgCl	92 kΩ	849 nF/ 0.35	107 Ω	91.3 kΩ	235 nF/ 0.85	800 Ω

Table 3.3: Components values corresponding to the electrical circuit model represented in figure 3.31 for the Ag/AgCl electrode EIS simulation.

thin film electrodes prepared in the same way as for the EIS measurements. The average roughness for those electrodes are almost the same. The difference in charge-transfer resistance (see table 3.2) can therefore not be explained by the difference in roughness. As it will be demonstrated in the next section, Pt is a highly polarisable material and there is virtually no electron transfer occurring at the interface with the electrolyte, no free charge carriers cross the double layer [4]. The Ag electrode can more easily transfer charges to the electrolyte, especially with Cl^-, which implies a lower charge-transfer resistance. Figure 3.35 a and b show respectively Ag/AgCl thin film electrodes, realised with 2.5 and 5 mA/cm^2 applied galvanostatic current for chlorination. The value of roughness represented in table 3.4 show that Ag/AgCl electrodes have a much higher roughnesses than Pt or Ag electrodes, and that the roughness increases with higher deposition cur-

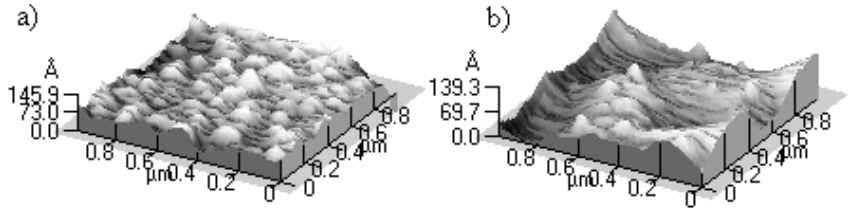

Figure 3.34: AFM measurements on 1 μm^2 of the metal thin film electrodes: a) Pt and b) Ag.

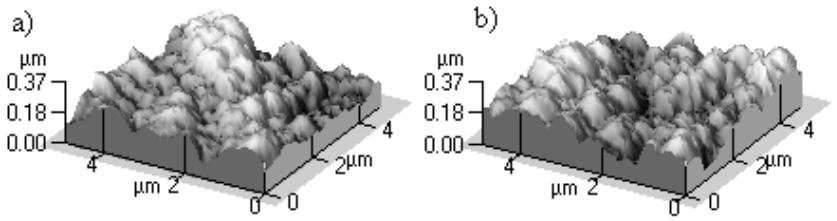

Figure 3.35:AFM measurements on 25 µm^2 of Ag/AgCl thin film electrodes: a) 2.5 mA/*cm^2 and b) 5* mA/*cm^2 as applied galvanostatic current for chlorination.*

Roughness	Pt	Ag	Ag/AgCl 2.5	Ag/AgCl 5
Pk to pk [Å]	100	71	3370	3550
Average [Å]	11	8	483	498

*Table 3.4: Surface roughness for different metal electrodes measured by Atomic Force Microscope (AFM). For Ag/AgCl electrodes, the numbers 2.5 and 5 represent the galvanostatic current applied for chlorination (in m*A/*cm^2*).

rents. This confirms the much larger effective electrode surface of the Ag/AgCl electrode, hence a lower charge-transfer resistance.

However, as AgCl is a poor conductor (resistivity of 10^5 to 10^6 Ωcm) [77], if the chlorination is sufficient such as to create a “closed” AgCl layer (less pores or even no more pores) [97], the surface resistance will start to increase. This effect is underlined in figure 3.36 showing the Bode plot of the EIS impedance measurement for different 1 mm^2 thin film Ag/AgCl and Ag electrodes using the HP4194A impedance analyser (100 Hz to 2 MHz). One can observe that until 3 mA/cm^2, the impedance loci decrease, and for higher galvanostatic deposition current densities, the impedance loci start to increase again. One can also mention that the standard value chosen in section 3.3.2 for the galvanostatic current is in the increasing impedance range. However, we chose our standard value, 5 mA/cm^2, following adhesion and potential stability (pseudo-reference electrode) characteristics which are crucial for our application, more than low impedance electrode characteristics (more decisive for current-carrying applications). Figure 3.37 shows the phase of the EIS measurements presented in figure 3.36. One can

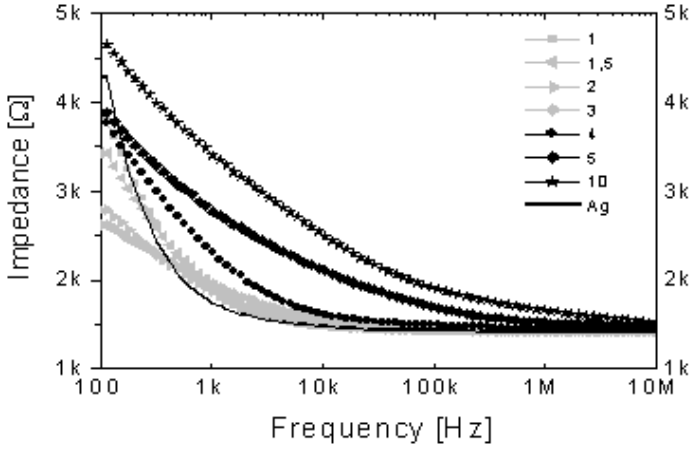

Figure 3.36: Bode plot of the EIS impedance measurement for different 1 mm^2 thin film Ag/AgCl and Ag electrodes using the HP4194A impedance analyser (100 Hz to 2 MHz). The numbers labelling the curves correspond to the current density applied in mA/cm^2 (see section 3.3.2).

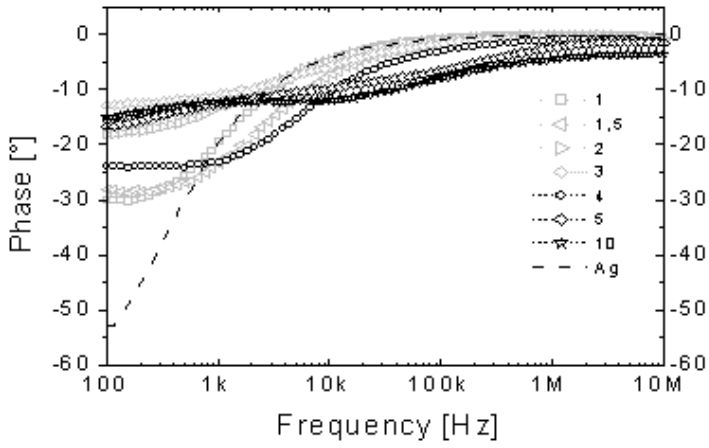

Figure 3.37: Bode plot of the EIS phase measurement corresponding to the impedance measurements of figure 3.36.

observe that starting with more than 3 mA/cm^2, the phase show the double peak characteristic of a double interface with the electrolyte.

3.5 CYCLIC VOLTAMETRY

3.5.1 INTRODUCTION

Cyclic voltammetry (CV) [4, 69, 70, 98, 99] is an electroanalytical technique for rapidly observing the redox behaviour of a compound over a wide potential range. It consists in the measurement of the current which flows at an electrode as a function of the cycled potential applied to the electrode, the result being represented in a voltammogram.

Practically, the potential of the working electrode (WE) is controlled versus a reference electrode (RE), the potential of which is known and constant (+ 197 mV for a silver/silver chloride reference electrode in 3 M NaCl) via a potentiostat. We have to consider the ohmic drop (IR drop) between the RE and the WE which will give rise to a shift in the actual potential of the WE. Thus, the WE and RE have to be positioned as close as possible. Also, we have chosen to compensate this ohmic drop using a software's option. A counter or auxiliary electrode (CE) such as carbon or platinum is used in our case, to close the current circuit. Figure 3.38 presents the experimental set-up for a CV experiment. We have used an EG&G 263 A Potentiostat/Galvanostat instrument with the PowerCV^{TM} software from PerkinElmer^{TM} instruments for CV experiments. Figure 3.39 shows a typical excitation signal for cyclic voltammetry, a linear potential scan with a triangular waveform with switching potentials at E^- and E^+ versus a Ag/AgCl reference

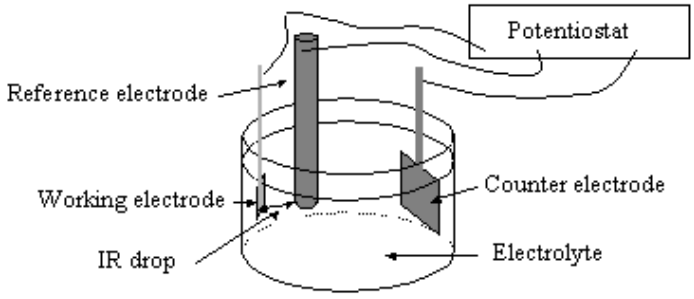

Figure 3.38: Schematic showing the CV experimental set-up (modified from [99]).

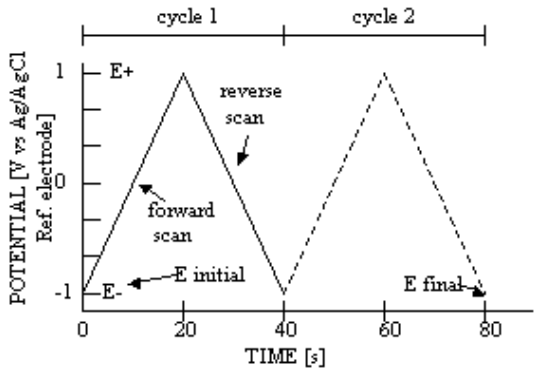

Figure 3.39: Graph showing a typical excitation signal for cyclic voltammetry, a triangular potential waveform with switching potentials at -1 and 1 V versus a Ag/AgCl reference electrode (modified from [99]).

electrode, which is applied in between the working and the reference electrode. The switching potentials are set depending on the reaction we want to observe. The scan rate (100 mV/s as standard value) has an effect on the size of the current peaks. Clearly the voltammogram will take longer, as the scan rate is decreased. Therefore the size of the ion-depleted diffusion layer above the electrode surface will be different depending upon the voltage scan rate used. In a slow voltage scan, the diffusion layer will grow much further from the electrode in comparison to a fast scan. Consequently the ion flux to the electrode surface is considerably smaller at slow scan rates than it is at faster rates. As the current is proportional to the flux towards the electrode, the magnitude of the current will be lower for slow scan rates than for high rates. Multiple cycles can be applied, and the electrode surfaces can be covered with a passive film as an oxide. We have performed cyclic voltammetry experiments on Pt, Ag and Ag/AgCl thin films.

3.5.2 EXPERIMENTS ON DIFFERENT ELECTRODES

- Pt thin film electrode:

  It was often claimed in the past that Pt is an inert material and does not undergo oxidation. But it was demonstrated, using cyclic voltammetry, that it is not the case in reality [98]. This can be observed in the cyclic voltammogram of figure 3.40, where a Pt thin film is used as WE, a large Pt wire as CE and NaCl 0.1 M as electrolyte. The observed peaks are due to the oxidation and reduction of Pt at the surface of the electrode and to

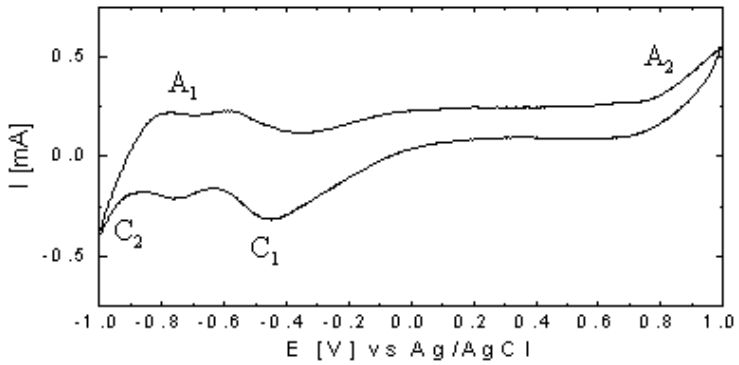

Figure 3.40: Graph showing the fifth cycle of a cyclic voltammetry experiment in 0.1 M NaCl for a Pt thin film, scan rate = 100 mV s^{-1}.

the reactivity of the electrode towards hydrogen oxidation and reduction [69, 79, 100]. The first anodic peak A_1 is a result of the oxidation of adsorbed hydrogen (several peaks), while the second one, A_2, is the formation of adsorbed oxygen and platinum oxide layers. During the backwards scan, the first cathodic peak encountered C_1 is the reduction of the oxide layers and the second one C_2 is for the reduction of adsorbed hydrogen (several peaks). The adsorption phenomena are very sensitive to the electrode surface. Therefore cyclic voltammograms are quite irreproducible for Pt. A pre-treatment is needed to obtain constant responses. A chemical cleaning (hot nitric acid) can be applied, although not for biosensor applications. Instead, a pre-polarisation step can be used at low negative voltage near the C_2 peak. However, as it will be shown further in this section, the currents involved in the reactions with Pt are quite low in proportion to other metals like Ag, thus making Pt a strongly polarisable electrode material.

- Ag and Ag/AgCl thin film electrode:

Figure 3.41 shows the cyclic voltammogram of a silver thin-film electrode in a NaCl 0.1 M solution. The main process occurring in this triangular scan is the formation and reduction of a AgCl film on the Ag electrode. During the anodic scan, the excess electrons are given off at the cathode (Pt electrode) and reduction takes place, whereas at the positive Ag electrode, the excess electrons are collected, and oxidation occurs. This giving and taking of electrons creates an electric

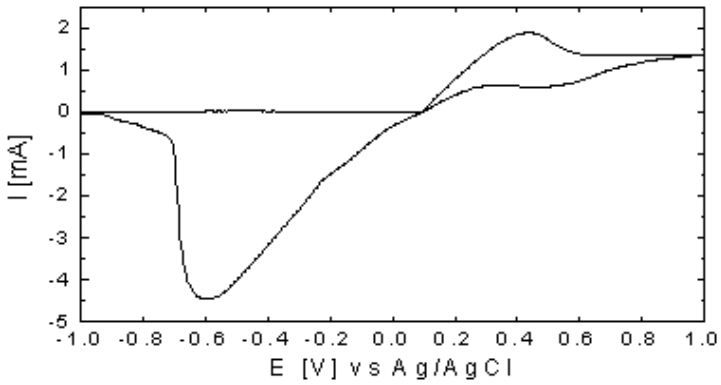

Figure 3.41: Graph showing the fifth cycle of a cyclic voltammetry experiment of a Ag thin film electrode in 0.1 M NaCl, scan rate = 100 mV s^{-1}.

current [101-103]. When scanning to positive potentials, the process starts at E^0=220 mV vs NHE under the following reaction (there is a slight shift to a more positive potential probably due to a bad IR drop compensation):

$$Ag_{(film)} + Cl^- \rightarrow AgCl_{(film)} + e^-$$

During the back scan to negative voltage (starting again at 220 mV vs NHE), the AgCl layer starts to decompose and Ag precipitates in the solution.

$$AgCl_{(film)} + e^- \rightarrow Ag \downarrow + Cl^-$$

The integration of the curve for higher potentials than 0 V vs Ag/AgCl is equal to the integration of the curve for lower potential than 0 V vs Ag/AgCl. This underlines the reversibility of the reaction as the same amount of charge is involved for increasing and decreasing potentials. Actually, Ag/AgCl electrodes are reversible electrodes of the second kind, which means that they have a solid phase in the form of a sparingly soluble salt in equilibrium with a saturated solution of this salt participating in the electrode reaction [97].

Remark: Ag and AgCl electrodes show identical voltammograms under the same conditions as they undergo the same reactions (except for the negative potentials of the first cycle of the Ag/AgCl electrode).

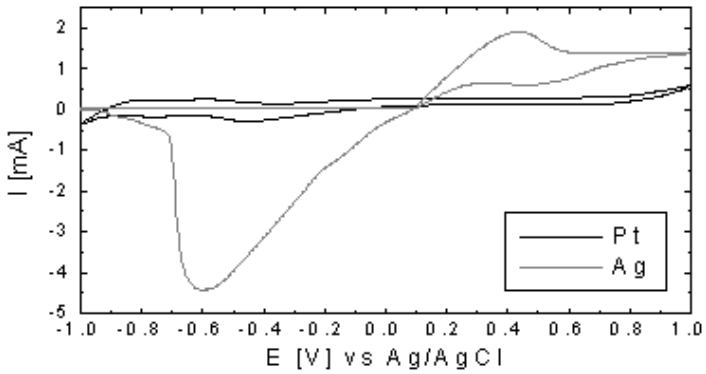

Figure 3.42: Graph showing the fifth cycle of a cyclic voltammetry experiment in 0.1 M NaCl for Pt and Ag thin films, scan rate = 100 mV s^{-1}.

Figure 3.42 shows the Ag and Pt voltammogram using the same current scale. The Pt shows a very flat voltammogram over a wide potential range and almost no electron transfer occurs, i.e. no free charge carriers cross the double-layer or flow in the solution. Pt is therefore a strongly polarisable electrode material, in contrast with a Ag/AgCl which is a non-polarisable electrode [4].

3.5.3 POTENTIAL STABILITY OF ELECTRODES

Figure 3.43 shows the voltage response to ± 1 µA, 1 s controlled input current pulses followed by a 2 s no-current rest time for three different electrode materials in a test device filled with a NaCl 0.1 M solution. The application of such current pattern is standard for the measurements of the transepithelial resistance and transepithelial voltage of epithelial cell mono-layers. One can observe the better response to the input current for Ag/AgCl electrodes compared to Ag and Pt electrodes. The potential at a Ag/AgCl electrode is defined by the Cl^- activity of the solution as exposed in section 3.2, that is to say, two Ag/AgCl electrode in the same solution will have an almost zero millivolt bias potential [77, 83, 84]. On the contrary, Ag and Pt electrodes do not have a well defined potential in solution [4], whereby, the bias potential without input current in the cell is unstable and fluctuating over several millivolts as shown in figure 3.44. As we want the voltage changes in a real cell experiment to be a response to transepithelial currents (Ite) flowing through the cell membrane, one can easily understand the preferred choice of Ag/AgCl as an electrode material for potential measurement.

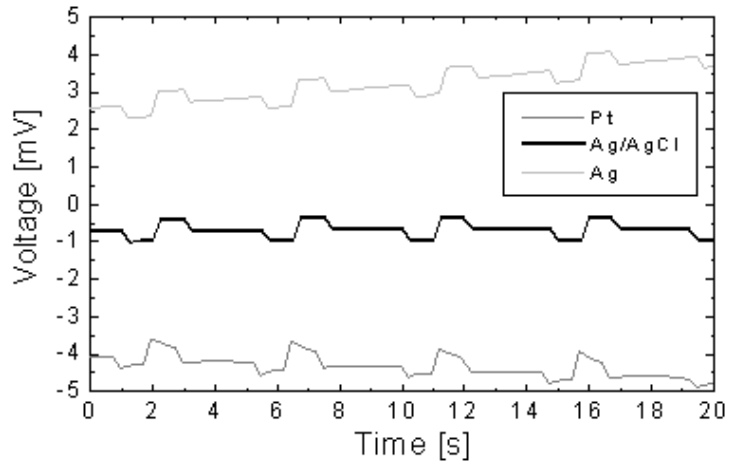

Figure 3.43: Graph showing the voltage response to ± 1 µA and 1 s current pulses for three different electrode materials.

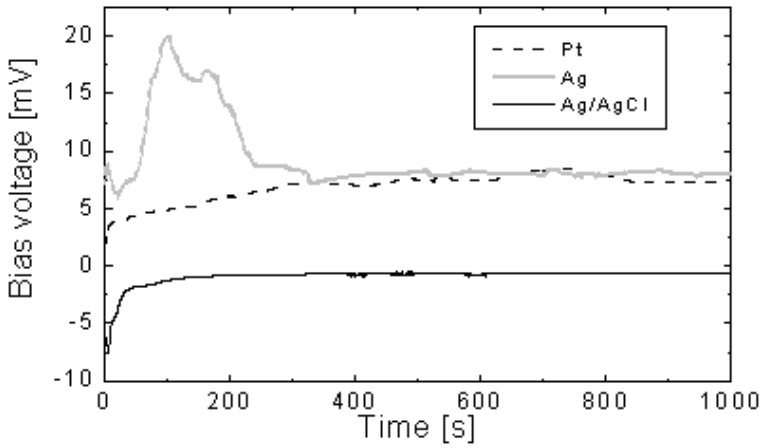

Figure 3.44: Graph showing the bias voltage between two identical thin film electrodes for Pt, Ag and Ag/AgCl in 0.1 M NaCl.

Figure 3.45 is a graph showing the theoretical (according to Nernst equation (eq. 3.7)) and experimental Cl^- concentration dependence of the potential of a Ag/AgCl thin film electrode versus a normal hydrogen electrode (NHE). One can

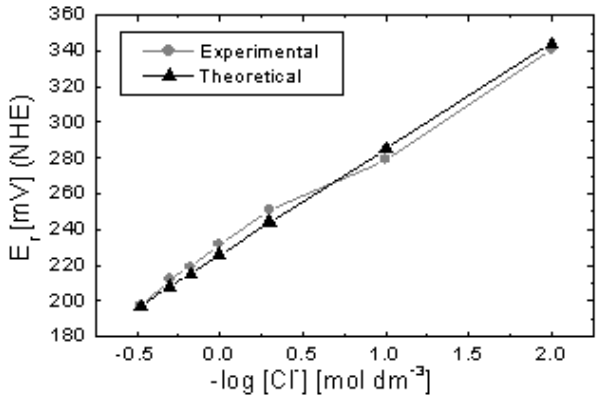

Figure 3.45: Graph showing the theoretical (according to Nernst equation (see eq. 3.7)) and experimental Cl^- concentration dependence of the potential of a Ag/AgCl thin film electrode versus a normal hydrogen electrode (NHE) in NaCl solutions.

observe a good potential behaviour of our thin film electrode as the experimental results follow quite smoothly the theoretical values. After having demonstrated the good potential properties of our silver/silver chloride electrodes, one important point to characterise is the lifetime of those electrodes.

The evolution in time of the bias voltage between two identical thin film Ti/Ag/AgCl electrodes in 0.1 M NaCl is show in figure 3.46. On this graph, a nice stable curve at zero millivolt can be seen, until about 7 days when a severe drift of bias voltage occurs before loss of electrical contact. We have found out that the problem came from non-adhesion of the Ag/AgCl thin film on its Ti adhesion layer. When a substantial portion of the AgCl layer is detached from the Ag layer, some portions remain working as the Ag/AgCl electrode, while other portions show a mixed potential derived from equilibrium relations other than Ag/AgCl [104]. Actually, if two or more electrochemical reactions are involved at the interface, a mixed potential is observed and a nonequilibrium state arises, which can explain the sudden drift of potential shown in figure 3.46 before the complete loss of adhesion. We were already using Ag/AgCl electrode with less than 30% of Ag converted to AgCl, which had proved to be the best for a good adhesion as explained in section 3.3.2. To extend the lifetime of the electrodes, we decided to work on the adhesion layer. Previously published results [69] were reported on adhesion layers for Ag/AgCl thin film electrodes. It was shown that the best adhe-

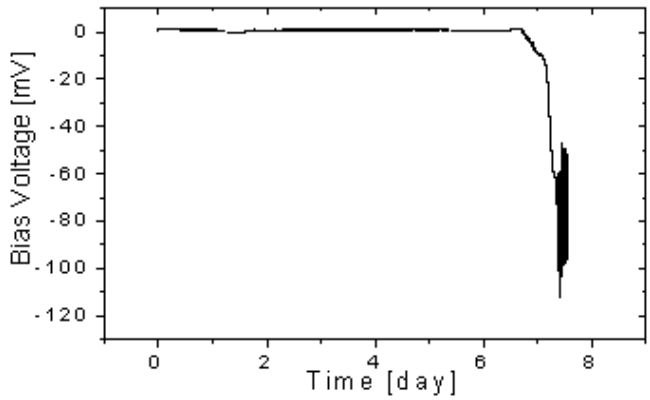

Figure 3.46: Graph showing the evolution in time of the bias voltage between two identical thin film electrodes in Ti/Ag/AgCl in 0.1 M NaCl.

sion layer was a Ti/Pd bilayer. The adhesion problem will be more developed in the next section. After realising Ti/Pd/Ag/AgCl thin film electrodes, the same voltage stability experiment was performed. The results presented in figure 3.47 show less than 1 mV bias voltage for more than 40 days in solution. The insert in figure 3.47 is an enlargement of three days of the first week of experiment. The first 24 days of the experiment were performed under daylight conditions, while for the following days, an opaque box was covering the electrochemical cell. One can easily remark that there's a one day period variation in day light conditions, variation not to be seen when the electrochemical cell is in the dark. The low peaks correspond to the time of the day when the sun rays arrive directly on the experiment's table. As, the temperature nearby the experiment was measured and no variation was observed (air conditioned laboratory), we thought of a probable photovoltaic effect which will as well be discussed in the next section. However, even with controlled conditions (temperature and light), there can still be offsets up to 0.5 mV, due to geometrical or electrochemical dissymetries in the devices.

We have now shown that a thin film Ti/Pd/Ag/AgCl electrode of our fabrication can stand more than 40 days in a 0.1 M solution (which is comparable in terms of Cl^- concentration to the physiological solution) without voltage drift (less than 1 mV). This result is encouraging for the linear device which is disposable, and even more for the modular device which is re-usable and has to stand several times 4-8 days of culture in physiological solution.

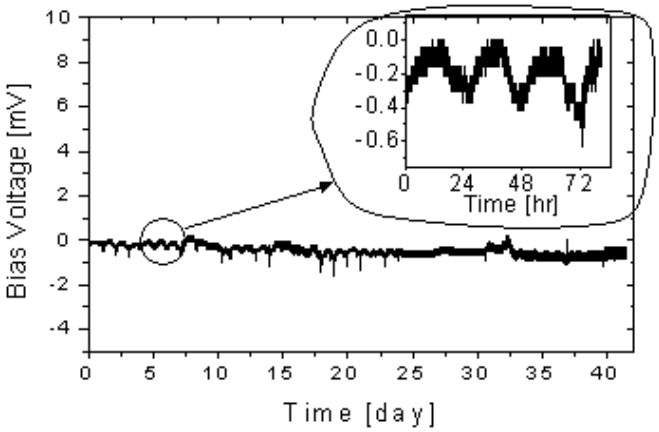

Figure 3.47: Graph showing the evolution in time of the bias voltage between two identical thin film electrodes in Ti/Pd/Ag/AgCl in 0.1 M NaCl. The insert is an enlargement of three days showing a day period variation.

3.5.4 CAUSE OF VOLTAGE INSTABILITIES

- Thermal effect:

  The Nernst equation (eq. 3.7), determining the potential of an electrode in solution, is temperature dependent [87]. As an example, if there is a change from 20 °C to 40 °C in a NaCl 0.1 M solution, the potential of an Ag/AgCl electrode will change from V=278.15 mV to V=282.13 mV. However, we use a voltage differential measurement between two Ag/AgCl electrodes for our application. Consequently, both electrodes should theoretically undergo the same drift. We have heated an electrochemical cell (two thin film Ag/AgCl electrodes in a NaCl 0.1 M solution) with a hot air gun for 10 second sequences. The temperature was measured just above the solution, and does not correspond to the temperature of the solution. The drift that can be seen on figure 3.48 corresponds to the difference of drift undergone by both electrodes. Even in an ambient temperature of 40 °C (the incubator that will be used for cell culture is at 37 °C), the drift is less than 1 mV, which is insignificant for our application. Although it can't be seen on the graph, when the temperature was maintained for longer periods than 10 seconds, such as 10 minutes, no further increase in drift was observed.

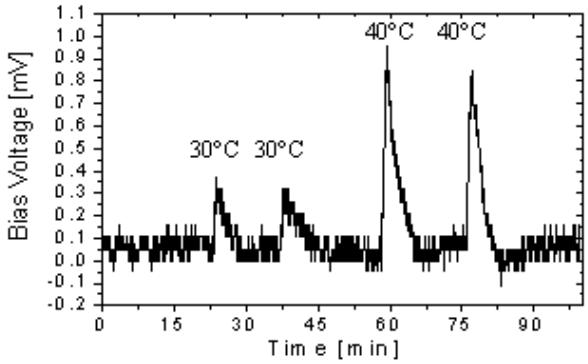

Figure 3.48: Graph showing the bias voltage response to temperature peaks in a NaCl 0.1 M solution.

- Light effect:

  As AgCl is photoreactive to ultraviolet light [81, 97], the colour of the electrode after chlorination depends on the amount of light present during preparation. The less light, the darker the electrode becomes. No lifetime nor stability dependence on the colour of the electrode was observed.

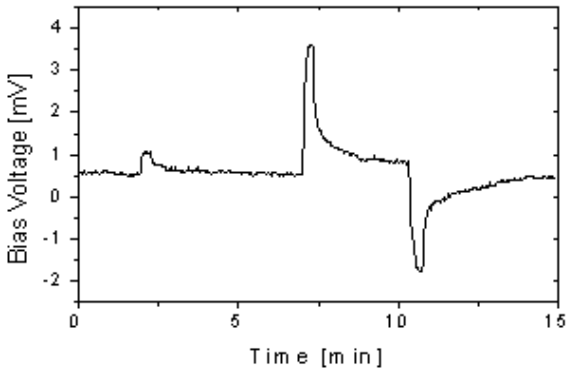

Figure 3.49: Graph showing the bias voltage response to UV light in a NaCl 0.1 M solution. The first peak is the response to UV light on both electrodes, as the second and third peak are the response to UV light on one of the electrodes only.

AgCl decomposes in presence of UV light [81]. As used in photography, light causes the following chemical reaction producing silver metal (black spot on the film):

$$AgCl + h\upsilon \rightarrow Ag_0 + Cl_2$$

But as shown on figure 3.47 where the first 24 days were measured under natural light, no damage or consequence on stability is observed. A photovoltaic effect [81, 97] of AgCl can as well be measured. Figure 3.49 shows the bias voltage response to UV light on our electrochemical cell. The first peak corresponds to the voltage drift difference, when both electrodes are illuminated with a UV light source, and the second and third peaks are the response to UV light on one of the electrodes. As for the thermal effect, the differential drift is less than a millivolt and is insignificant for our application.

- Non-adhesion of thin film electrode:

As mentioned in the preceding section, we have observed a degradation of the adhesion of the Ag/AgCl film after more or less one week in chlorine solution, as shown in figures 3.50 and 3.51.

It was then demonstrated (see figure 3.47) that, with the inclusion of a Pd layer between the Ti and the Ag layer, the electrode was stable for a much longer period of time. A few reasons for this change of behaviour were advanced by

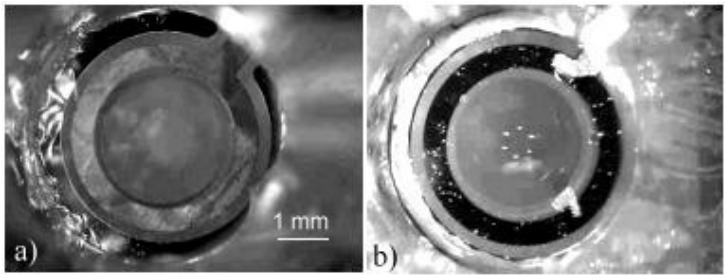

Figure 3.50: Optical photograph showing the top reservoir of a linear device. One can observe the Ti/Ag current electrode (external one) and the Ti/Ag/AgCl voltage electrode (inner one) around the culture site. a) before use. b) after a 7 days culture, the Ag/AgCl layer of the voltage electrode has peeled off the Ti layer.

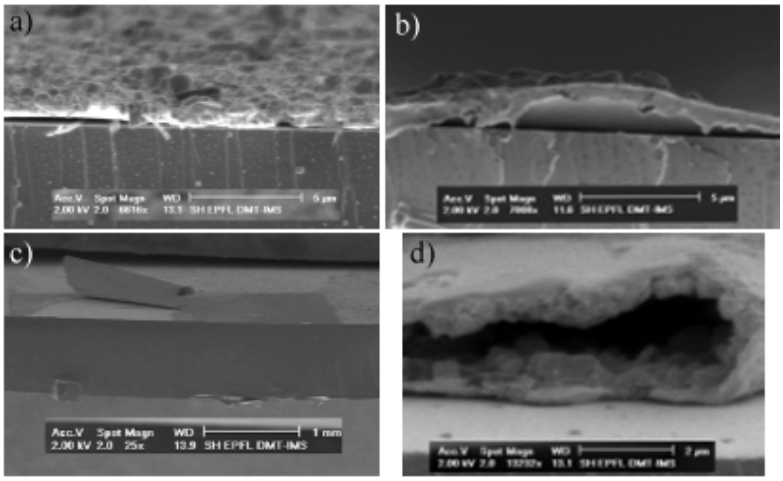

Figure 3.51: SEM photographs showing detached Ti/Ag/AgCl electrodes.

Lambrechts *et al.* [69]. They relate the excellent corrosion resistance to a modification of the anodic potential of the active metal (Ag) by the introduction of Pd, thereby forming a passive oxide with exposure to an electrolyte. Moreover, Pd serves as diffusion barrier for oxygen and moisture, inhibiting the corrosion of the Ti layer, hence preserving the adhesion of the Ag film.

A mechanical “scratch” test was used to compare the adhesion of the Ag/AgCl film on its adhesion layer. Figure 3.52 and 3.53 are optical photographs showing the results of the scratch test on a Ag/AgCl electrode after 7 days in a NaCl 0,1 M solution, respectively with Ti and Ti/Pd as adhesion layers. One can observe that for the Ti/Ag/AgCl, the whole Ag/AgCl layer is peeled off the Ti

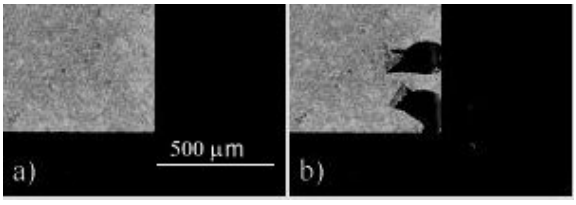

Figure 3.52: Optical photograph showing a Ti/Ag/AgCl test electrode: a) after 7 days in a NaCl 0.1 M solution, b) same electrode after a slight scratching with a tip, the Ag/AgCl layer is peeling off the Ti layer.

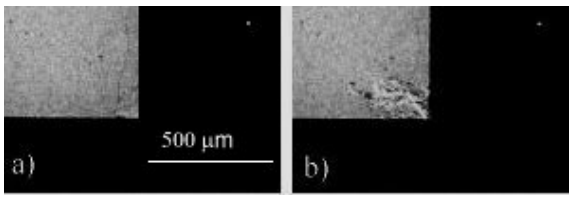

Figure 3.53: Optical photograph showing a Ti/Pd/Ag/AgCl test electrode: a) after 7 days in a NaCl 0.1 M solution, b) same electrode after a slight scratching with a tip, a part of the Ag/AgCl layer is damaged but no peeling is occurring.

layer (although difficult to distinguish on this figure, but can be seen better in figure 3.50), whereas with the introduction of a intermediate Pd layer, the Ag/AgCl layer can be mechanically damaged locally but without loss of adhesion.

- Evaporation of the physiological solution:

As the top reservoirs of our devices are uncovered, evaporation occurs, leading to a difference in ion concentration between the top and the bottom reservoirs, thus giving rise to an offset in voltage measurements as well as osmotic imbalance on the cell level. On the other hand, cell culture is performed after introducing our devices in a Petri dish (to avoid bacterial contamination) and then in an incubator saturated with water (see section 1.1.3); consequently very little evaporation takes place during cell culture. Nevertheless, during the cell culture experiments presented in the next chapter, both the solution in the top reservoir and in the bottom channel was replaced every two days.

Yet the evaporation was characterised in a Petri dish but in more unfavourable conditions (laboratory conditions, 22 °C and approximately 30% of humidity). Figure 3.54 shows the bias voltage response during 6 days for one culture site of three linear devices filled with a NaCl 0.1 M solution. After three days, the solutions were replaced in the top reservoirs, with the bias voltages showing sudden increase to approximately 0 mV. One can observe that, even in those unfavourable conditions, the offset due to evaporation is less than 5 mV. Moreover, in our experiment without cell layer, the voltage stability is favoured by the diffusion of NaCl from the top to the bottom reservoir during evaporation, by which the concentrations are balanced again.

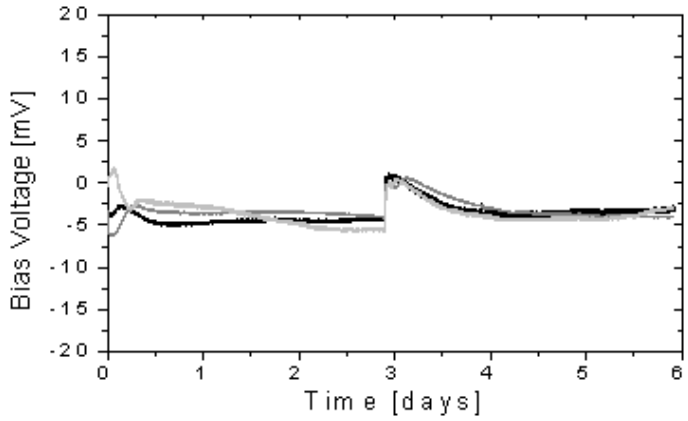

Figure 3.54: Graph showing the bias voltage response during 6 days for one culture site of three linear devices filled with a NaCl 0.1 M solution. The solution was replaced in the top reservoirs after three days.

3.6 CELL CULTURE DEVICE RESISTANCE

In this section, only the linear and the modular devices will be characterised in terms of resistance of the cell culture sites without cell, as both of them are final versions, incorporating all improvements mentioned before (for example the voltage stability).

3.6.1 LINEAR DEVICE

Figure 3.55 shows the resistance of the culture sites of four linear devices with 1 mm of diameter sites and voltage Ti/Pd/Ag/AgCl electrodes, filled with NaCl 0.1 M. The measurement set-up used is the DC four-point set-up (see section 3.2.2). The resistances of the culture sites without cells are quite reproducible with a mean value of 2.15 kΩ. The small deviations are due to geometrical differences on each culture site. Actually, the size of each culture site is defined primarily by a moulded PDMS layer with four holes (see figures 2.27d and 2.29a) and secondly by a proper gluing of the membrane; as a result, there can be slight differences in surface of free polycarbonate membrane.

In order to confirm the right choice for the design of the bottom common current and voltage electrode (see figure 2.27b), we have tried three new configura-

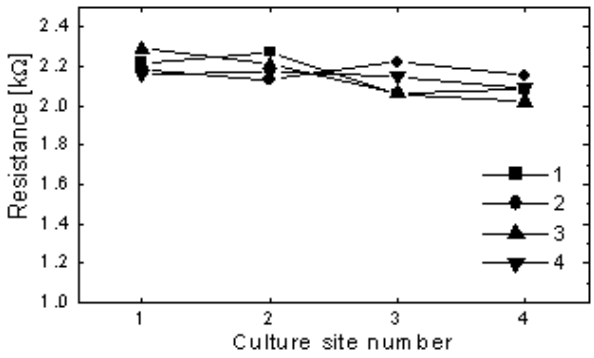

Figure 3.55: Graph showing the resistance of the culture sites of four linear devices with 1 mm of diameter sites and voltage Ti/Pd/Ag/AgCl electrodes, filled with NaCl 0.1 M.

tions. Figure 3.56 presents a schematic of the four bottom electrode configurations we have tested, configuration a) being the standard one for the linear device. Figure 3.57a shows the resistance of the four culture sites of four linear devices with 1 mm diameter sites, voltage Ti/Pd/Ag/AgCl electrodes, but with different bottom electrode configurations. One can observe that except for configuration a) where the electrodes pass under each culture site, the further the culture site is from the electrodes, the higher resistance is measured. This is typical as the pathway through the bottom channel is longer, hence the ohmic resistance is higher (although negligible after cell culture compared to the resistance of the cell layer). The tendency is even more obvious in figure 3.57b where a correction was applied on the resistance of culture site n° 2 after having optically measured the surface of each culture site, culture site n° 2 being slightly larger than the others. This clearly

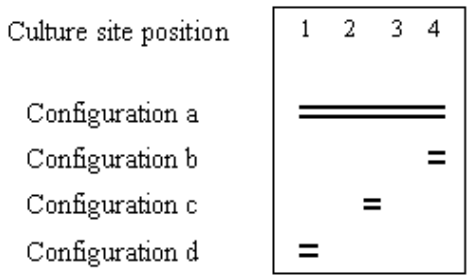

Figure 3.56: Schematic description of bottom electrode configurations.

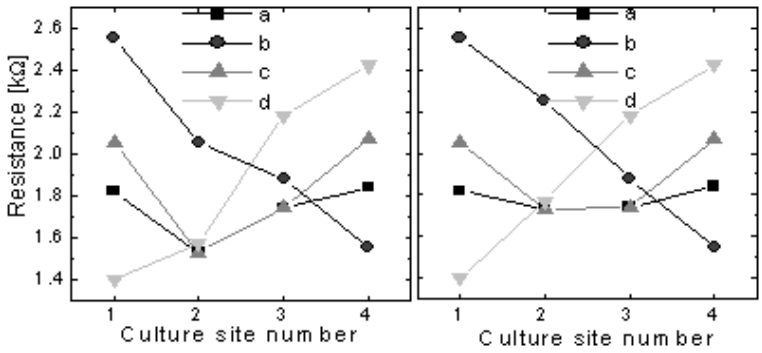

Figure 3.57:a) Graph showing the resistance of the four culture sites of four linear devices with 1 mm diameter sites, voltage Ti/Pd/Ag/AgCl electrodes but different bottom electrode configurations a, b, c and d. b) Same graph as a) but with a correction on site number two due to a difference of site surface compared to the others.

confirms the choice of configuration a) for a better uniformity of resistance for the four culture sites.

3.6.2 MODULAR DEVICE

Figure 3.58 shows the resistance of the culture sites of three modular devices with voltage Ti/Pd/Ag/AgCl electrodes. Two devices used with 1 mm diameter sites and one device with 3 mm diameter sites are measured. As for the linear device, the resistance of the culture sites without cells are quite reproducible with a mean value of 2.25 kΩ for the 1 mm of diameter sites. When using 3 mm of diameter sites, the resistance decreases to 1 kΩ. This shows that the main contribution to the resistance of a culture site without cell is the size of the culture site itself, as its cross-section is the smallest in the whole current path from the bottom to the top electrodes.

3.6.3 POLYCARBONATE MEMBRANE

The polycarbonate porous membrane, basis for the cell culture, has been electrically characterised using the set-up presented in the insert of figure 3.59 and the HP 4194A impedance analyser. One measures 3 Ohm at 1 MHz for a surface of 16 mm^2. So even with a surface of 0.785 mm^2 (surface of one cell culture site of the linear device), the membrane resistance without cell is about 60 Ohm,

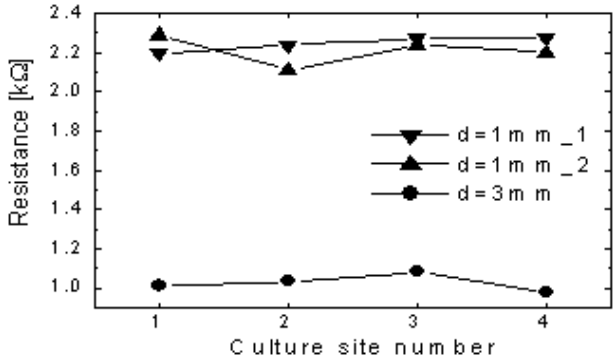

Figure 3.58: Graph showing the resistance of the culture sites of three modular devices with voltage Ti/Pd/Ag/AgCl electrodes. Two devices were used with 1 mm of diameter sites and one device with 3 mm of diameter sites.

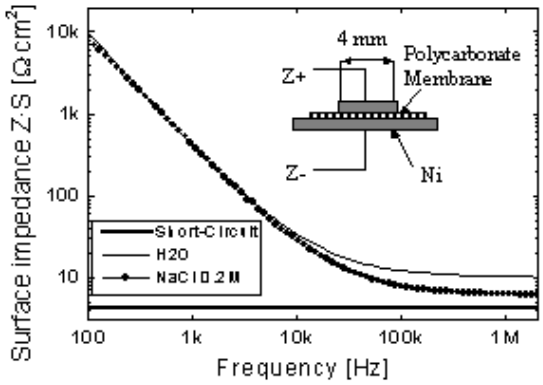

Figure 3.59: Graph showing the frequency dependent two-point impedance measurement of a polycarbonate membrane with 0.4 μm pores and a surface area S = 16 mm^2. We used two flat Ni electrodes to have the electrical field perpendicular to the membrane and distilled water and NaCl 0.1 M solution (ρ ≅ 60 Ω cm) as pores filling solution.

which is negligible with respect to the resistance value of a device. This is confirmed with a measurement done in the linear device with silver/silver chloride electrodes, using the same NaCl 0.1 M solution (the resistivity of which is com-

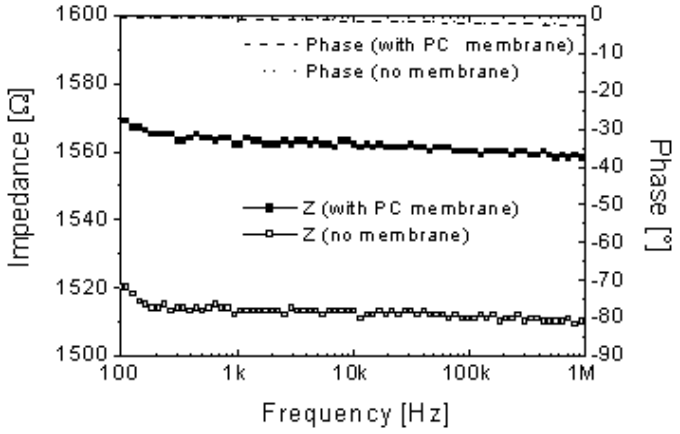

Figure 3.60: Graph showing the frequency dependent two-point impedance measurement of a culture site of a linear device with and without the polycarbonate membrane.

parable to the physiological solution resistivity). One can observe on figure 3.60 that the phase with or without the membrane is almost zero, giving the indication that the impedance is a simple resistance. The difference between the impedance curve shape in figure 3.59 and 3.60 are due to the very low surface impedance of silver/silver chloride electrodes used for the measurement of figure 3.60. We can measure a resistance difference of about 60 Ohm as expected for a surface of 0.785 mm^2.

3.7 CONCLUSION

In this chapter, we have demonstrated by means of experiments and simulation, that the four-point impedance probe is the best electrode system for the measurement of the transepithelial resistance. The experiments carried out to characterise the electrodes have led us to the comprehension of impedimetric and voltammetric properties of different electrode materials. Thereby, we have defined the best deposition and chlorination method for the fabrication of stable and durable pseudo-reference silver/silver-chloride thin film electrodes.

4 BIOLOGICAL EXPERIMENTS

Working with biological material is always a very delicate task, especially for an engineer in microtechnology. The best way to proceed is to create a close collaboration with people specialised in the field and use their feedback to improve the biosystems. That is what we tried to do and I think we've succeeded collaborating with three different academic work groups: the group of Prof. W. Hunziker from the Institute of Biochemistry at the University of Lausanne, the group of Prof. Van der Goot from the Department of Biochemistry at the University of Geneva and the group of Prof. J.D. Horisberger from the Institute of Pharmacology and Toxicology at the University of Lausanne.

4.1 TRANSEPITHELIAL RESISTANCE STUDY (WITH PROF. HUNZIKER)

Figure 4.1 is a photograph of an epithelial cell monolayer grown on our glass based device [52]. As it has been introduced in section 2.2.3, we have used an epoxy glue, the Araldit®, for the gluing of the PC membrane. Although it is not supposed to be biocompatible, the growth of an epithelial cell monolayer in our glass based device supposes no toxicity to the cell culture. Madin-Darby Canine Kidney (MDCK) cells possess characteristics similar to the principal cells of the collecting kidney duct and form tight epithelial-like monolayers, when grown on permeable supports. Cells (originally obtained from K. Matlin, Boston) were cultured as described [105] and plated on the micro-structures at a density of $5x10^4$ / cm^2 for 3 days to obtain a confluent monolayer. The cells on the micro-structures where then fixed in ethanol/acetic acid (3:1; 5 min at –20°C), washed in H_2O (5 min, room temperature) and the nuclei stained with the Hoechst 33258 bisbenziamid fluorochrome (50 ng/ml in H_2O for 30 min at 37°C). After washing in H_2O (5 min at room temperature), the cells on the micro-structure were covered with a drop of Moviol embedding solution and viewed with a Zeiss Axiophot microscope using a 63x Apachromat oil immersion lens, epifluorescence and fluorescein filters. The cell-growth experiments demonstrate the potential of our microsystem for miniaturised biological applications.

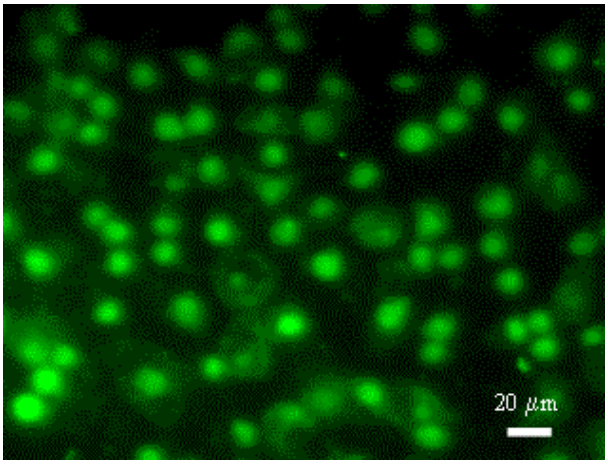

Figure 4.1: Optical photograph of fluorescently labelled cell nuclei of an epithelial cell layer grown into our glass based microsystem (Madin-Darby Canine Kidney (MDCK) cells are used).

Figure 4.2 shows the surface resistance measurement in our glass based devices before and after an MDCK cell culture. Four point surface resistance measurements were performed using the EVOM™ described in chapter 1 (see figure 1.5) in six nominally identical culture sites of our glass based microsystems. The insert shows the difference of surface resistance before and after cell culture. The dashed line represents the mean value. The mean difference of surface resistance value is of about 40 $\Omega \cdot cm^2$ with a considerable standard deviation. As we have used only devices with a nano-porous membrane fixed using our special gluing procedure and, hence, completely free of residual glue on the membrane, this resistance variation is not due to the gluing procedure but due to the non-uniformity of current lines in our device, combined with slight geometrical differences between the culture sites. Indeed, when locating the measurement electrodes very close to the membrane, the measurement will become very sensitive (as practically the resistance of the fluid does not contribute to the measured resistance), but the exact measured value will strongly depend on contact symmetry, positioning with respect to the cell chamber, etc…. The mean value for the surface resistance is of the same order of magnitude as the results on the 'macroscopic' epithelial cell culture devices (see figure 1.4), where we found a value of 70 $\Omega \cdot cm^2$. The difference in surface resistance between the standard cell culture devices and our microsystem approach could be due to edge effects of the membrane during cell culture or due to non-uniform measuring currents (for the 'macroscopic' devices).

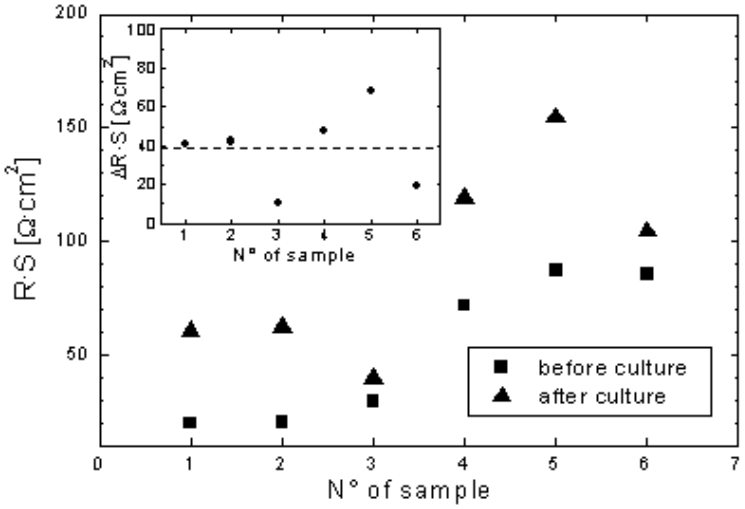

Figure 4.2: AC four point surface resistance measurements at 12.5 Hz in six nominally identical culture sites of our glass based microsystems, before and after MDCK epithelial cell culture. The insert shows the difference of surface resistance before and after cell culture. The dashed line represents the mean value.

Despite this slight difference compared to value obtained with commercial tissue culture multi-well plates, the biocompatibility has been demonstrated as well as the four-point impedance probe principle.

4.2 TRANSEPITHELIAL RESISTANCE STUDY (WITH PROF. VAN DER GOOT)

We have been able to launch an epithelial cell culture just before the end of this PhD work with the group of Prof. Van der Goot from the Department of Biochemistry at the University of Geneva. The cells used were Madin-Darby Canine Kidney (MDCK) cells as used for cultures in the group of Prof. Hunziker (see section 4.1). The purpose of these cultures is to perform transepithelial resistance (TER) measurements and observe their evolution under specific conditions and addition of certain compounds and drugs. Actually, only preliminary tests have been performed: TER measurements are reported until MDCK cell complete

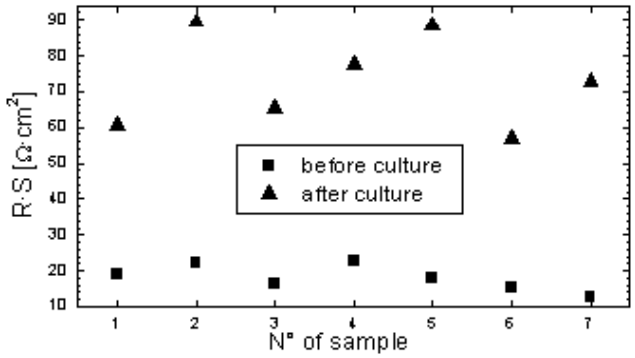

Figure 4.3: AC four point surface resistance measurements at 12.5 Hz in seven nominally identical culture sites of linear microsystems, before and after MDCK epithelial cell culture.

mono-layer formation. The biosystem used was the linear device with cell culture sites of 1 mm in diameter.

Figure 4.3 shows the surface resistance measurements in seven nominally identical culture sites of our linear microsystems. The values presented were measured before cell culture and after 5 days of culture. The increase in surface resistance is shown in figure 4.4 with the full line representing the mean value.

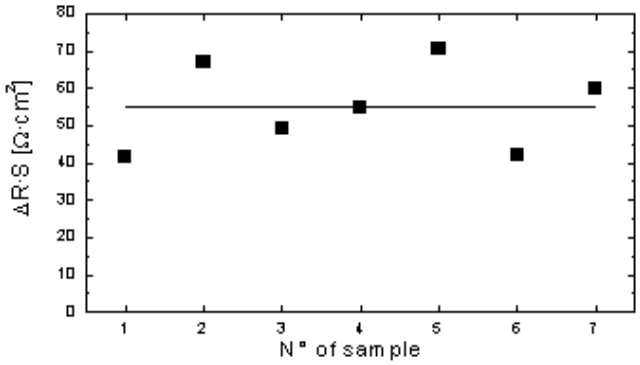

Figure 4.4: Graph showing the difference of surface resistance before and after cell culture for the experiments presented in figure 4.3. The full line represents the mean value (55 Ω·cm^2).

The mean value of surface resistance increase is of about 55 $\Omega \cdot cm^2$ which is of the order of the value measured in the glass based device (see figure 4.2). On the other hand, the standard deviation is smaller than for the measurements performed with the glass based device. Actually, the gluing of the membrane has been improved in the linear device by the use of a glue characterised by less diffusion on the polycarbonate porous membrane such as to have a more reproducible cell culture site surface. However, compared to experiments performed in standard cell culture wells (see section 1.4) our system offers a large enhanced stability. In addition, since our devices have integrated electrodes with external connectors that can be connected to a computer, for the first time, on-line TER kinetic measurements could be achieved. Moreover, the miniaturised size (80 µl of physiological solution in each top reservoir, 330 µl in the bottom reservoir and electrodes at respectively 1.5 and 3 mm distance from the culture membrane) allows the testing of compounds in minute amounts.

4.3 TRANSEPITHELIAL RESISTANCE AND ION TRANSPORT STUDY (WITH PROF. HORISBERGER)

We finally used our devices (linear, modular and macro) for the characterisation of the sodium transport through the epithelial cell sodium channel [14]. The micro-chambers were tested with cell lines with well known properties such as mCCD cell lines (cortical collecting duct cells) with the collaboration of Prof. J.D. Horisberger from the Institute of Pharmacology and Toxicology at the University of Lausanne. Figure 4.5 shows the transepithelial resistance (Rte) evolution of three culture sites of a linear device seeded with mCCD cells of transgenic mice in a standard mammalian physiological solution [57, 106]. The resistance increases gradually until the 7^{th} day, when 10 µM of amiloride (A) is added to the apical side of the cell monolayer (top of the membrane). This product is meant to block temporarily the active transport of Na^+ by inhibiting the Na^+ channels present in the apical membrane of these cells and then has to be rinsed before continuation of further cell growth. No effect of amiloride on Rte is detected, probably because of the relatively low value of the total transepithelial resistance. The resistance is then quite stable until the 10^{th} day when 10 µM Amiloride is added again to the apical side of the cells. The resistance drops after one more day in the incubator (probably due to bad rinsing of amiloride). Figure 4.6 shows the transepithelial voltage (Vte) evolution for the same experiment as for figure 4.5. Vte is the voltage induced in the device by the transepithelial current (Ite), which has its origin in the spontaneous transport of Na^+ ions through the cell layer. This volt-

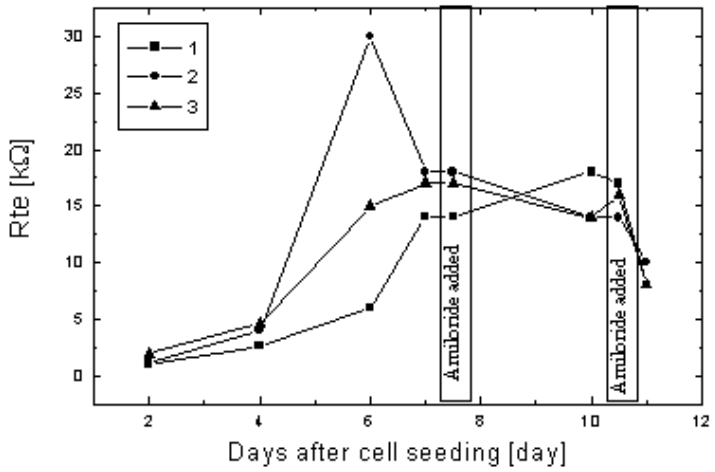

Figure 4.5: Transepithelial resistance (Rte) evolution of three culture sites seeded with mCCD cells. 10 µM of amiloride (A) are added to the apical side of each site after the 7th and 10th day.

age strongly increases after the fourth day of culture, when a tight monolayer of epithelial cells have grown on the polycarbonate membrane; these cells are characterised by an active Na^+ transport, which is the origin for the measured potential difference across the membrane. The consequence of the amiloride addition to the cells after 7 and 10 days is a voltage drop which confirms the temporary suppression of transport through the cells, although we would expect a drop to initial voltage. The presence of Cl^- ion transepithelial transport (not affected by amiloride) or the drift of the open voltage potential of the Ag/AgCl electrodes can be the origin of the relatively small decrease of Vte.

Prof. J.D. Horisberger from the Institute of Pharmacology and Toxicology at the University of Lausanne, gave us some reference values based on his measurements in standard cell culture wells. He used to measure about 50 µA of Ite for a cultured surface of 4 cm^2. As our linear and modular devices have culture sites of 1 mm in diameter, so 0.785 mm^2 in surface, we should measure a Ite in the order of 100 nA. From figure 4.5, we have measured 15kΩ of Rte (which is a relatively low value compared to standard values measured by Prof. Horisberger) when the cell mono-layer is complete. Consequently, for measuring 100 nA with our devices, we should be able to measure voltages in the order of 1-2 mV, which is

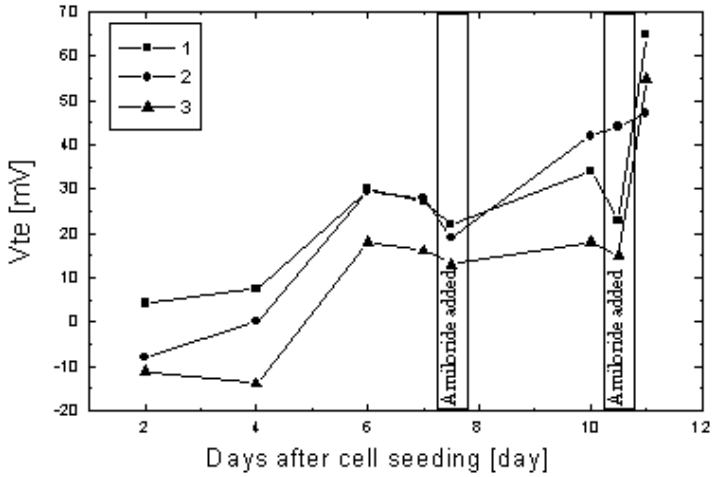

Figure 4.6: Transepithelial voltage (Vte) evolution of three culture sites seeded with mCCD cells. 10 µM of amiloride (A) are added to the apical side of each site after the 7th and 10th day.

just above the stability variation of our Ag/AgCl electrodes (see section 3.5.3 and figure 3.47).

With these experiments, the functionality of our devices was proved. Further investigations are now possible, especially a first application of our tissue culture and electrical characterisation systems with samples removed from transgenic mice. Unfortunately, several logistical and timing problems didn't allow us to carry on those experiments. Thus, this last application will be described in the next section as an outlook of this work.

4.4 CONCLUSION

We have successfully experienced epithelial culture with three different academic biochemistry work-groups, showing the biocompatibility of our devices. Transepithelial resistance measurements were carried out for each culture experiments, demonstrating the potential of our four-point impedance probe for measuring the resistance of a cell monolayer separating two compartments. The values of surface resistance for MDCK cells cultured in our devices are comparable to values obtained for the same experiment in commercially available systems. The pos-

sibility of measuring the transepithelial current using integrated silver/silver-chloride thin film electrodes as pseudo-reference electrodes (defined potential at a certain Cl^- concentration) opens interesting perspectives for miniaturised electrophysiological measurement systems.

CONCLUSIONS AND OUTLOOK

CONCLUSION:

Many different designs of microsystems for the culture and electrical characterisation of epithelial cell layers for biomedical diagnostic purposes were realised during this work.

We have first realised a microsystem based on silicon substrates, allowing us to use well know micromachining technologies such as photolithography, wet etching and dry etching procedures, metal thin film deposition, high temperature humid silicon oxidation, as well as anodic bonding to a pyrex wafer. These standard silicon microfabrication procedures, available in our clean room, allowed us to design a complex structure of channels, vias, side connections and integrated electrodes. Having started with a two-point impedance probe, we have observed a unfavourable behaviour of the insulating silicon dioxide layer for high frequency measurements. This last point, adding to the costs of such a silicon microsystem for a disposable use, made us decide to design a new microsystem based on glass substrates with the use of a four-point impedance probe. A new glass etching process was introduced, powder-blasting, which is a non-cleanroom process. The result was a simplified structure which was tested in real biological experiments with Madin-Darby Canine Kidney (MDCK) cell culture, showing promising results.

The second development step was to simplify again the microfabrication steps by using PDMS moulded channels and vias, as well as the use of galvanostically deposited silver/silver-chloride electrodes for better electrical characterisation. Finally, we opted for two structures, a linear disposable structure and a modular reusable structure, both of them with four miniaturised (1 mm^2) culture sites, based on glass substrates, PDMS moulded elements and Ag and Ag/AgCl electrodes as four-point impedance probe. Our systems are with integrated electrical electrodes, micro-fluidic channels and feed-throughs, making it extremely compact and easy-to-use to avoid cell function perturbation by manipulations.

The linear and the modular structures were electrochemically characterised, and the glass based and the linear devices were tested in cell culture experiments. The biocompatibility was demonstrated with epithelial cell growth and the functionality of the impedance probe was confirmed with a better accuracy of the transepithelial resistance and current. A specific study on micro-electrodes for stable dc potential measurements was carried out using several electrochemical characterisation methods such as impedance spectroscopy and cyclic voltammetry. Our structures facilitate control of the cell layer growth, the measurement of the cell layer resistance, the transport and diffusion of biological or pharmacological molecules through the cell layer and accurate measurement of (bio-) chemically induced resistance variations.

Direct collaborations with different biological research groups gave us the possibility to demonstrate the potentiality of such devices for biomedical diagnostic purposes and we hope that our device will open new perspectives for fundamental research and cell based diagnostic applications.

OUTLOOK:

With our linear and modular devices, the renal and bronchial epithelia functions of two experimental models, that reproduce human hereditary affections, can be tested. Those affections are the Liddle syndrome [12] and the primary pseudohypoaldosteronism, which are both induced by an epithelial sodium channel dysfunction. The use of a transgenic mice strategy is often practically limited by the difficulty of performing complex physiological measurements on animals, especially when studying young or new-born animals, obviously because of their small size. The possibility of establishing a culture and studying the epithelial tissues of those animals as a primary culture, is a challenge to answer questions that can practically not be resolved at present. Furthermore, the microsystems could be used with tissues obtained from patient biopsies. Tissues are often sampled for establishing histopathological diagnosis. As cultures can be started from a fraction of those biopsies, it would become possible to do in vitro studies of the functional characteristics of certain patients epithelium. This would allow, on the one hand, to settle down the diagnosis of epithelial function troubles, and on the other hand, to realise scientific studies on specific functional properties of human epithelia.

Also, the modular device, allowing the separation of the culture substrate and its PDMS sandwich from the total measuring structure (see figure 2.33 and 2.34), can be used for optical measurements such as following the pathway of certain fluorescent compounds in an epithelial cell or cell layer.

In order to obtain a complete epithelial cell culture and electrical characterisation system, a student is presently developing a portable four-point resistance and voltage meter. A square 1 μA current with a rest time between the periods is injected to the biosystem through two ports and the voltage is measured using two other ports. Actually, it is realized with integrated multiplexing unit for measuring the four culture sites of the linear or modular devices. Direct measurements can be performed or can be programmed to measure each of the 4 wells every 2 hours during 7-10 days of culture. The measured values can be kept in the internal memory before downloading on a PC or directly sent to a PC for on-line TER kinetic measurements.

APPENDIX

1 MACHINES AND INSTRUMENTS FOR MICROMACHINING

1.1 IN CLEAN ROOM

1) Manual coaters for positive resist, Karl Süss RC8.

2) Proximity/contact double side mask aligners, Karl Süss MA6/BA6.

3) Proximity/contact double side mask aligner, MA-150 aligner.

4) Wet bench for resist development and resist strip, Coillard, using Microposit developer 351 and remover 1165.

5) Wet bench for oxide and metal etch, Coillard, with baths for Al etch, Cr etch, dip HF and oxide etch (BHF 1:7).

6) Inspection microscope, Nikon 200.

7) HMDS dispense oven, YES LPIII.

8) Wet bench for anisotropic silicon etching (KOH), Plade.

9) Microwave plasma stripper, Tepla 300.

10) Single chamber multi-target sputtering system, BAS-450.

11) E-gun evaporator, Alcatel EVA 600.

12) Profilometer, TENCOR Alphastep 500.

13) Chlorine chemistry high density plasma etcher, STS Multiplex ICP.

14) Wet bench for piranha (1 x H_2O_2 + 3 x H_2SO_4) cleaning procedure, UFT Bench.

1.2 OUT OF CLEAN ROOM

15) Disco dicing saw machine DAD321.

16) Kulicke & Soffa saw machine 984-6.

17) Multipurpose oven (250°C), Memmert.

18) High temperature oven (1200°C), Nabertherm.

19) Several Zeiss microscopes.

20) Lab fabricated anodic bonding installation

21) Powder-blasting set-up

2 SUBSTRATES

Denomination	Diameter [mm]	Thickness [µm]	Orientation	Conductivity type	Dopant	Resistivity range [ohm-cm]
Silicon prime wafers double-side polished	100 ± 0.2	380 ± 10	<100>	P	Boron	0.1 -0.5
Silicon prime wafers single-side polished	100 ± 0.2	380 ± 10	<100>	P	Boron	0.1 -0.5
Silicon Nitride wafers double-side polished	100 ± 0.2	380 ± 10	<100>	P	Boron	0.1 -0.5

Denomination	Diameter [mm]	Thickness [µm]	Composition
Floatglass wafer, FLOAT/DS	100 0/-0.3	550 ± 10 and 2000 ± 20	SiO2: 70.8%, Na2O: 13.9%, K 2O: 0.4%, CaO: 8.4%, MgO: 4.4%, Al2O3: 1.5%, Fe2O3: 0.08%, SO3: 0.3%
Pyrex wafers, Pyrex/DS	100	525	SiO2: 81%, Na2O: 4%, Al 2O3: 2%, B2O3: 13% + traces elements

3 CLEAN ROOM FABRICATION RUN-CARD

3.1 SILICON BASED DEVICE

Starting with one silicon wafer double-side polished, one silicon wafer single-side polished and one Pyrex wafer.

Step		Material	Parameters	Results
With a double-side polished silicon wafer 4"				
Photolithography	HMDS dispense	oven, YES LPIII	150°C	
	resist spinning	S1818 (Shipley) manual coater	30 sec. 2500 rpm	2.45 µm
	prebake	hotplate	1 min. 115°C	
	backside exposition without align.	mask bh $7mW/cm^2$	20 sec.	
	development	developer	1 min.	
	rinsing	H_2O DI		
	postbake	hotplate	1min. 115°C	
Anisotropic etching	programme Serge	Plasma STS	4µm/min.	etching of 250-270 µm

Step		Material	Parameters	Results
Photolithography	HMDS dispense	oven, YES LPIII	150°C	
	resist spinning	S1818 (Shipley) manual coater	30 sec. 2500 rpm	2.45 µm
	prebake	hotplate	1 min. 115°C	
	frontside exposition with align.	mask fh 14mW/cm^2	12 sec.	
	development	developer	1 min.	
	rinsing	H_2O DI		
	postbake	hotplate	2 min. 115°C	
Anisotropic etching	programme Serge	Plasma STS	4µm/min. with blue tape on backside	etching of 110-130 µm
	resist stripping	plasma stripper and acetone + isopropanol + piranha		
Wet oxidation	for a 0.5 µm thick SiO_2 layer	high temperature oven + N_2 charged with H_2O	T profile: 20°C->1h->700°C 700°C->1h15->1000°C 2h at 1000°C	0.6 µm thick SiO_2
With a Pyrex wafer				

Step		Material	Parameters	Results
Photoli-thography	backside protec-tion	blue tape		
	resist spinning	S1818 (Shipley) manual coater	30 sec. 2500 rpm	2.45 µm
	prebake	hotplate	1 min. 115°C	
	frontside exposi-tion without align.	mask frontelec 7mW/cm^2	20 sec.	
	development	developer	1 min.	
	rinsing	H_2O DI		
	postbake	hotplate	2 min. 115°C	
Frontside etching in BHF	BHF etching	BHF (100nm/5min.)	30min. -> 0,6 µm	
		take out of BHF every 5 min. and bake 1 min. 115°C		
Metallisa-tion	Cr/Au 50/200 or Ta/Pt 20/200	E-gun evaporator or sputtering sys-tem, BAS-450		
Lift-off		acetone + ultra-sound		
With the two preceding wafers silicon and Pyrex				
Anodic bonding	Si and Pyrex cleaning	acetone + ultra-sound		
		isopropanol then H_2O DI then Drying		

Step		Material	Parameters	Results
		Piranha then H_2O DI then Drying		
	alignment and assembly			
	Bonding Si-Pyrex	Bonding installation (lab fabricated)	700 V at 350°C 5 min.	
with one silicon nitride wafer for KOH etching				
Photolithography	Standard as preceding process frontside without align.			
Anisotropic etching	programme Si_3N_4	Plasma STS	7 min.	0.5 µm
Anisotropic etching	KOH etching	KOH 40% 60°C	20 µm/min.	
	rinsing	H_2O DI		
Nitride etching		H_3PO_4 180°C	5 min.	
	rinsing	acetone + isopropanol + H_2O DI		
Wet oxidation	for a 0,5 µm thick SiO_2 layer	high temperature oven + N_2 charged with H_2O	T profile: 20°C->1h->700°C 700°C->1h15->1000°C 2h at 1000°C	0.6 µm thick SiO_2
with a single-side polished silicon wafer for fabrication of a shadow mask				

Step		Material	Parameters	Results
Photolithography	Standard as preceding process frontside without align.			
Metallisation through shadow mask	Cr/Au 50/200 or Ta/Pt 20/200 on frontside of silicon KOH etched wafer through shadow mask	E-gun evaporator or sputtering system, BAS-450		

3.2 GLASS BASED, LINEAR AND MODULAR DEVICES

For those three devices, just one procedure is realised in the clean room, that is the deposition of the electrodes on floatglass wafers.

Step		Material	Parameters	Results
With a double-side polished silicon wafer 4"				
Cleaning procedure	Piranha bath	Wet bench	10 min. Piranha (1 x H_2O_2 + 3 x H_2SO_4)	
	rinsing	H_2O DI and drying		
HMDS deposition	HMDS for resist adhesion on wafer	HMDS oven	20 min. at 150°C	
Resist deposition	resist spinning	S1818 (Shipley) manual coater	30 sec. 2500 rpm	2.35 µm
	prebake	hotplate	1 min. 115°C	

Step		Material	Parameters	Results
Illumination	frontside exposition without align.	10mW/cm^2	8 sec.	
	development	developer	90 sec.	
	rinsing	H_2O DI		
	postbake	hotplate	1min. 115°C	
Slight recess etching for electrode deposition	BHF etching	BHF 1:7	90 sec.-> 1.4 µm	
Metallisation	Cr/Au 50/ 200nm or Ta/Pt 20/ 200nm or Ti/Ag 20/ 300nm or Ti/Pd/Ag 20/ 20/500nm	E-gun evaporator or sputtering system, BAS-450		
Lift-off		acetone + ultrasound		

4 PDMS MOULDING

The PDMS used was bought from Distrelec (Switzerland) under the denomination of Sylgard 184™ from Dow Corning. It is a two component product: silicone and curing agent. The mixing proportions are respectively, 10 to 1. After mixing, the PDMS is placed in a vacuum chamber at 0.15 mbar for 10 min. in order to eliminate the air bubbles trapped in the PDMS during mixing. We then used a fast curing, 115°C for 5 min.

5 POWDER BLASTING

The basic element of our set-up (figure 4.7) is an HP-2 Texas Airsonic abrasive jet machine, which is connected to a 6 bar pressurised air source [53, 54]. The eroding powder consists of 30 µm size alumina particles (Al_2O_3) and is dosed to an exit nozzle by a vibration feeder in an air jet. The erosion process can be tuned by varying parameters like the air pressure and the flux of particles in the air flow. The distance from the nozzle exit to the substrate can be varied from 1 cm up to 9 cm. The substrate surface can be uniformly exposed to the powder beam by the use of an x-axis and a y-axis translation stage for the substrate and the nozzle, respectively. Selective erosion can be obtained using a protective steel mask, containing the desired structure features. We typically use laser-cut 0.5 mm thick masks. If holes are to be etched through deposited circular electrodes, the wafer has to be eroded from the other side (with no electrode) and the electrodes can be protected with blue-tape.

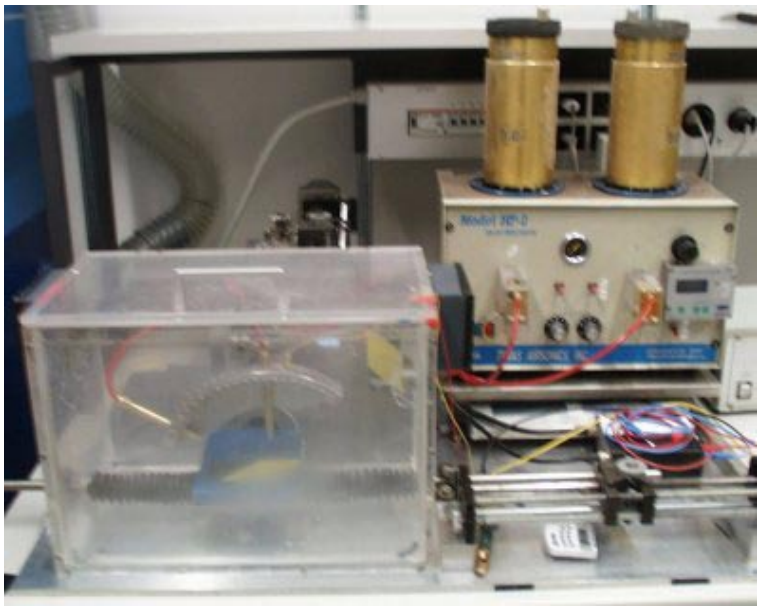

Figure 4.7Photograph of the powder-blasting set-up, showing on the left-hand side, the powder blasting chamber and on the right-hand side, the HP-2 Texas Airsonic abrasive jet machine.

Parameters used for cylindrical through-holes:

substrate	process	nozzle distance	pressure	exposure time
floatglass 0.5 mm of thick-ness	frontside	5 cm	3.5 bar	15 sec.
floatglass 2 mm of thick-ness	frontside	4 cm	4 bar	45 sec.
	backside	4 cm	4 bar	30 sec.

6 MASKS FOR POWDER-BLASTING

The mask were designed using the same CleWin software as for photolithography. They were then reproduced in metallic (Ac inox) plates of thickness 0.5 or 1 mm by laser-cutting, which is available in the Institute of Applied Optics (IOA) at the EPFL. Figure 4.8 shows the design of the metallic mask for powder-blasting the top level of the modular device.

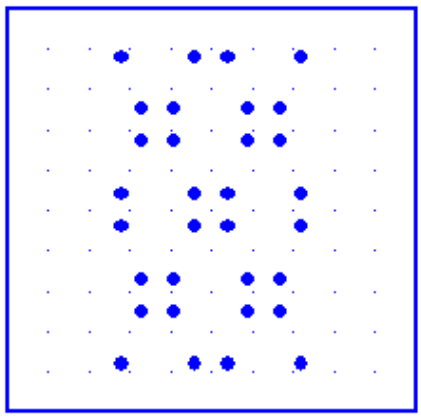

Figure 4.8: Design of the metallic mask for powder-blasting the top level of the modular device. Four structures can be seen on that mask for a 4 inch wafer process (refer to figure 4.11). In each structure, the four centre holes are the vias to the cell culture sites, and the four external are the holes for mounting on the Al base by means of four screws.

7 MASKS FOR PHOTOLITHOGRAPHY

The masks have been designed using the CleWin software from WieWeb software in the Netherlands. We have used a demo version of CleWin 2.75. As no dimension smaller than 100 µm was needed, the mask is silk-screen printed on a transparency with a 3600 dpi resolution which can be directly used as a mask or reproduced on a chrome-blank (glass plate with pre-deposited Cr layer and a photoresist layer).

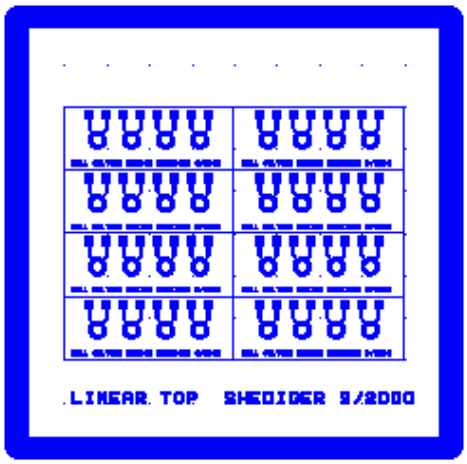

Figure 4.9: Design of the mask for the photolithographic process of the top wafer of the linear device. Eight structures can be seen on that mask for a 4 inch wafer process.

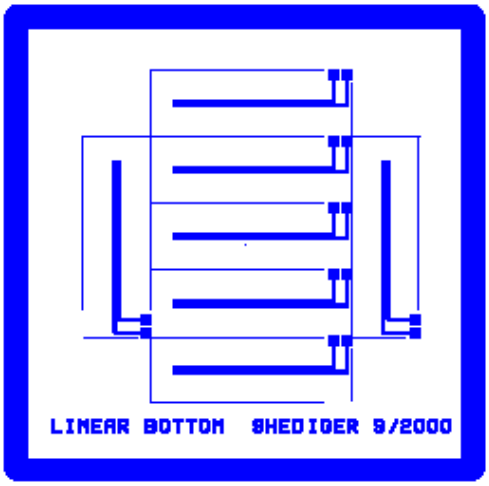

Figure 4.10: Design of the mask for the Photolithography process of the low wafer of the linear device. Seven structures can be seen on that mask for a 4 inch wafer process.

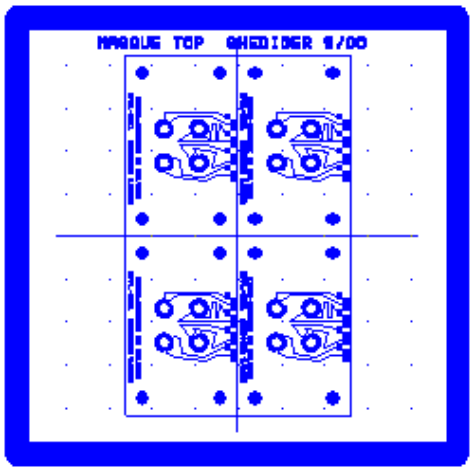

Figure 4.11: Design of the mask for the photolithography process of the top wafer of the modular device. Four structures can be seen on that mask for a 4 inch wafer process.

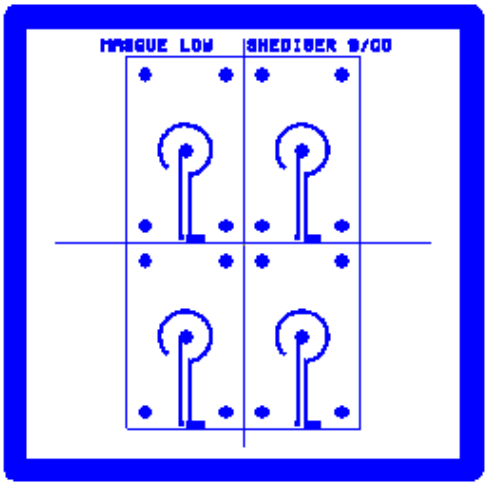

Figure 4.12: Design of the mask for the photolithographic process of the low wafer of the modular device. Four structures can be seen on that mask for a 4 inch wafer process.

REFERENCES

[1] G. Fuhr, "*Examples of three-dimensional microstructures for handling and investigation of adherently gowing cells and submicron particles*", Analyt. Methods and Instrumentation, Special Issue µTAS '96, pp. 39-54, (1996).

[2] G. Fuhr and S. G. Shirley, "*Cell handling and characterization using micron and submicron electrode arrays: state of the art and perspectives of semiconductor microtools*", Journal of Micromechanics and Microengineering, vol. 5, pp. 77-85, (1995).

[3] N. B. Standen, P. T. A. Gray, and M. J. Whitaker, "*Microelectrode techniques*", The Company of Biologists Ltd., Cambridge, (1987).

[4] S. Grimmes and O. G. Martinsen, "*Bioimpedance & Bioelectricity Basics*", Academic Press, San Diego, (2000).

[5] L. C. Milks, M. J. Brontoli, and E. B. Cramer, "*Epithelial Permeability and the Transepithelial Migration of Human Neutrophils*", J. Cell Biol., vol. 96, pp. 1241-1247, (1983).

[6] D. S. Misfeldt, S. T. Hammamoto, and D. R. Pitelka, "*Transepithelial Transport in Cell Culture*", Proc. Natl. Acad. Sci. USA., vol. 73, pp. 1212-1216, (1976).

[7] Falcon® product literature, Becton Dickinson, NJ USA , (1998).

[8] Corning Costar® product literature, MA USA , (1999).

[9] M. Madou, "*Fundamentals of microfabrication*", CRC Press, New York, USA, (1997).

[10] D. W. Selding and G. Giebisch, "*The Kidney: Physiology and pathology*", vol. 1, Raven Press, New York, (1985).

[11] A. J. Vander, J. H. Sherman, D. S. Luciano and J. R. Gontier, "*Physiologie humaine*", McGraw-Hill, New York, (1989).

[12] S. J. Scheinman, L. M. Guay-Woodford, V. Thakker and D. G. Warnock, "*Mechanisms of Disease: Genetic Disorders of Renal Electrolyte Transport*", New England Journal of Medicine, vol. 340, pp. 1177-1187, (1999).

[13] E. Hummler, P. Barker, C. Talbot, Q. Wang, C. Verdumo, B. Grubb, J. Gatzy, M. Burnier, J.-D. Horisberger, F. Beermann, R. Boucher and B. C. Rossier, "*A mouse model for the renal salt-wasting syndrome pseudohypoaldosteronism*", Proc.Natl.Acad.Sci. U.S.A, vol. 94, pp. 11710-11715, (1997).

[14] M. Mall, A. Wissner, H. Seydewitz, J. Kuehr, M. Brandis, R. Greger and K. Kunzelmann, "*Defective cholinergic Cl(-) secretion and detection of K(+) secretion in rectal biopsies from cystic fibrosis patients*", American Journal of Physiology-Gastrointestinal & Liver Physiology, vol. 278, pp. 617-624, (2000).

[15] N. A. Campbell, J. B. Reece, and L. G. Mitchell, "*Biology*", Benjamin/Cummings, Menlo Park, CA, (1999).

[16] H. H. Ussing and K. Zerahn, "*Active transport of sodium as the source of electric current in the short-circuited isolated frog skin.*", Acta Physio. Scan., vol. 23, pp. 110-127, (1951).

[17] World Precision Instruments web page (http://www.wpiinc.com)

[18] Y. Yamamoto, T. Yamamoto, and P. A. Oberg, "*Impedance Plethysmography in Human Limbs .1. On Electrodes and Electrode Geometry*", Medical & Biological Engineering & Computing, vol. 29, pp. 419-424, (1991).

[19] Y. Yamamoto, T. Yamamoto, and P. A. Oberg, "*Impedance Plethysmography For Blood-Flow Measurements in Human Limbs .2. Influence of Limb Cross-Sectional Area*", Medical & Biological Engineering & Computing, vol. 30, pp. 518-524, (1992).

[20] E. J. Woo, P. Hua, J. G. Webster, W. J. Tompkins and R. Pallasareny, "*Skin Impedance Measurements Using Simple and Compound Electrodes*", Medical & Biological Engineering & Computing, vol. 30, pp. 97-102, (1992).

[21] A. O. Ragheb, L. A. Geddes, J. D. Bourland and W. A. Tacker, "*Tetrapolar Electrode System For Measuring Physiological Events By Impedance*", Medical & Biological Engineering & Computing, vol. 30, pp. 115-117, (1992).

[22] K. R. Visser, "*Electric-Conductivity of Stationary and Flowing Human Blood At Low-Frequencies*", Medical & Biological Engineering & Computing, vol. 30, pp. 636-640, (1992).

[23] B. Sakmann and E. Neher, "*Single-channel recording*", Plenum Press, New York, (1995).

[24] O. P. Hamill, A. Marty, E. Neher, B. Sakmann and F. J. Sigworth, "*Improved patch-clamp techniques for high-resolution current recording from cells and cell-free membrane patches*", Pflügers Arch.: Eur. J. Physiol., vol. 391, pp. pp. 85-100, (1981).

[25] Cytion web page (http://www.cytion.ch)

[26] H. E. Ayliffe, R. D. Rabbitt, P. A. Tresco and A. B. Frazier, "*Micromachined cellular characterization system for studying the biomechanics of individual cells*", Proc. The International Conference on Solid-State Sensors and Actuators (Tranducers' 97), Chicago, IL, USA, June 16-19, pp.1307-10, (1997).

[27] H. E. Ayliffe, A. B. Frazier, and R. D. Rabbitt, "*Development of a microfabricated device to measure the electric impedance of individual leukocytes*", American Society of Mechanical Engineers, Bioengineering Division (Publication) BED, vol. 35, pp. 485-486, (1997).

[28] H. E. Ayliffe, A. B. Frazier, and R. D. Rabbitt, "*Electric impedance spectroscopy using microchannels with integrated metal electrodes*", Journal of Microelectromechanical Systems, vol. 8, pp. 50-57, (1999).

[29] G. Blankenstein, L. Scampavia, J. Branebjerg, U. D. Larsen and J. Ruzicka, "*Flow swith for analyte injection and cell/particle sorting*", Proc. The 1st International Symposium on micro Total Analysis Systems (μTAS'96), Basel, Switzerland, (1996).

[30] U. D. Larsen, G. Blankenstein, and J. Branebjerg, "*Microchip coulter particle counter*", Proc. International Conference on Solid-State Sensors and

Actuators (Transducers'97), Chicago, USA, June 16-19, pp. 1319-1322, (1997).

[31] S. Gawad, L. Schild, and P. Renaud, "*Micromachined impedance spectroscopy flow cytometer for cell analysis and particle sizing*", Lab on a Chip, vol. 1, pp. 76 - 82, (2001).

[32] H. Thielecke, T. Stieglitz, H. Beutel, T. Matthies, H. H. Ruf and J. U. Meyer, "*Fast and precise positioning of single cells on planar electrode substrates*", IEEE-Engineering-in-Medicine-and-Biology-Magazine, vol. 18, pp. 48-52, (1999).

[33] H. Thielecke, T. Stieglitz, H. Beutel, T. Matthies and J. U. Meyer, "*A novel technique for positioning of single cells on sensor microstructures*", Proc. European medical and biological engineering conference (EMBEC99), Wien, Austria, November 4-7, pp. 598-599, (1999).

[34] A. Manz, N. Graber, and H. M. Widmer, "*Miniaturized total analysis systems: a novel concept for chemical sensors*", Sensors & Actuators B, vol. 1, pp. 244, (1990).

[35] A. Manz, D. J. Harrison, E. M. J. Verpoorte, J. C. Fettinger, A. Paulus, H. Ludi and H. M. Widmer, "*Planar Chips Technology For Miniaturization and Integration of Separation Techniques Into Monitoring Systems - Capillary Electrophoresis On a Chip*", Journal of Chromatography, vol. 593, pp. 253-258, (1992).

[36] C. S. Effenhauser, A. Manz, and H. M. Widmer, "*Glass Chips For High-Speed Capillary Electrophoresis Separations With Submicrometer Plate Heights*", Analytical Chemistry, vol. 65, pp. 2637-2642, (1993).

[37] D. J. Harrison, A. Manz, Z. Fan, H. Ludi and H. M. Widmer, "*Capillary electrophoresis and sample injection systems integrated on a planar glass chip*", Anal. Chem., vol. 64, pp. 1926, (1992).

[38] J. Wegener, M. Sieber, and H. J. Galla, "*Impedance analysis of epithelial and endothelial cell monolayers cultured on gold surfaces*", Journal of Biochemical and Biophysical Methods, vol. 32, pp. 151-170, (1996).

[39] M. P. Maher, H. Dvorak-Carbone, J. Pine, J. A. Wright and Y. C. Tai, "*Microstructures for studies of cultured neural networks*", Medical & Biological Engineering & Computing, vol. 37, pp. 110-118, (1999).

[40] M. P. Maher, J. Pine, J. Wright and Y. C. Tai, "*The neurochip: a new multielectrode device for stimulating and recording from cultured neurons*", Journal of Neuroscience Methods, vol. 87, pp. 45-56, (1999).

[41] M. O. Heuschkel, "*Fabrication of multi-electrode array devices for electrophysiological monitoring of in-vitro cell/tissue cultures*", Series in Microsystems vol. 13, Hartung-Gorre Verlag, Konstanz, Germany, (2001).

[42] S. Tacic-Lucic and Y. C. Tai, "*Silicon-micromachined neurochips for in vitre studies of cultured neural networks*", Proc. International conference on solid-state sensors and actuators (Transducers'93), Yokohama, Japan, November, pp.943-946, (1993).

[43] J. A. Wright and S. Tacic-Lucic, "*Towards a functional MEMS neurowell by physiological experimentation*", Proc. International mechanical engineering congress and exposition (ASME 1996), Atlanta, USA, November, pp. 333-338, (1996).

[44] B. W. Kristensen, J. Noraberg, P. Thiebaud, M. Koudelka-Hep and J. Zimmer, "*Biocompatibility of silicon-based arrays of electrodes coupled to organotypic hippocampal brain slice cultures*", Brain Research, vol. 896, pp. 1-17, (2001).

[45] P. Thiebaud, C. Beuret, M. Koudelka-Hep, M. Bove, S. Martinoia, M. Grattarola, H. Jahnsen, R. Rebaudo, M. Balestrino, J. Zimmer and Y. Dupont, "*An array of Pt-tip microelectrodes for extracellular monitoring of activity of brain slices*", Biosensors & Bioelectronics, vol. 14, pp. 61-65, (1999).

[46] P. Jacobs, A. Varlan, and W. Sansen, "*Design Optimization of Planar Electrolytic Conductivity Sensors*", Medical & Biological Engineering & Computing, vol. 33, pp. 802-810, (1995).

[47] P. Jacobs, J. Suls, and W. Sansen, "*Performance of a Planar Differential-Conductivity Sensor For Urea*", Sensors and Actuators B-Chemical, vol. 20, pp. 193-198, (1994).

[48] R. S. Newbower and E. D. Trautman, "*Sensor For Catheter-Based Measurements of Electrical- Conductivity*", IEEE Trans. Biomed. Eng., vol. 33, pp. 182-188, (1986).

[49] A. R. Varlan, P. Jacobs, and W. Sansen, "*New design technique for planar conductometric haematocrit sensors*", Sensors and Actuators B-Chemical, vol. 34, pp. 258-264, (1996).

[50] Rai-Choudhury, "*Handbook of microlithography, micromachining, and microfabrication*", SPIE Optical Engineering Press, Bellingham, Washington, USA, (1997).

[51] S. M. Sze, "*Semiconductor devices: physics and technology*", John Wiley & Sons, New York, USA, (1985).

[52] S. Hediger, J. Fontannaz, A. Sayah, W. Hunziker and M. A. M. Gijs, "*Biosystem for the culture and characterisation of epithelial cell tissues*", Sensors and Actuators B, vol. 63, pp. 63-73, (2000).

[53] E. Belloy, S. Thurre, E. Walckiers, A. Sayah and M. A. M. Gijs, "*The Introduction of Powder Blasting for Sensor and Microsystem Applications*", Sensors and Actuators A, vol. 84, pp. 330-337, (2000).

[54] E. Belloy, A. Sayah, and M. A. M. Gijs, "*Powder Blasting for Three Dimensional Microstructuring of Glass*", Sensors and Actuators A, vol. 86, pp. 231-237, (2000).

[55] Osmonics Lab Store web page (http://www.osmolabstore.com)

[56] O. Thoumine and A. Ott, "*Comparison of the mechanical properties of normal and transformed fibroblasts*", Biorheology, vol. 34, pp. 309-326, (1997).

[57] S. Hediger, A. Sayah, J. D. Horisberger and M. A. M. Gijs, "*Modular microsystem for epithelial cell culture and electrical characterisation*", Biosensors & Bioelectronics, vol. 16, pp. 689-694, (2001).

[58] R. Schmukler, "*A Brief-History of Bioelectrodes*", Annals of Biomedical Engineering, vol. 20, pp. 265-268, (1992).

[59] R. Schmukler and R. P. Buck, "*Special Issue - Bioelectrodes - Introduction*", Annals of Biomedical Engineering, vol. 20, pp. 263-264, (1992).

[60] B. Rigaud, J. P. Morucci, and N. Chauveau, "*Bioelectrical impedance techniques in medicine .1. Bioimpedance measurement - Second section: Impedance spectrometry*", Critical Reviews in Biomedical Engineering, vol. 24, pp. 257-351, (1996).

[61] E. T. McAdams and J. Jossinet, "*Tissue Impedance - a Historical Overview*", Physiological Measurement, vol. 16, pp. A1-A13, (1995).

[62] L. A. Geddes, "*Historical evolution of circuit models for the electrode- electrolyte interface*", Annals of Biomedical Engineering, vol. 25, pp. 1-14, (1997).

[63] I. Fried, "*The chemistry of electrode processes*", Academic Press, New York, (1973).

[64] J. O. M. Bockris and A. K. N. Reddy, "*Modern electrochemistry*", vol. 2, Plenum Press, New York, (1970).

[65] H. Helmholtz, "*Studien uber electrische Genzschichten*", Ann. Phys. Chem., vol. 7, pp. 337-382, (1879).

[66] Research Solutions & Resources web page (http://www.consultrsr.com/resources/eis/warburg2.htm)

[67] E. T. McAdams, A. Lackermeier, J. A. McLaughlin, D. Macken and J. Jossinet, "*The linear and non-linear electrical properties of the electrode-electrolyte interface*", Biosensors & Bioelectronics, vol. 10, pp. 67-74, (1995).

[68] D. Landolt, "*Corrosion et chimie de surfaces des métaux*", Traité des matériaux vol. 12, Presses Polytechniques et Universitaires Romandes, Lausanne, (1997).

[69] M. Lambrechts and S. W, "*Biosensors: Microelectrochemical Devices*", Institute of Physics Publishing, New York, (1992).

[70] A. J. Bard and L. R. Faulkner, "*Electrochemical methods: fundamentals and applications*", John Wiley & Sons, New York, (2001).

[71] L. A. Geddes, "*Who introduced the tetrapolar method for measuring resistance and impedance?*", Ieee Engineering in Medicine and Biology Magazine, vol. 15, pp. 133-134, (1996).

[72] R. J. Guanti and P. J. Moran, "*Measurement of electrolyte conductivity in highly conducting solutions*", Journal-of-Applied-Electrochemistry, vol. 16, pp. 678-82, (1986).

[73] R. J. Guanti and P. J. Moran, "*4 Electrode Technique For the Measurement of Electrolyte Conductivity*", Journal of the Electrochemical Society, vol. 130, pp. C336-C336, (1983).

[74] Z. Moron, Z. Rucki, and Z. Szczepanik, "*The possibility of employing a calculable four-electrode conductance cell to substitute for the secondary standards of electrolytic conductivity*", Ieee Transactions On Instrumentation and Measurement, vol. 46, pp. 1268-1273, (1997).

[75] J. Z. Tsai, H. Cao, S. Tungjitkusolmun, E. J. Woo, V. R. Vorperian and J. G. Webster, "*Dependence of apparent resistance of four-electrode probes on insertion depth*", Ieee Transactions On Biomedical Engineering, vol. 47, pp. 41-48, (2000).

[76] R. Tamamushi and K. Takahashi, "*Instrumental study of electrolytic conductance measurements using four-electrode cells*", Journal-of-Electroanalytical-Chemistry-and-Interfacial-Electrochemistry, vol. 50, pp. 277-84, (1974).

[77] G. J. Janz and D. J. G. Ives, "*Silver-silver chloride electrodes*", Ann. N.Y. Acad. Sc., vol. 148, pp. 210-221, (1968).

[78] M. Steyaert, M. Lambrechts, and W. Sansen, "*Noise Power Spectrum Density Analysis of Planar Ag/Agcl Electrodes*", Sensors and Actuators, vol. 12, pp. 185-192, (1987).

[79] H. Suzuki, T. Hirakawa, S. Sasaki and I. Karube, "*An integrated three-electrode system with a micromachined liquid-junction Ag/AgCl reference electrode*", Analytica Chimica Acta, vol. 387, pp. 103-112, (1999).

[80] H. Suzuki, T. Hirakawa, S. Sasaki and I. Karube, "*Micromachined liquid-junction Ag/AgCl reference electrode*", Sensors and Actuators B-Chemical, vol. 46, pp. 146-154, (1998).

[81] C. D. Ferris, "*Introduction to bioelectrodes*", Plenum Press, New York, (1974).

[82] H. Suzuki and H. Shiroishi, "*Development of thin-film liquid-junction Ag/AgCl reference electrodes and their application to one-chip micro chemical sensors*", Proc. Transducers, Sendai, Japan, 1180-1183, (1999).

[83] H. Suzuki, A. Hiratsuka, S. Sasaki and I. Karube, "*Problems associated with the thin-film Ag/AgCl reference electrode and a novel structure with improved durability*", Sensors and Actuators B-Chemical, vol. 46, pp. 104-113, (1998).

[84] F. Crenner, F. Angel, and C. Ringwald, "*Ag/Agcl Electrode Assembly For Thin Smooth-Muscle Electromyography*", Medical & Biological Engineering & Computing, vol. 27, pp. 346-356, (1989).

[85] D. M. Zhou, E. T. McAdams, A. Lackermeier and J. G. Jones, "*AC impedance of Ag/AgCl reference electrodes for use in disposable biosensors*", Annual International Conference of the IEEE Engineering in Medicine and Biology Society - Proceedings, vol. 16, pp. 832-833, (1994).

[86] M. Koudelka, "*Performance-Characteristics of a Planar Clark-Type Oxygen Sensor*", Sensors and Actuators, vol. 9, pp. 249-258, (1986).

[87] J. Kulys, J. A. Munk, T. Buchrasmussen and H. E. Hansen, "*The Preparation in-Situ of a Silver Silver-Chloride Reference Electrode*", Electroanalysis, vol. 6, pp. 945-952, (1994).

[88] J. R. McDonald, "*Impedance spectroscopy*", John Wiley & Sons, New York, (1987).

[89] R. Greef, R. Peat, L. M. Peter, D. Pletcher and J. Robinson, "*Instrumental methods in electrochemistry*", John Wiley & Sons, Chichester, (1985).

[90] E. T. McAdams, "*Effect of surface topogaphy on the electrode-electrolyte interface impedance, Part 1. The high frequency, small signal interface impedance*", Surface topography, vol. 2, pp. 107-122, (1989).

[91] R. de Levie, "*The influence of surface roughness on electrochemical measurements*", J. Electrochem. Soc., vol. 107, pp. 113-130, (1965).

[92] L. A. Geddes, C. P. Da Costa, and G. Wise, "*The impedance of stainless steel electrodes*", Med. & Biol. Eng., vol. 9, pp. 511-521, (1971).

[93] H. Fricke, "*The theory of electrolytic polarization*", Phil. Mag., vol. 7(14), pp. 310-318, (1932).

[94] V. Pollack, "*Computation of the impedance characteristics of metal electrodes for biological investigations*", Med. Bio. Eng., vol. 14, pp. 460-464, (1974).

[95] A. J. Bard, "*Electronanalytical chemistry*", vol. 15, Marcel Dekker Inc., New York, (1989).

[96] Y. J. Kingma, J. Lenhart, K. L. Bowes, M. M. Chambers and N. G. Durdle, "*Improved Ag/AgCl pressure electrodes*", Med. Biol. Eng. Comput., vol. 21, pp. 351-357, (1983).

[97] G. J. Janz and D. J. G. Ives, "*Reference electrodes*", Academic Press, New York, (1961).

[98] R. N. Adams, "*Electrochemistry at solid electrodes*", Marcel Dekker Inc., New York, (1969).

[99] P. T. Kissinger and W. R. Heineman, "*Cyclic Voltammetry*", Journal of Chemical Education, vol. 60, pp. 702-706, (1983).

[100]J. J. Vanbenschoten, J. Y. Lewis, W. R. Heineman, D. A. Roston and P. T. Kissinger, "*Cyclic Voltammetry Experiment*", Journal of Chemical Education, vol. 60, pp. 772-776, (1983).

[101]S. Jaya, T. P. Rao, and G. P. Rao, "*Monolayer and Multilayer Formation Studies of Silver-Chloride On Silver Electrodes From Chloride-Containing Solutions*", Journal of Applied Electrochemistry, vol. 17, pp. 635-640, (1987).

[102]B. Kolodziej, "*The anodic behavior of silver in concentrated chloride solutions*", Polish Journal of Chemistry, vol. 74, pp. 349-360, (2000).

[103]V. I. Birss and C. K. Smith, "*The Anodic Behavior of Silver in Chloride Solutions .1. the Formation and Reduction of Thin Silver-Chloride Films*", Electrochimica Acta, vol. 32, pp. 259-268, (1987).

[104]H. Suzuki, H. Ozawa, S. Sasaki and I. Karube, "*A novel thin-film Ag/AgCl anode structure for microfabricated Clark-type oxygen electrodes*", Sensors and Actuators B-Chemical, vol. 53, pp. 140-146, (1998).

[105]W. Hunziker and I. Mellman, "*Expression of macrophage-lymphocyte Fc recepors in Madin-Darby canine kidney cells: polarity and transcytosis differ for isoforms with or without coated pit localisation domains*", J. Cell Biol., pp. 3291-3302, (1989).

[106]M. Bens, V. Vallet, F. Cluzeaud, L. Pascual-Letallec, A. Kahn, M. E. Rafestin-Oblin, B. C. Rossier and A. Vandewalle, "*Corticosteroid-dependent sodium transport in a novel immortalized mouse collecting duct principal cell line*", J.Am.Soc.Nephrol., vol. 10, pp. 923-934, (1999).

ACKNOWLEDGMENTS

First of all, I would like to thank my direct collaborators on my project, so let me introduce them all. This thesis has been done at the Institute of Microsystems at the Swiss Federal Institute of technology (EPFL) in Lausanne. It has been proposed to me and supervised by Prof. Martin Gijs which is head of the Technology group. So I want to thank him warmly for giving me the opportunity to achieve this thesis in a favourable and dynamic atmosphere, and for the kindness he always showed me. In the same time, I want to thank Dr. Abdeljalil Sayah, senior staff of our group, for the scientific and morale support he gave me during our long discussions.

I would like to thank my partners for the biological part, Prof. W. Hunziker from the Institute of Biochemistry at the University of Lausanne, PhD student K. Sobo from the research group of Prof. Van der Goot at the Department of Biochemistry at the University of Geneva and Prof. J.D. Horisberger from the Institute of Pharmacology and Toxicology at the University of Lausanne. They have done all the biological experiments for me with much patience and good feedback even when, our device were encountering several problems...

My special thanks to all the people from different institutes of the EPFL for the unilateral help they gave me: MM. G. Vaucher and P. Bruehlmeier from the accort for all the PCBs and the wire bonding they did for me, Dr. P. Kern from the LMCH for the experiments we've done and the discussions we've had on the subject of electrodes and interfaces, as well as Dr. S. Gilbert from Crystal Vision Microsystems, B. Senior for the help on the SEM microscope, all the mechanical workshop staff, especially G. Perrenoud, for the numerous mechanical parts they tooled for me, all the CMI staff for their availability and their advice in the cleanroom which gave me the chance to always come out of the cleanroom with the exact device I had designed in my office...

I was also very happy to work with students who helped me to advance in my project, J. Fontannaz, G. Chambon and S. Dey. A greeting to all the people of the IMS with whom I had always good contacts and unofficial collaborations, to R-

M. Apothéloz, our secretary who is always in a good mood although taking care of our heavy administration, and a special thought to D. Solignac who shared an office with me during three happy years.

Finally, I'd like to thank my family for giving me the opportunity to have a good education for a valuable start in the life, and my wife Celestina for being by my side during these four long but very pleasant years.

CURRICULUM VITAE

Personal Data

First name, name	**Serge Hediger**
Date and place of birth	April 12th 1973 in Vevey, Switzerland
Nationality	Swiss
Civil status	married

Education

1991	Federal maturity, scientific orientation, Gymnase de La Cité, Lausanne, Switzerland.
1992-1997	Engineering degree in microengineering, with a specialisation in integrated products, Swiss Federal Institute of Technology (EPFL), Lausanne, Switzerland.
1996-1997	Diploma work, Ceramics Laboratory (EPFL-DMX-LC), Fabrication and characterisation of a silicon piezoelectric accelerometer.
1998-2002	PhD candidate at the Institute of Microsystems (EPFL-IMS), Biosystem for epithelial cell culture and electrical characterisation.

Journal publications

P. A. Passeraub, P. A. Besse, S. Hediger, C. de Raad and R. S. Popovic, "*High-resolution miniaturized inductive proximity sensor: characterization and application for step-motor control*", Sensors and Actuators a-Physical, vol. 68, pp. 257-262, (1998).

P. A. Passeraub, P. A. Besse, A. Bayadroun, S. Hediger, E. Bernasconi and R. S. Popovic, "*First integrated inductive proximity sensor with on-chip CMOS read-*

out circuit and electrodeposited 1 mm flat coil", Sensors and Actuators a-Physical, vol. 76, pp. 273-278, (1999).

J. Baborowski, S. Hediger, P. Muralt and C. Wuethrich, "*Fabrication and characterization of micromachined accelerometers based on PZT thin films*", Ferroelectrics, vol. 224, pp. 711-718, (1999).

S. Hediger, A. Sayah, and M.A.M. Gijs, "*Fabrication of a novel microsystem for the electrical characterisation of cell arrays*", Sensors and Actuators B Vol. 56, pp.175-180, (1999).

S. Hediger, J. Fontannaz, A. Sayah, W. Hunziker, and M.A.M. Gijs, "*Biosystem for the culture and characterisation of epithelial cell tissues*", Sensors and Actuators B, vol. 63, pp. 63-73, (2000).

S. Hediger, A. Sayah, J.D. Horisberger, and M.A.M. Gijs, "*Modular microsystem for epithelial cell culture and electrical characterisation*", Biosensors & Bioelectronics, vol. 16/9-12, pp. 689-694, (2001).

Conference publications

S. Hediger, A. Sayah, and M.A.M. Gijs, "*Microsystem for living cell electro-optical characterisatio*n", Proc. The 3rd International Symposium on micro Total Analysis Systems (μTAS'98), Banff, Canada, October 13-16, 1 page, (1998).

S. Hediger, A. Sayah, and M.A.M. Gijs, "*Microsystem for living cell electro-optical characterisatio*n", Proc. The 2nd European Conference on Micro and Nanoscale Technologies for Biosciences (Nanotech'98), Montreux, Switzerland, November 24-26, 1 page, (1998).

S. Hediger, J. Fontannaz, A. Sayah, W. Hunziker and M.A.M. Gijs, "*Biosystem for culture and characterisation of epithelial cell tissues*", Proc. The 3rd European Conference on Micro and Nanoscale Technologies for Biosciences (Nanotech'99), Montreux, Switzerland, November 28- December 1, 3 pages, (1999).

S. Hediger, A. Sayah, W. Hunziker, M.A.M. Gijs, "*Biosystem for culture and characterisation of epithelial cell tissues*", Proc. The 6th World Congress on Biosensors (Biosensors 2000), San Diego, USA, May 24-26, p. 397, (2000).

S. Hediger, J. Fontannaz, A. Sayah, W. Hunziker and M.A.M. Gijs, "*Biosystem for culture and characterisation of epithelial cell tissues*", Proc. 4th International Symposium on micro Total Analysis Systems (μTAS'00), Twente Enschede, Netherlands, May 14-18, pp. 99-102, (2000).

S. Hediger, G. Chambon, A. Sayah, W. Hunziker and M.A.M. Gijs, "*Modular biosystem for the culture and characterisation of scarce epithelial cell tissues*", Proc. 11th International conference on solid-state sensors and actuators (Transducers'01 Eurosensors XV), Munich, Germany, June 10-14, 4 pages, (2001).

S. Hediger, A. Sayah, K. Sobo, F.G. Van der Goot and M.A.M. Gijs, "*Biosystem for epithelial cell culture and electrical characterisation*", Proc. The 5th European Conference on Micro and Nanoscale Technologies for Biosciences (Nanotech'01), Montreux, Switzerland, November 27-29, 2 pages, (2001).